



Patel, Amrita (2018) *Structural and biochemical characterisation of RING E3 mediated ubiquitination*. PhD thesis.

<http://theses.gla.ac.uk/9025/>

Copyright and moral rights for this work are retained by the author

A copy can be downloaded for personal non-commercial research or study, without prior permission or charge

This work cannot be reproduced or quoted extensively from without first obtaining permission in writing from the author

The content must not be changed in any way or sold commercially in any format or medium without the formal permission of the author

When referring to this work, full bibliographic details including the author, title, awarding institution and date of the thesis must be given

Enlighten: Theses

<https://theses.gla.ac.uk/>
research-enlighten@glasgow.ac.uk



Structural and biochemical characterisation of RING E3- mediated ubiquitination

Amrita Patel
M.Sc., M.Res

Submitted to the University of Glasgow in fulfilment of
the requirements for the
Degree of Doctor of Philosophy

Cancer Research UK Beatson Institute
College of Medical, Veterinary and Life Sciences
University of Glasgow

September 2017

Abstract

The ubiquitination pathway involves a cascade of three enzymes (E1, E2 and E3) that work together to conjugate ubiquitin (Ub) to protein substrates. RING E3s are the biggest family of E3s and are the major focus of my research project. RING E3s are characterised by the presence of a RING domain that binds E2~Ub and a protein-protein interaction domain that binds substrate(s). To facilitate Ub transfer, RING E3s perform several functions. Firstly, RING E3s bind E2~Ub and prime the E2~Ub thioester bond in a configuration that is optimal for catalysis. Secondly, RING E3s recruit substrate and juxtapose the E2~Ub thioester bond and ϵ -amino group of a lysine residue from the substrate to facilitate Ub transfer. Lastly, RING E3s recruit additional E2~Ub to catalyze polyUb chain formation. How RING E3s achieve these steps remains elusive. My research project focuses on understanding how RING E3s activate E2~Ub and catalyze Ub chain formation.

Previously, our lab has shown that Ub bound non-covalently to the surface of UbcH5B opposite its active site (“backside” bound Ub or Ub^B) stimulates ubiquitin transfer in both RING-dependent and RING-independent manners, but with a more prominent effect in RING-dependent transfer. In this earlier work, we used a monomeric RING E3, RNF38, for structural analyses. To assess whether the mechanism of Ub^B-stimulation is conserved for other RING E3s, I report the structure of a dimeric RING E3, cIAP1 (also known as BIRC2), bound to UbcH5B–Ub and Ub^B. This complex structure is the first structure of a dimeric RING E3 bound to E2–Ub and Ub^B. It is also the first structure of the cIAP1 RING domain bound to E2–Ub. Using structural and biochemical analysis, I show residues within the RING-UbcH5B–Ub and Ub^B-UbcH5B interfaces that are important in Ub transfer. I have also shown that the mechanism of Ub^B-stimulation is conserved throughout the UbcH5 family (UbcH5A, UbcH5B, UbcH5C and UbcH5D) of E2’s.

Previous studies suggest that UbcH6 lacks a Ub^B-binding ability despite sharing sequence and structural homology with the UbcH5 family. To investigate this, I performed NMR experiments that showed very weak binding between UbcH6 and Ub. To investigate further I performed autoubiquitination and lysine discharge assays using wild type UbcH6 (WT) and UbcH6 with Ser68 mutated to Arg to abrogate backside binding and found that Ub transfer was slower with UbcH6 S68R. Together

my results show that UbcH6 binds Ub non-covalently via its backside, but the binding is weak compared to the UbcH5 family of E2s.

Finally in chapter 5, I describe my attempts to elucidate how RING E3s promote Ub transfer from E2~Ub onto a lysine residue of substrate. I developed a model system containing an E3 bound to E2~Ub and a monoubiquitinated substrate mimetic. Initially, I used Cbl and UbcH5B for my model since many Cbl structures have been determined and Cbl's substrates are also well characterised. In the beginning, generating monoubiquitinated substrate mimetics was challenging, but later I standardised a method and showed that my substrate mimetics were functional *in vitro*. I then set up crystallisation experiments with various combinations of E3-E2-Ub and substrate mimetics, but unfortunately all my crystals diffracted poorly. After many attempts to improve the diffraction quality of my crystals, I did not manage to get data of sufficient resolution to determine a complex structure.

Acknowledgements

I would like to take this opportunity and express my sincere gratitude and thank my supervisor, Prof. Danny T. Huang, for all his guidance, support and motivation throughout my Ph.D. Without his constant guidance and encouragement, this thesis would have not been possible. I am fortunate to be in his lab, and having him as my supervisor has motivated me to elevate my scientific thinking and research. I would also like to thank my advisor Dr. Shehab Ismail and my review panel members Prof. Mike Olson, Dr. Daniel Murphy and Dr. Karen Blyth who guided and advised me on my yearly progress.

I would like to thank other members of my lab, Lori Buetow, Karolina Majorek, Mark Nakasone, Helge Magnussen, Feroj Ahmed, Mads Gabrielsen, Gary Sibbet, Dominika Kowalczyk and Alexander Schüttelkopf (DDP), for their support in the lab and thoughtful discussion, without which I would not be able to achieve these results. I would also like to thank previous students from our lab, Marta Klejnot, Gabriele Marcano and Hazel Aitkenhead, for giving me support when I first joined the lab. I am also very grateful to Prof. Richard Cogdell and his group at University of Glasgow who inspired me to pursue my research interests in structural biology.

A very big thank to my husband Sanjay Patel, whose love, encouragement, support, and trust overcame long distances and allowed me to continue my studies. I would like to thank my parents Mrs. Alka Patel and Mr. Natwar D. Patel and my brother Vikrant Patel for the love and support they have given me. I am very lucky to have so many friends in Glasgow. A big thank you to my best friends Neha Malviya and Gaurav Malviya for their friendship and for making my experience enjoyable and memorable. I would like to thank the Beatson services, including Molecular Technology Services, the Proteomics Facility, and Central Services, for their tremendous help and support. I would also like to thank Diamond Light Source (DLS) for beamtime and assistance in data collection. Finally, yet importantly, I am very grateful to Cancer Research UK (CRUK) for funding my studies and research.

Author's Declaration

I declare that I am the sole author of this thesis and the work presented here is entirely my own, except where acknowledged to others. This thesis does not include work that has been submitted for consideration for another degree in this or any other university.

Amrita Patel

Table of Contents

Abstract	2
Acknowledgements	4
Author's declaration	5
Table of contents	6
Abbreviations	13
1. Introduction	16
1.1 Ubiquitin.....	16
1.2 Ubiquitin conjugation system.....	17
1.3 Significance of ubiquitination.....	19
1.4 E1s.....	19
1.5 E2s.....	20
1.5.1 UbcH5 family.....	21
1.5.2 Non-covalent Ub binding to the UbcH5 family of E2s.....	23
1.5.3 Non-covalent Ub binding to the UbcH6 family of E2s.....	24
1.6 E3s.....	25
1.6.1 Characteristics of HECT E3 ligases.....	26
1.6.2 Characteristics of RING E3 ligases.....	27
1.6.3 Characteristics of RBR ligases.....	29
1.6.4 RING E3-E2 interfaces.....	30
1.6.5 RING domains activate E2~Ub.....	30
1.6.5.1 Direct interactions between RING E3s and E2~Ub.....	32
1.6.5.2 Indirect role of RING E3s for optimal Ub transfer.....	35
1.6.6 Substrate recognition by RING E3s.....	39
1.6.7 Methods to identify RING E3-substrate interactions.....	39
1.7 Cbl proteins.....	41
1.7.1 Discovery.....	41
1.7.2 Domain organisation.....	41
1.7.3 Cbl activity and functions.....	42
1.7.4 Cbl as a ubiquitin ligase.....	42
1.8 Cellular Inhibitor of Apoptosis (cIAPs).....	43
1.8.1 Role of IAPs in signalling pathways.....	43
1.8.2 IAPs as ubiquitin ligases.....	45

1.8.3	Available structures of cIAPs.....	46
	Thesis Objectives.....	48
2.	Materials and Methods.....	49
2.1	Materials.....	50
2.2	Methods.....	50
2.2.1	Primer design and molecular cloning.....	50
2.2.2	Expression and purification of proteins.....	57
2.3	Purification of ubiquitin.....	59
2.4	Purification of pc-Cbl and pCbl-b.....	59
2.5	Purification of <i>Arabidopsis thaliana</i> Uba1.....	61
2.6	Purification of UbcH5B.....	62
2.7	Purification of UbcH5A, UbcH5C and UbcH5D.....	64
2.8	Purification of UbcH5B~Ub.....	65
2.8.1	Purification of UbcH5B _{C85K} -Ub.....	65
2.9	Purification of cIAP2(255-C).....	66
2.10	Crystallisation.....	67
2.10.1	cIAP1R-UbcH5B _{C85K} -Ub-Ub ^B complex.....	67
2.10.2	Data collection and processing.....	68
2.11	Lysine discharge assays.....	68
2.11.1	Lysine discharge assays with UbcH5B~Ub.....	69
2.11.2	Lysine discharge assays with UbcH6(43-C)~Ub.....	69
2.11.3	Lysine discharge assays with UbcH6(43-C)~Ub using ubiquitinated cIAP.....	70
2.11.4	Non-radioactive lysine discharge assays.....	70
2.12	Ubiquitination assays.....	71
2.12.1	Autoubiquitination of cIAP1 and cIAP2.....	71
2.12.2	SMAC substrate ubiquitination by cIAP1.....	72
2.12.3	Ub-peptide substrate ubiquitination.....	72
2.13	Surface plasmon resonance (SPR).....	72
2.14	Nuclear Magnetic Resonance (NMR).....	73
3	Role of non-covalent ubiquitin in cIAP1 mediated ubiquitin transfer.....	75
3.1	Aims and Objectives.....	76
3.2	Results.....	77
3.2.1	Purification of His-GST RING (cIAP1R) domain with TEV.....	77

3.2.2	Ub ^B enhances cIAP1's affinity for UbcH5B~Ub.....	78
3.2.3	Ub ^B stimulates cIAP1R catalysed Ub transfer.....	80
3.2.4	Crystallisation of cIAP1R-UbcH5B-Ub-Ub ^B complex.....	80
3.2.5	Structure of cIAP1R-UbcH5B-Ub-Ub ^B complex.....	81
3.2.6	Interactions between cIAP1R and UbcH5B-Ub.....	84
3.2.7	Comparison between cIAP1 and cIAP2 to understand ubiquitin transfer.....	89
3.2.8	Ub ^B as an allosteric activator of cIAP1-mediated Ub transfer.....	90
3.2.9	Ub ^B stimulation mechanism observed across UbcH5 family.....	95
3.3	Discussion.....	97
4	Study of UbcH6's backside binding mechanism.....	100
4.1	Aims and Objectives.....	101
4.2	Results.....	102
4.2.1	Purification of UbcH6 ^{core} WT and S68R.....	102
4.2.2	Ub binds to UbcH6 ^{core} weakly.....	103
4.2.3	SPR with UbcH6.....	106
4.2.4	Ub ^B -mediated stimulation of UbcH6-catalysed Ub transfer	107
4.2.5	Assessing the effects of Ub ^B on cIAP1-UbcH6 catalysed autoubiquitination.....	108
4.2.6	Ubiquitinated cIAP1 acts as a source of Ub ^B	111
4.2.7	Ubiquitination of cIAP2 with UbcH6 ^{core} WT and S68R.....	112
4.3	Discussion.....	114
5	Study of RING E3-mediated substrate polyUbiquitination.....	116
5.1	Aims and Objectives.....	118
5.2	Results.....	120
5.2.1	Generation of Ub fused to Cbl substrate peptides (Ub-peptide)....	120
5.2.2	Test expression and purification of Ub-peptides.....	122
5.2.3	Test expression and purification of re-engineered Ub-fused peptides.....	123
5.2.4	Developing a method to separate tyrosine phosphorylated and unphosphorylated Ub-ZAP70.....	125
5.2.5	Biochemical assay to validate Ub-ZAP70p as a substrate.....	126

5.2.6 Assembling pCbl-E2-Ub complex bound to phosphorylated Ub-peptides.....	128
5.2.6.1 pc-Cbl-UbcH5B _{S22R} -Ub-Ub-3ggs-Srcp.....	129
5.2.6.2 pc-Cbl-UbcH5B _{C85K} -Ub-Ub-3ggs-Srcp with free Ub.....	130
5.2.6.3 pc-Cbl-UbcH5B-Ub-Ub-3ggs-ZAP70p.....	131
5.2.6.4 Other E3-E2-Ub-substrate complexes.....	131
5.3 Discussion.....	133
6. Conclusions and future work.....	135

List of Figures

Figure 1-1: The ubiquitin pathway.....	18
Figure 1-2: E1-E2-E3 system and its complexity.....	19
Figure 1-3: Crystal structures of Uba1 with Ub and with Ubc4.....	21
Figure 1-4: Overview of UBC domain of E2.....	22
Figure 1-5: Structures of UbcH5 family E2s.....	23
Figure 1-6: Structures of UbcH5C-Ub ^B and UbcH5B-Ub ^B	24
Figure 1-7: Structural comparison of UbcH5C-Ub ^B and UbcH6.....	25
Figure 1-8: E3 Ubiquitin ligase families.....	27
Figure 1-9: Domain architecture and characterisation of HECT E3 ligases.....	28
Figure 1-10: Domain architecture of RING E3s.....	29
Figure 1-11: Structures of Parkin and HOIP/E2-Ub of RBR ligases.....	31
Figure 1-12: Illustration of RING E3-E2 binding.....	32
Figure 1-13: Mechanism for stabilising E2~Ub by RING E3s.....	35
Figure 1-14: Phosphorylation of a conserved tyrosine residue activates Cbl.....	37
Figure 1-15: E3 binding to E2's backside enhances E2~Ub transfer.....	39
Figure 1-16: Cbl activity and functions.....	42
Figure 1-17: Canonical and non-canonical pathways of NF- κ B signalling.....	45
Figure 1-18: Domain organisation of human IAP family of proteins.....	46
Figure 1-19: Available structures of cIAP2.....	48
Figure 2-1: Generation of Ub fused peptide using multiple rounds of PCR.....	52
Figure 2-2: Purification steps of pCbl.....	61
Figure 2-3: Purification of Uba1.....	62
Figure 2-4: Protein purification of UbcH5B WT.....	63

Figure 2-5: Purification of UbcH5B–Ub.....	64
Figure 2-6: Purification of UbcH5B _{C85K} –Ub.....	66
Figure 2-7: Protein purification of cIAP2(255-C).....	67
Figure 2-8: Lysine discharge assay.....	69
Figure 2-9: Ubiquitination assay.....	71
Figure 2-10: SPR experimental setup.....	73
Figure 3-1: S75/1660 elution of cIAP1R.....	77
Figure 3-2: SPR binding data showing representative sensograms and binding Curves.....	79
Figure 3-3: Lysine discharge assays of UbcH5B WT and S22R.....	80
Figure 3-4: Crystallisation of cIAP1R-UbcH5B–Ub-Ub ^B	81
Figure 3-5: Crystal structure of cIAP1R-UbcH5B–Ub-Ub ^B	83
Figure 3-6: Interactions of cIAP1R C-terminal tail.....	86
Figure 3-7: Interactions between Ub ^D and UbcH5B.....	88
Figure 3-8: Structural comparison of cIAP1R-UbcH5B–Ub and cIAP2R- UbcH5B.....	90
Figure 3-9: Mechanistic aspects of Ub ^B -stimulation.....	91
Figure 3-10: Comparing Ub ^B from cIAP1R-UbcH5B–Ub-Ub ^B with RNF38-UbcH5B–Ub-Ub ^B and UbcH5C-Ub ^B	93
Figure 3-11: Ub ^B -stimulation is conserved in the UbcH5 family.....	97
Figure 4-1: Purification of UbcH6 ^{core} WT.....	103
Figure 4-2: Chemical perturbation shifts plots of Ub bound to UbcH5B and UbcH6 ^{core}	104
Figure 4-3: Chemical shift perturbation data for UbcH6 ^{core} interactions with Ub..	105
Figure 4-4: CSPs mapped on Ub’s surface.....	106
Figure 4-5: SPR binding data showing representative sensograms.....	107
Figure 4-6: Lysine discharge of UbcH6 ^{core} WT and S68R with and without Ub.....	108
Figure 4-7: Ubiquitination assays with UbcH6 ^{core} WT and S68R.....	110
Figure 4-8: Non-reduced autoradiogram showing disappearance of UbcH6 ^{core}	111
Figure 4-9: Autoubiquitination assays of cIAP2 with UbcH6 WT and S68R.....	113
Figure 5-1: Structures of Cbl with E2 and ZAP70 peptide.....	119
Figure 5-2: Modelled Ub-ZAP70 substrate peptide mimetic bound to pCbl-b-UbcH5B–Ub.....	120
Figure 5-3: Generation of Ub fusion peptides to function as substrates to elucidate RING-mediated substrate polyUbiquitination.....	121

Figure 5-4: Small-scale purifications of Ub-ZAP70 co-expressed with different kinases.....	122
Figure 5-5: Trouble-shooting Ub-peptide cleavage in <i>E.coli</i>	123
Figure 5-6: SDS PAGE of Ub-ZAP70 with C-terminal Ala-Ala –Pro substitution after Ni ²⁺ -affinity pull down and cleavage with thrombin.....	124
Figure 5-7: Western blot of purified Ub-ZAP70 from co-expressions with tyrosine kinases.....	125
Figure 5-8: Separation of phosphorylated and unphosphorylated Ub-ZAP70.....	126
Figure 5-9: SDS-PAGE showing ubiquitination of Ub-ZAP70p catalysed by pCbl.....	127
Figure 5-10: SDS-PAGE showing ubiquitination of Ub-ZAP70p with varying linker lengths catalysed by pCbl.....	128
Figure 5-11: Results from crystallisation experiments obtained from Table 5.2.....	130

List of Tables

Table 2-1: Constructs and primers used.....	51
Table 2-2: List of proteins purified.....	58
Table 3-1: Dissociation constants for interactions between cIAP1R, UbcH5B, UbcH5B–Ub with and without excess Ub.....	78
Table 3-2: Diffraction and refinement statistics of cIAP1R-UbcH5B–Ub-Ub ^B complex.....	82
Table 5-1: Substrate peptide sequences from ZAP70, Src, EGFR and c-MET ...	121
Table 5-2: Other E3-E2–Ub-Ub-peptide complexes.....	132

Abbreviations

APC	anaphase promoting complex
BIR domain	Baculovirus IAP repeat domain
BIRC	Baculoviral IAP repeat-containing
BIRC7	Baculoviral IAP repeat-containing 7
BSA	Bovine serum albumin
CBL	Casitas B-lineage lymphoma
cIAP1/2	Cellular inhibitor of apoptosis proteins 1 and 2
CIN85	CBL-interacting protein of 85kDa
CSPs	Chemical shift perturbations
CUL	Cullin family proteins
DLS	Diamond Light Source
DUB	Deubiquitinase
DTT	Dithiothreitol
E1	Ubiquitin-activating enzyme
E2	Ubiquitin-conjugating enzyme
E3	Ubiquitin ligase
EDTA	Ethylenediaminetetraacetic acid
EGFR	Epidermal growth factor receptor
IAP	Inhibitor of apoptosis
IPTG	Isopropyl β -D-thiogalactopyranoside
JMML	Juvenile myelo-monocytic leukaemia
K0Ub	Ubiquitin in which all seven lysine residues are mutated to Arg
k_{cat}	Catalytic constant
K_d	Dissociation constant
LHR	Linker helix region in CBL
LRR	Linker helix region and the RING domain in CBL
NF- κ B	Nuclear factor κ B
NMR	Nuclear magnetic resonance
PCR	Polymerase chain reaction
PDB	Protein Data Bank
PMSF	Phenylmethylsulfonyl fluoride

PTK	Protein tyrosine kinase
RBR	RING between RING
RING	Really Interesting New Gene
RTK	Receptor tyrosine kinase
SDS-PAGE	Sodium dodecyl sulfate polyacrylamide gel electrophoresis
SH2	Src homology 2
SH3	Src homology 3
Smac/DIABLO	Second mitochondriaderived activator of caspases / Direct IAP binding protein with low pI
SPR	Surface plasmon resonance
Syk	Spleen tyrosine kinase
TC	Thrombin cleavage
TEV	Protease found in the tobacco etch virus
TKBD	Tyrosine kinase-binding domain
Ub	Ubiquitin
Ub ^B	Ub back
Ubl	Ubiquitin-like protein
UBA	Ubiquitin associated domain
XIAP	X-linked inhibitor of apoptosis
ZAP-70	Zeta chain associated protein kinase 70
Å	Ångström
A ₆₀₀	Absorbance at 600 nm
kDa	kilodalton
M	molar
mg	milligram
mg/ml	milligram per millilitre
min	minute
ml	millilitre
mM	millimolar
r.m.s.d	root-mean-square deviation
s	second
μg	microgram

Chapter 1

Introduction

1 Introduction

1.1 Ubiquitin

Ubiquitin (Ub) is a small 76-residue polypeptide found ubiquitously in all eukaryotes. It is attached to amino groups on target proteins and alters the function of these target proteins. One of the best-characterised functions of Ub-targeting is Ub-mediated proteolysis in which proteins tagged with Ub are directed to the 26S proteasome for degradation. There are seven lysine residues (Lys6, Lys11, Lys27, Lys29, Lys33, Lys48 and Lys63) present on Ub's surface. Ub can be conjugated to its targets as a single moiety at one or multiple amino sites or as a polyUb chain that is linked via one of the seven lysine residues in Ub or via Ub's N-terminal methionine. Different types of Ub modification lead to distinct biological consequences [1]. For example lysine 48-linked polyUb chains target protein substrates to the 26S proteasome [2] for degradation, whereas lysine 63-linked polyUb chains are involved in protein trafficking and lysosomal degradation [3]. Lys48 and Lys63-linked polyUb chains are the most abundant linkages found in cells and hence their function is better characterised. Other chains are not well-characterised, but recent studies have deciphered some of their roles. For example, Lys6-linked polyUb chains have shown an increase in abundance in mitochondrial outer membrane proteins upon organelle polarisation [4, 5]. The exact cellular function of Lys6 chain linkages is not well understood. Previous studies showed that inhibition of the proteasome does not increase the abundance of Lys6-linked polyUbiquitinated proteins, suggesting a non-degradative role for this chain linkage [6, 7]. Lys6- along with Lys27-linked polyUb chains have been characterised as mitochondrial damage markers. Lys11-linked chains have shown to play an important role in proteosomal degradation and in cell cycle regulation. They have been identified as the specific chain linkage types utilised by anaphase promoting complex (APC) during mitosis [5, 8]. Lys27-along with Lys33-linked polyUb chains help in regulating innate immunity [9-12]. Lys29-linked polyUb chains are abundantly present during inhibition of the 26S proteasome, suggesting Lys29-linked chains function as a potential proteosomal degradation marker [6, 8]. Lys33-linked chains are involved in many biological processes. They play an important role in regulating the enzymatic activity of AMPK-related kinases along with Lys29-linked polyUb chains [13].

1.2 Ubiquitin conjugation system

Post-translational modification of proteins by ubiquitin (Ub) is a key regulatory mechanism involved in a myriad of cellular processes including apoptosis, cell cycle and division, DNA transcription and repair, immune response and inflammation. The ubiquitination pathway involves a cascade of enzymes that work together to conjugate ubiquitin (Ub) to protein substrates. First, Ub is activated by ubiquitin-activating enzyme (E1) resulting in the formation of a thioester intermediate between the C-terminus of Ub and the catalytic cysteine of E1. E1 then recruits a ubiquitin-activating enzyme (E2) and transfers Ub via its C-terminus to the E2's catalytic cysteine, resulting in the formation of an E2~Ub thioester intermediate (~ indicates a thioester bond). Finally, a ubiquitin-ligase (E3) binds E2~Ub and substrate and mediates transfer of the C-terminus of Ub from E2 to the α -amino group of the N-terminal methionine or an ϵ -amino group of a lysine side chain on substrate, resulting in the formation of an isopeptide bond (Figure 1-1).

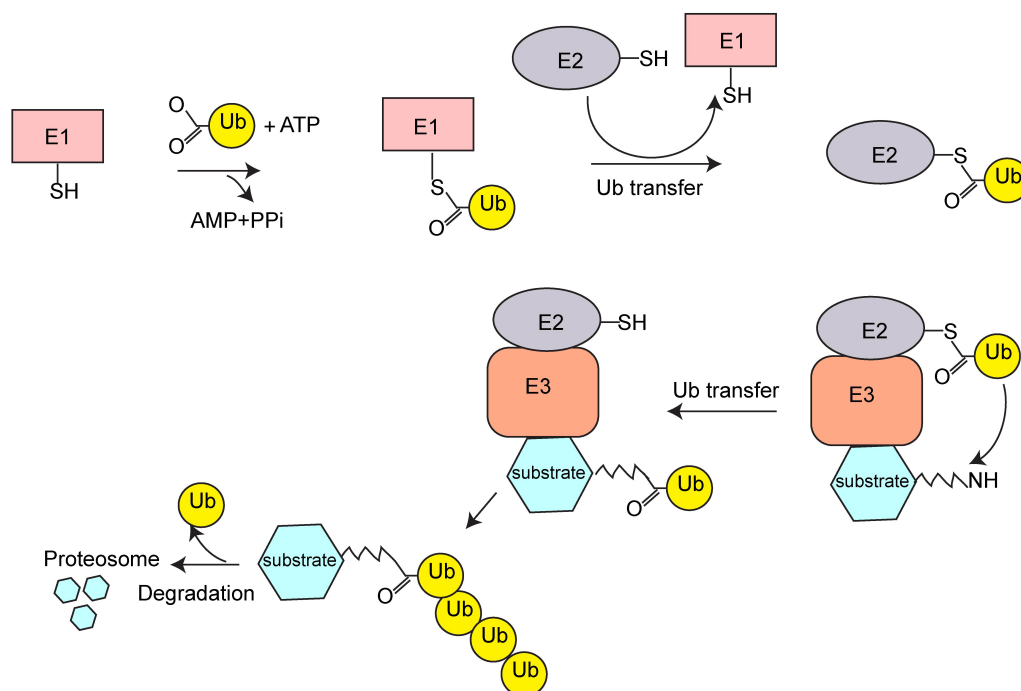


Figure1-1: The ubiquitin pathway. E1 activates Ub in an ATP-dependent manner and forms a thioester intermediate via its catalytic cysteine to Ub. Ub is then transferred to E2 and finally to E3. In the last step E3 recruits both E2 and substrate and transfers Ub from E2 onto a substrate amino group. Figure modified from Julie Maupin-Furlow (2011).

After the discovery of Ub in the early 1970s, other ubiquitin-like molecules were identified and classified into a family of proteins called the ubiquitin-like proteins (Ubls) [14]. The best-characterised Ubls are SUMO and NEDD8. SUMO plays important roles in substrate localisation and protein interactions [15], whereas NEDD8 plays important roles in activation of Cullin-RING ligases and helps in regulating p53 and destabilising SCF complexes [16, 17]. Ubls have their own dedicated E1-E2-E3 conjugation systems and often compete with Ub for the same lysine sites on some substrates. For example, Ub, SUMO-1 and NEDD8 modify certain lysines on p53. [18]

In the human genome, there are 2 E1s, ~30 E2s and more than 600 E3s. E3s play a pivotal role in determining substrate specificity and specifying the type of Ub chain that is attached to the substrate (Figure 1-2). There are four major groups of E3s that have been characterised based on their Ub transfer mechanism: HECT, RING, U-box and RING-between-RING (RBR). These E3s are discussed in detail in Section 1.6.

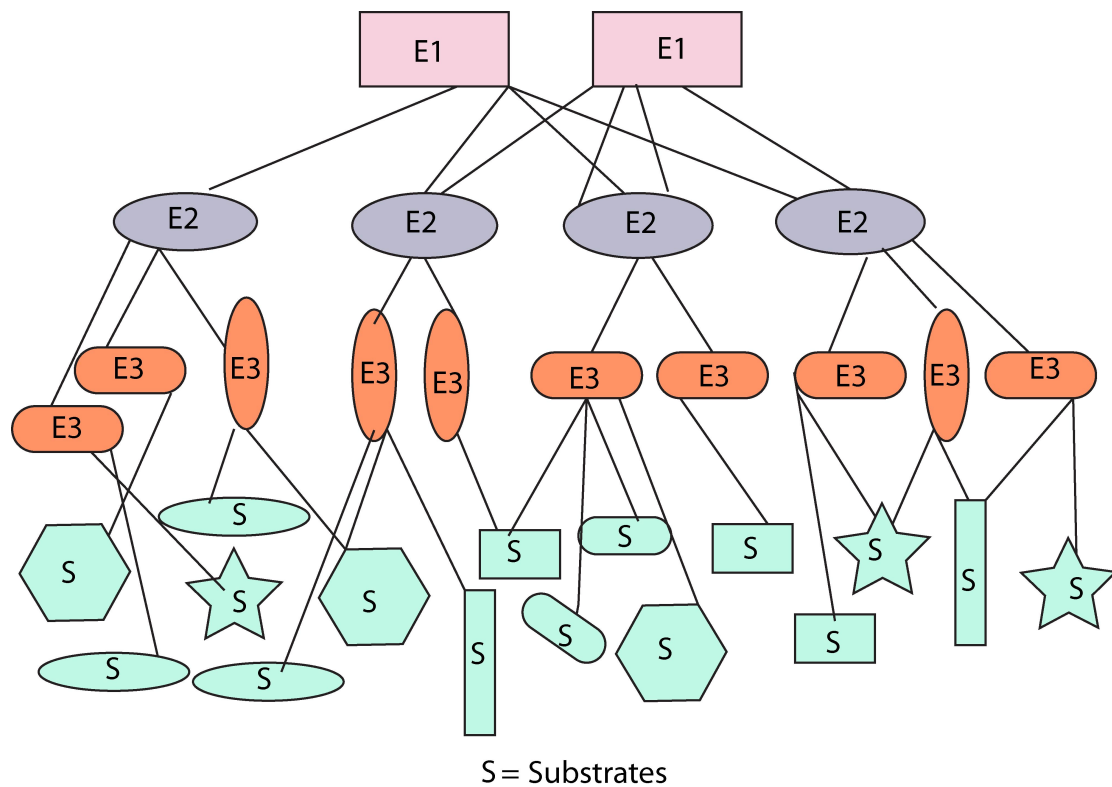


Figure 1-2: E1-E2-E3 system and its complexity. There are two E1s, which activate dozens of E2s. These E2s then activate hundreds of E3s, which in turn target thousands of substrates. Figure modified from Nalepa et al. (2006).

1.3 Significance of ubiquitination

Given the complexity of the Ub chain types that are involved in various signaling pathways, it is not surprising that defects in the Ub conjugation system are frequently associated with various diseases including cancers. Moreover, components of the Ub conjugation system are frequently elevated in cancer cells. The success of the proteasome inhibitor Velcade in treating patients with multiple myeloma has prompted the investigation of other therapeutic opportunities in the Ub-proteasome system. Based on this success, there is also great interest in targeting E1s, E2s, E3s and deubiquitinating enzymes (enzymes that remove Ub from the substrate, hereby referred to as DUBs). It is clear that a better understanding of the molecular mechanisms of these enzymes will assist in future therapeutic development.

1.4 E1s

E1s have a central role in the ubiquitination pathway. They initiate the ubiquitin conjugation cascade by activating the C-terminus of Ub. There are only two E1 genes present in eukaryotes, *Uba1* and *Uba6*. *Uba1* and *Uba6* are monomers of about 120 kDa. *Uba1* consists of four domains: an adenylation domain, a catalytic cysteine domain containing the catalytic cysteine, a four-helix bundle present between the adenylation domain and the catalytic cysteine domain, and a C-terminal Ub-fold domain (Figure 1-3) [19-22]. The adenylation domain of *Uba1* binds Mg^{2+} -ATP to activate Ub's C-terminal tail. Cys from the catalytic cysteine domain binds to the C-terminal tail of Ub, resulting in the formation of a thioester bond between the two [23, 24]. *Uba1* subsequently also activates another molecule of Ub, thereby binding two Ub molecules simultaneously: one is bound covalently via the catalytic Cys and another is bound non-covalently to the adenylation active site. Ub from E1's active site Cys is then transferred to an active site Cys on an E2 [24-26]. Crystal structures of *Uba1* and *Uba1* complexes (Figure 1-3A and B) show that the E2 *Ubc4* binds to a site proximal to the catalytic Cys of the E1 whereas the body of Ub binds to adenylation domain, suggesting that *Uba1* undergoes major conformational changes to catalyse the reaction [27].

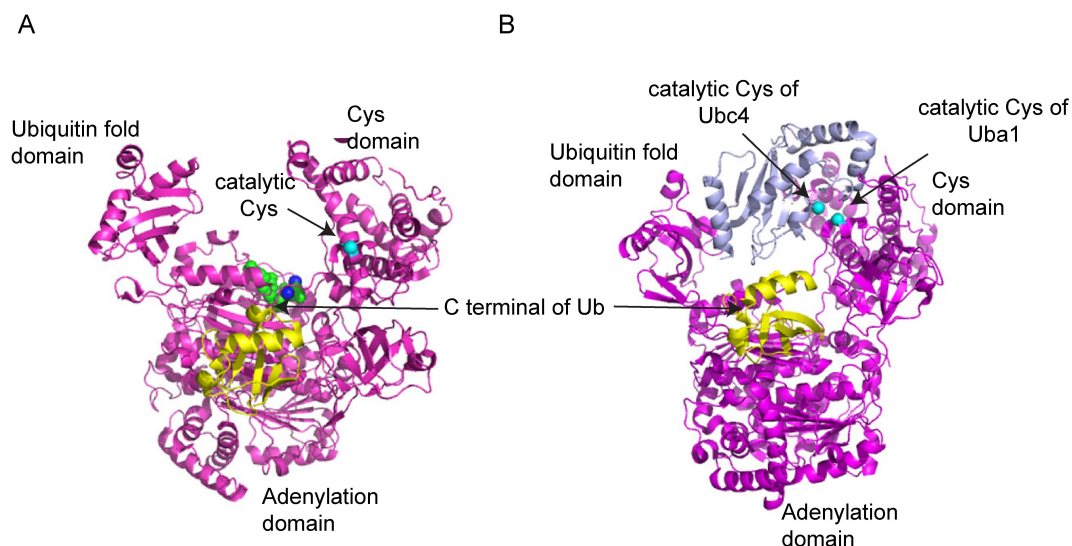


Figure 1-3: Crystal structures of Uba1 with Ub and with Ubc4 (A) Cartoon representation of the crystal structure of the Uba1-Ub complex. Uba1 is coloured magenta and Ub is coloured yellow. ATP and Mg²⁺ are respectively shown as green and blue spheres. Uba1's catalytic cysteine is shown as a cyan coloured sphere (PDB ID: 4II3). (B) Cartoon representation of the crystal structure of the Uba1-Ubc4-Ub complex. Ubc4 is coloured in light blue. The catalytic cysteines of Ubc4 and Uba1 are shown as cyan coloured spheres (PDB ID: 4II2).

1.5 E2s

The human genome encodes ~40 E2s that are involved in the transfer of Ub or UbIs (e.g. SUMO, NEDD8, etc.). For RING E3s, the mechanism of Ub transfer from an E2 to a target protein has not been completely elucidated. To date, evidence suggests that the ϵ -amino group from a substrate lysine attacks the carbonyl of the E2~Ub thioester to form a tetrahedral intermediate [28]. There is a highly conserved His-Pro-Asn (HPN) triad near the active site of all known E2s (Figure 1-4). His and Pro from this triad support the structure near the active site whereas Asp helps in stabilising the oxyanion intermediate that occurs during isopeptide formation [29]. E2s are characterised by the presence of a conserved catalytic ubiquitin-conjugating (UBC) domain. This domain is comprised of five α -helices and four anti-parallel β -strands [30] and contains the catalytic cysteine residue that receives Ub from the E1 to form a thioester bond. E2s serve as the “middle man” in the ubiquitination cascade. They interact with E1 and E3 during the transfer of ubiquitin to substrate. The E2 residues that interact with E1 and E3 overlap, suggesting that E2s cannot bind both simultaneously [31, 32]. Some E2s have additional N-terminal or C-terminal extensions. Evolutionarily, the E2 family is divided based into four classes depending

on these additional N- or C-terminal extensions. Class I E2s are only comprised of a UBC domain; Class II E2s have a UBC domain with a C-terminal extension; Class III E2s have a UBC domain with an N-terminal extension and Class IV E2s have a UBC domain with C-terminal and N-terminal extensions. These extensions are responsible for the varied sizes and functions of E2s. For example, the N-terminal extension of UbcH10, a class III E2, plays an important role in regulation of substrate ubiquitination and the C-terminal extension of CDC34, a class II E2, is responsible for cell cycle progression, ubiquitination and localisation of E2s in cells [31, 33].

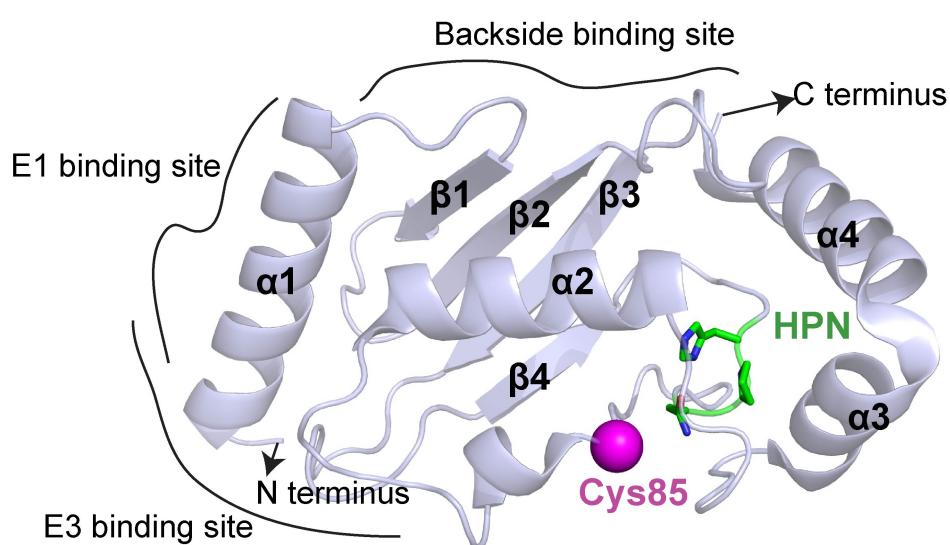


Figure 1-4: Overview of UBC domain E2. Cartoon representation of Ubch5B (PDB Id: 2FUH), a class I E2. The catalytic cysteine residue is shown as a sphere and coloured magenta. HPN motif residues are shown as sticks with C atoms coloured green, N atoms blue and O atoms red. The N-terminus and C-terminus are indicated by arrows. E1, E3 and backside binding sites are labelled.

1.5.1 Ubch5 family

The Ubch5 family of E2s has four homologues in humans: Ubch5A, Ubch5B, Ubch5C and Ubch5D. This family of E2s is homologous to Ubch4p and Ubch5p in yeast [34, 35]. Members of the Ubch5 family interact with a wide range of E3s from both the RING and HECT families of E3s. Ubch5A, Ubch5B and Ubch5C are well-characterised whereas not much is known about Ubch5D. The sequences of all four proteins in the family are highly conserved (Figure 1-5) and the structures of

UbcH5A, UbcH5B and UbcH5C are very similar; there are no available structures of UbcH5D.

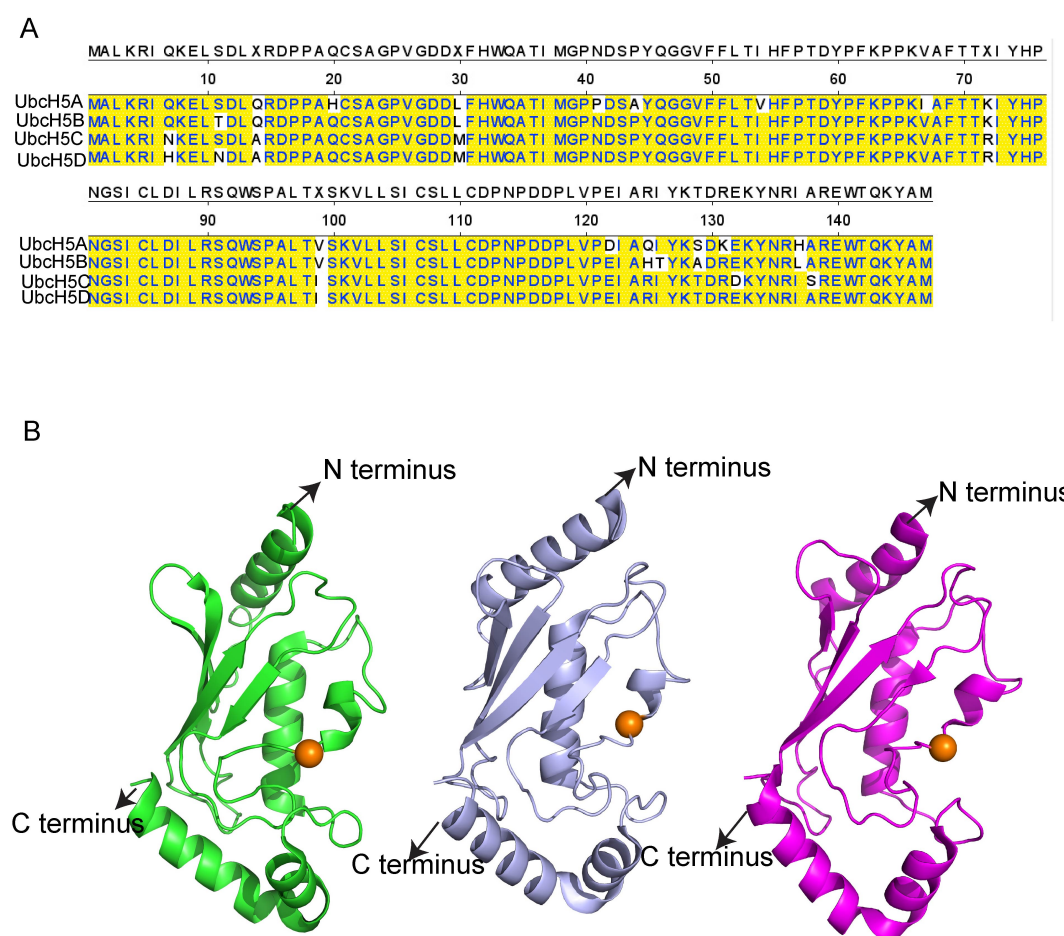


Figure 1-5: Sequence alignment and structures of the UbcH5 family. (A) Sequence alignment of UbcH5A, UbcH5B, UbcH5C and UbcH5D using megAlign. Identical residues highlighted in yellow. (B) Crystal structures of UbcH5A (green) (PDB ID: 2C4P), UbcH5B (light blue) (PDB ID: 2CLW) and UbcH5C (magenta) (PDB ID: 2FUH) [36]. The catalytic cysteines are shown as orange spheres and the N-terminal and C-terminal ends are marked.

UbcH5 family proteins are highly promiscuous in their lysine selection during Ub transfer. They do not discriminate, and will transfer Ub to any lysine residue near the catalytic cysteine. For this reason, they are widely used for *in vitro* studies [37].

1.5.2 Non-covalent Ub binding to the UbcH5 family of E2s

Brzovic *et al.*, in 2006 first reported non-covalent binding of Ub to a surface on UbcH5C opposite the active site [36]. They observed binding between the Ile44 surface of Ub and the β 1-3 surface of UbcH5C (Figure 1-6A). They showed that binding of non-covalent Ub to the backside of UbcH5C increases processivity of BRCA-1 directed polyUb chain formation. Mutation of Ser22 to Arg on the β -sheet of UbcH5C eliminated non-covalent binding of Ub. In two other studies it was postulated that self-assembled UbcH5B~Ub polymers bridge the gap between E2's active site and substrate lysine residues [38, 39]. All the above-mentioned studies showed that the β 1-3 surface of UbcH5 centring on Ser22 interacts with the hydrophobic patch of Ub surrounding Ile44. Disruption of this interaction abrogated RING E3 catalysed polyUb chain formation, but its mechanism was not well understood. In 2015, our lab determined the structure of RNF38 RING-UbcH5B~Ub bound to Ub^B (PDB ID: 4V3L) (Figure (1-6B)). Together these studies showed that non-covalent binding of Ub to the backside of UbcH5 family members UbcH5B and UbcH5C is conserved. Biochemical and structural data showed that Ub^B enhances RING-dependent and RING-independent UbcH5B~Ub transfer, with RING-dependent effects being more prominent. How this binding enhances RING-mediated E2~Ub transfer is discussed later in section 1.6.4.2

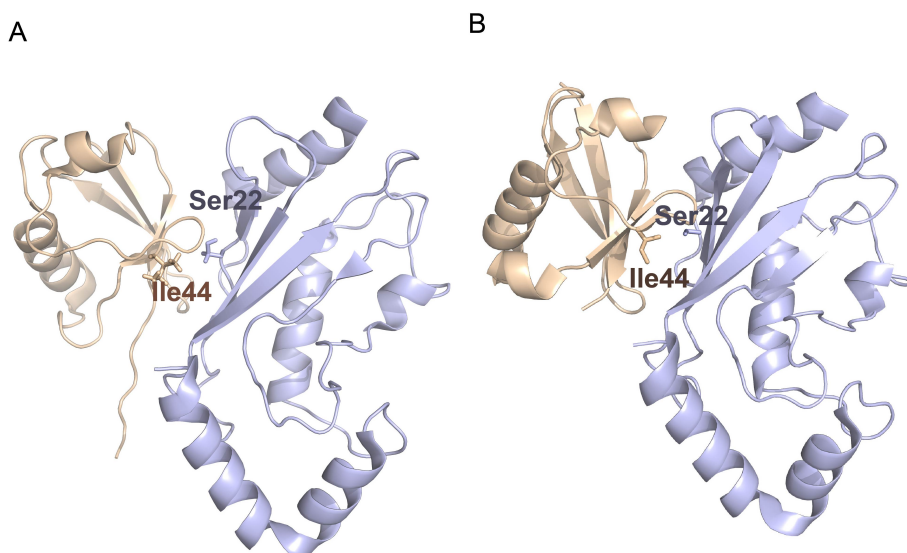


Figure 1-6: Structures of UbcH5C-Ub^B and UbcH5B-Ub^B. (A) UbcH5C-Ub^B (PDB ID: 2FUH) [36]. (B) UbcH5B-Ub^B from RNF38-UbcH5B~Ub-Ub^B (PDB ID: 4v3L) [40]. Ub^B is coloured in wheat and UbcH5B and UbcH5C in light blue.

1.5.3 Non-covalent backside binding to UbE2E family

The human UbE2E family of proteins has three members: UbE2E1, UbE2E2 and UbE2E3. All members of the UbE2E families have a conserved UBC domain and disordered N-terminal extensions of varied lengths [33, 41, 42]. These disordered extensions limit chain elongation and promote monoubiquitination whereas the core domain builds polyubiquitin chains [43]. To characterise the function of N-terminal residues in UbE2E proteins, autoubiquitination of cIAP2 and RNF4 with WT and K0Ub (Ub in which all seven lysines are mutated to Arg) were performed. Results from these experiments showed that the activity of the core domain of UbcH6 was restricted with K0Ub, whereas full length showed similar activity with WT and K0Ub. Residues 10-20 of the N-terminus were shown to be essential in limiting polyubiquitin chain formation.

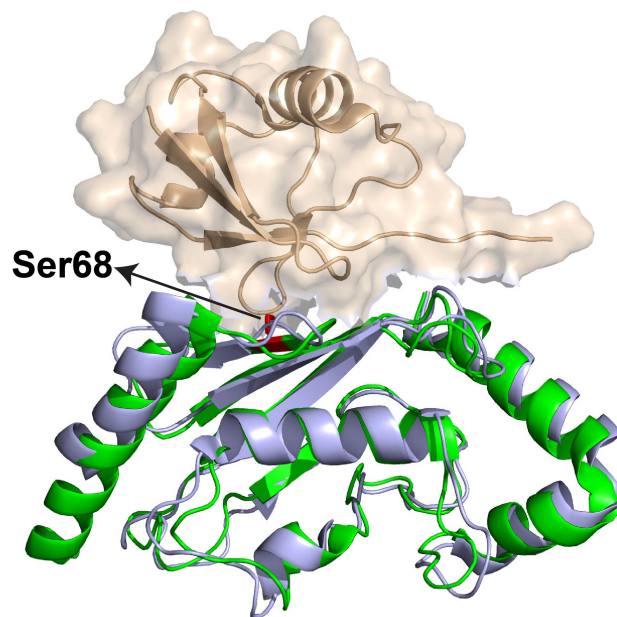


Figure 1-7: Structural comparison of UbcH5c-Ub^B and core domain of UbcH6 (43-C). Structure of UbcH6 in green (PDB ID: 3BZH) overlaid with structure of UbcH5C-Ub^B with UbcH5C in light blue and Ub^B in wheat (PDB ID: 2FUH). Ser68 of UbcH6 (shown as sticks in red) is equivalent to Ser22 of UbcH5C.

Although the structures of the UbcH6 and UbcH5 families are similar and both appear to have the capacity to bind Ub via the backside of the E2 (Figure 1-7), in 2013 Schumacher and colleagues [43] showed that backside binding of Ub involving

residue Ser68 (equivalent of Ser22 in UbcH5 family) on the β -sheet surface of UbcH6 does not influence polyubiquitin chain formation. Their results suggest that although the UbcH6 family of E2s is structurally similar to the UbcH5 family, the backside β -sheet surface might function differently than the UbcH5 family.

1.6 E3s

E3s, also known as ubiquitin ligases, are a large family of enzymes responsible for specifically targeting substrates for ubiquitination. There are four major groups of E3s that are characterised based on their Ub transfer mechanism: HECT, RING, U-box and RING-between-RING (RBR). Different E3s have different roles. Some are responsible for monoubiquitination of substrate whereas others regulate and catalyse substrate polyubiquitination [44]. All E3s function by either forming a covalent catalytic intermediate with ubiquitin during ubiquitin transfer (Figure 1-8C), or they transfer ubiquitin directly from E2~Ub to substrate (Figure 1-8A and B). The former mechanism is observed in HECT and RBR E3 ligases whereas the latter mechanism is a signature of RING and U-box E3 ligases [45]. RING domain of RING E3 ligases are characterised by the presence of two loops arranged in a cross brace configuration that are stabilised by Zn^{2+} which helps in binding E2s (Figure 1-8A,B); however, U-box E3 ligases lack Zn^{2+} ions and are stabilised via network of hydrogen bonds. Based on these similarities, U-box E3s are often grouped into the RING family of E3s (Figure 1-8) [45]. The RING-between-RING (RBR) class of E3s behave similarly to the HECT E3s, except Ub is transferred from active site of RING2 domain before transferring onto the substrate (Figure 1-8D).

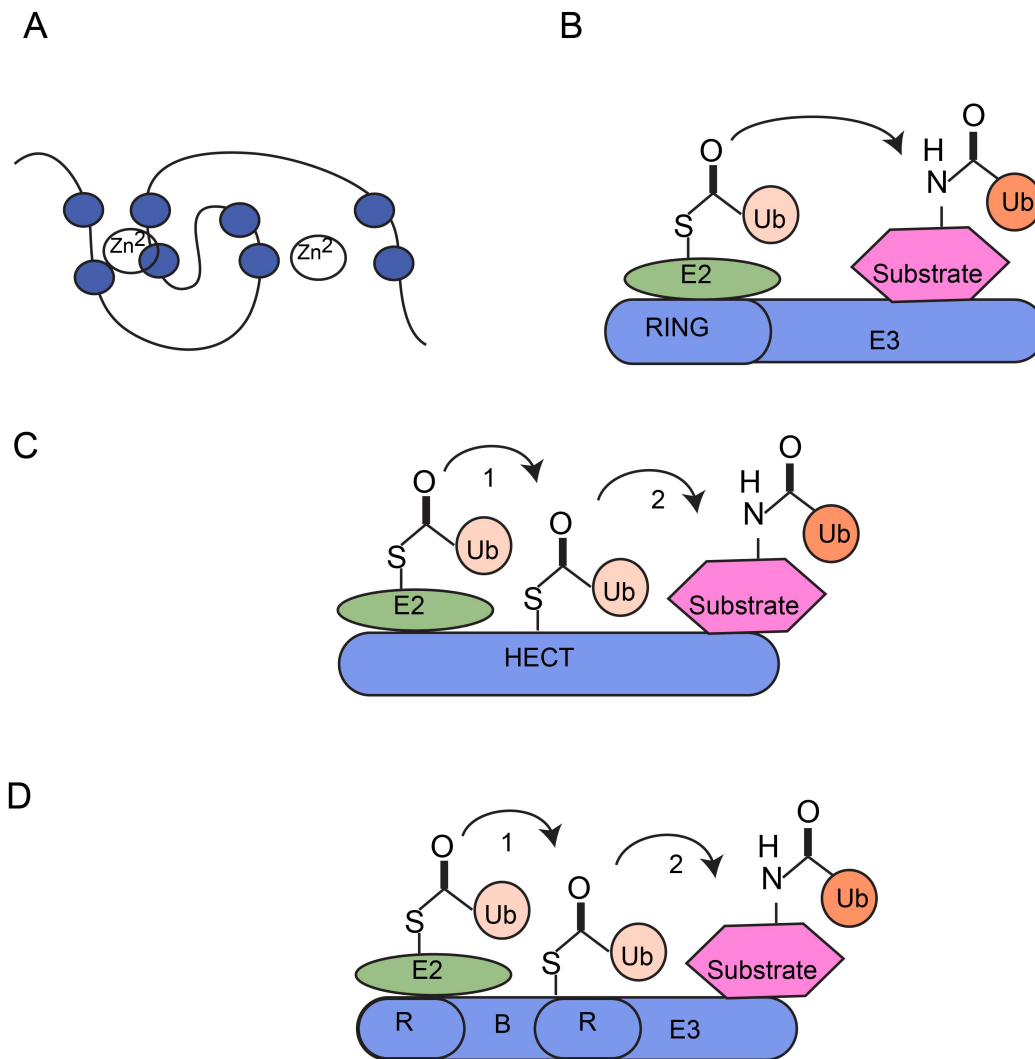


Figure 1-8: E3 Ubiquitin ligase families. (A) Zn²⁺-binding arrangement in RING E3 ligases. (B) RING-mediated Ub transfer mechanism. (C) HECT-mediated Ub transfer mechanism. (D) RBR-mediated Ub transfer mechanism. Figure modified from Francesca Ester Morreale and Helen Walden (2016)

1.6.1 Characteristics of HECT E3 ligases

The first family of E3s described were the HECT E3s in 1995 [46, 47]. There are about 28 HECT E3s in humans [48, 49]. The HECT domain is bilobal; the N-terminal lobe binds substrate and mediates substrate targeting whereas the C-terminal lobe (~350 amino acid) comprises the HECT domain, which contains the conserved catalytic cysteine (Figure 1-9A). Structural studies show that a hinge connecting the two lobes plays a critical role in juxtaposing the catalytic cysteines of E2 and E3 for ubiquitin transfer (Figure 1-9B) [50, 51]. HECT E3s are divided into three main classes depending on the presence of conserved domains or sequence motifs within the N-terminal region: (i) E3s containing WW domains are classified as

Nedd4/Nedd4-like; (ii) HERCS, which have N-terminal Rcc-1 like domain (RLD) and (iii) and other HECT E3s, which contain various other domains within their N-terminal regions (Figure 1-9C) [46, 52]

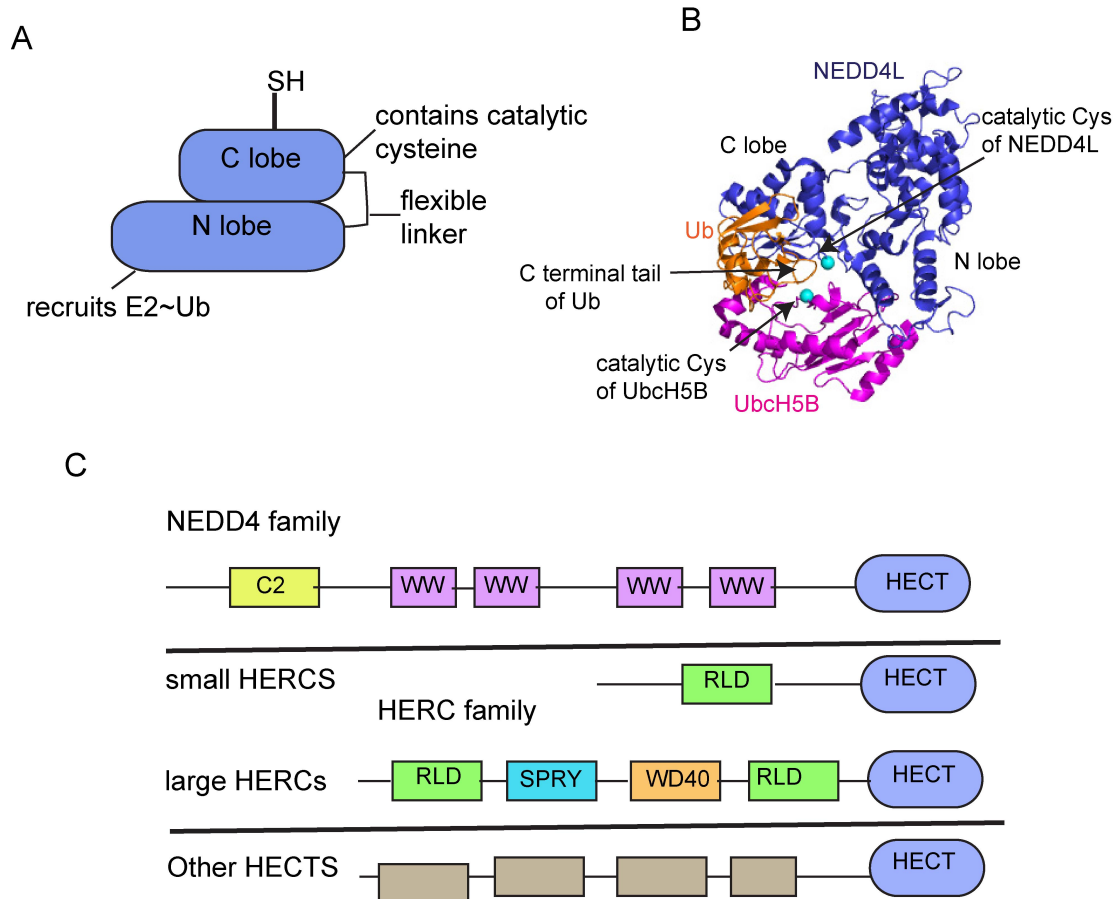


Figure 1-9: Domain architecture and characterisation of HECT E3 ligases. (A) HECT domains are bilobal. The N-lobe recruits E2~Ub and the C-lobe contains the catalytic cysteine that receives Ub from E2~Ub. A flexible linker between the N- and C-lobes is required to juxtapose Ub and its target. (B) Crystal structure of NEDD4L-UbcH5B-Ub (PDB ID: 3JWO). UbcH5B is coloured in magenta, NEDD4L in blue and Ub is in orange. Catalytic Cys of UbcH5B and NEDD4L are shown in cyan sphere. (C) Class I HECT E3 ligases containing WW domains. Class II HECT E3 ligases contain RLDS and HECT domains and class III contain various domains. Figure modified from Francesca Ester Morreale and Helen Walden (2016).

1.6.2 Characteristics of RING E3 ligases

There are more than 600 RING E3s found in mammalian cells, making it the largest family of E3 ligases. RING E3s are recognised by the presence of a RING domain. RING domains comprise ~75-100 amino acids and are characterised by the presence of two Zn^{2+} -coordinating loops (Figure 1-10A). These Zn^{2+} ions are required for

structural stability. RING domains recruit E2~Ub and promoting Ub transfer, Structural studies have shown that any mutation in these Zn²⁺-coordinating loops leads to functional aberrations [48, 53]. RING E3s can be divided into three major classes: monomeric, dimeric or multi-subunit complexes (Figure 1-10).

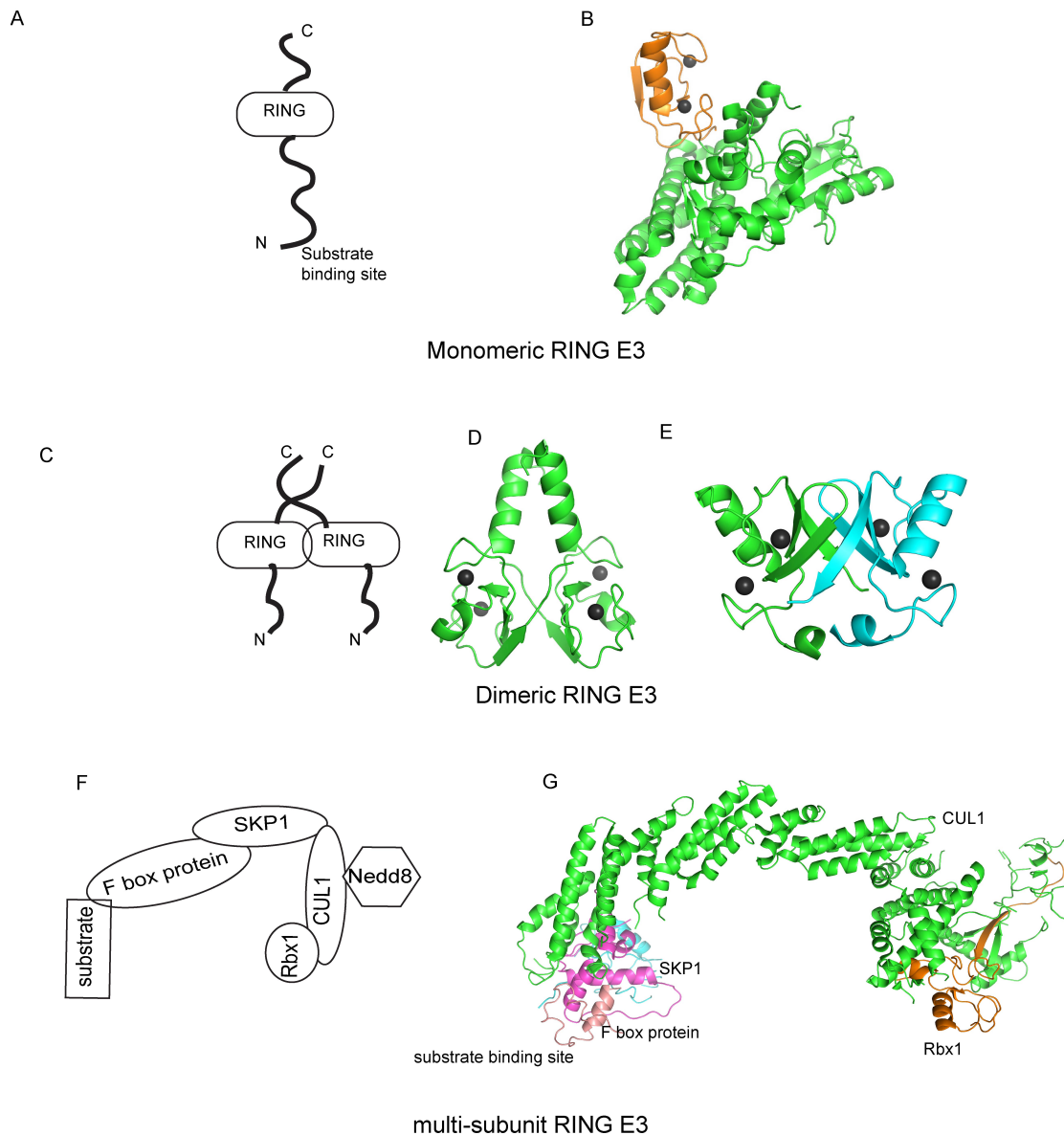


Figure 1-10: Domain architecture of RING E3s. (A) Schematic of a monomeric RING E3 (B) Crystal structure of the monomeric RING E3 c-Cbl (PDB ID: 2YIN), comprising a RING domain to recruit E2~Ub and a substrate-binding domain. The substrate binding domain is coloured green and the RING domain is orange. Zn²⁺ ions are shown as grey spheres. (C) Schematic of a dimeric RING E3. (D) Crystal structure of the homodimeric RING domain of CIAP2 (PDB ID: 3EB6) with Zn²⁺ ions shown as in B. (E) Crystal structure of the heterodimeric RING domain of MDM2-MDMX (PDB ID: 2VJE) MDM2 is coloured in green and MDMX in cyan

and Zn^{2+} ions are shown as in B. (F) Schematic of a multi-subunit RING E3. (G) Crystal structure of full length CRL2 (PDB ID: 5N4W). The Cul-2 subunit is coloured in green, the substrate-binding receptor in magenta, and Elongin B and Elongin C are in sand and blue, respectively. The RING subunit (Rbx1) is coloured in orange and Zn^{2+} ions are shown as in B.

Monomeric RING E3s like the Cbl family and RNF38 have a RING domain for recruiting E2~Ub and a substrate-binding domain or domain(s) encoded on a single polypeptide chain (Figure 1-11A). In RING E3 dimers, the RING domain and surrounding regions contribute to the dimer interface. Some RING E3s form homodimers as in cIAP (cellular inhibitor of apoptosis) (Figure 1-11B) and others form heterodimers as in MDM2 (murine double minute 2) with MDMX (known as MDM4) (Figure 1-11C). In some heterodimers like MDM2/MDMX, one of the RING domains lacks ligase activity and instead functions to stabilise E2~Ub binding by the second RING domain [50]. Multi-subunit RING E3 ligases like the Cullin RING E3 ligase (CRL) superfamily make up the largest number of RING E3s (Figure 1-11D). Each subunit of the CRL is encoded on a single polypeptide chain. CRLs consist of a Cullin subunit (Cul-1, 2, 3, 4a, 4b, 5 or 7), a RING subunit such as RBX1, RBX2, or Hrt1 and a substrate binding receptor subunit from the F-box, SOCS or BTB family. The Cullin domain acts as scaffold in which the RING and substrate receptor subunits are mounted [48]. The most studied CRL superfamily is the Skp1-Cul1-F-box protein (SCF) family. Another example of a multi-subunit RING superfamily is the anaphase promoting complex/cyclosome (APC/C) (Figure 1-11D). It consists of 19 subunits, including a RING subunit (APC11) and a Cullin-like subunit (APC2) [54].

1.6.3 Characteristics of Ring between Ring (RBR) ligases

The RING between RING (RBR) family of proteins is characterised by the presence of two RING domains. The N-terminal RING domain binds E2 and the C-terminal RING domain contains the catalytic Cys used to form the E3~Ub thioester. The N-terminal RING is followed by a cluster of cysteine and histidine residues that form the in between RING (IBR) region. In the best characterised members of the RBR E3s, namely Parkin and HOIP, the C-terminal IBR region contains a third RING domain that only binds one Zn^{2+} -ion and forms a hydrophobic core [55, 56]. In Parkin, this IBR RING domain is essential for function but this is not a feature common to all RBR ligases [57]. The catalytic cysteine of RBR E3s is frequently buried, suggesting

they are autoinhibited [58-61]. Recent structural studies on Parkin and HOIP reveal how RBR E3s are regulated (Figure:1-11A) and how they recruit E2~Ub (Figure:1-11B).

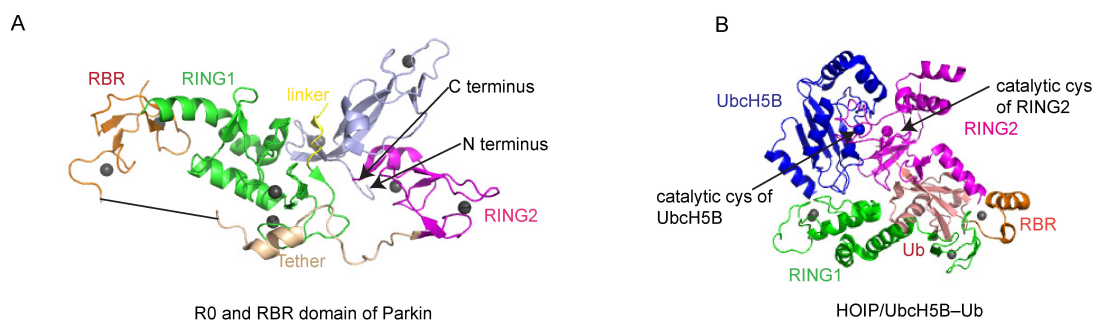


Figure 1-11: Structures of Parkin and HOIP/E2~Ub of RBR ligases (A) Crystal structure of a fragment of Parkin comprising the RING0 and RBR domains (PDB Id: 4I1F). (B) Crystal structure of a HOIP-UbcH5B~Ub complex (PDB ID:5edv). Each domain is labeled in the same colour in which it is shown.

Structural basis of RING E3 activity

RING E3 ligases serve as the biggest group of E3 ligases with ~600 RING E3s found in humans. Presence of RING E3 stimulates the Ub transfer from E2's active site onto the substrate's lysine site. The method of their stimulation was not very well understood until the first structure of c-Cbl-UbcH7-ZAP70 was solved [28, 40, 62, 63]. In the following sections, I have discussed about the RING E3-E2 interacting surface and how it activates E2~Ub transfer.

1.6.4 RING E3-E2 interface

The first step in E2~Ub activation by RING E3 ligases involves binding of the RING domain from the E3 to E2~Ub. The E3 selects E2~Ub and the target protein and the E3-E2~Ub pair determines how the substrate is modified [30]. A plethora of structural and molecular information on E3-E2 binding shows that the binding surfaces present on E3s and E2s are highly conserved, yet specific E2-E3 pairs exist in nature with some pairs being unique [33, 64, 65]. In all available complex structures of E3 bound to E2, loops 1 and 2 and the N-terminal α -helix of the E2 interact with the hydrophobic surface co-ordinated by Zn^{2+} -ions on the E3 RING domain [62, 66-69]. The first structure to show RING E3-E2 binding was that of c-Cbl bound to UbcH7

(Figure 12A). As shown in the figure below, Phe63 in loop 1 and Pro97 and Ala98 in loop 2 of UbcH7 pack closely within the groove between the Zn^{2+} -ions of the RING domain. Arg5 and Arg15 from the N-terminal α -helix of UbcH7 also interact with the linker region of c-Cbl [62] (Figure 12B). Although UbcH7 has been used in early structural studies with RING E3s, later studies have shown it to be reactive towards cysteine and not lysine. Therefore, UbcH7 can bind many RING E3s but is only reactive with HECT E3 ligases [63].

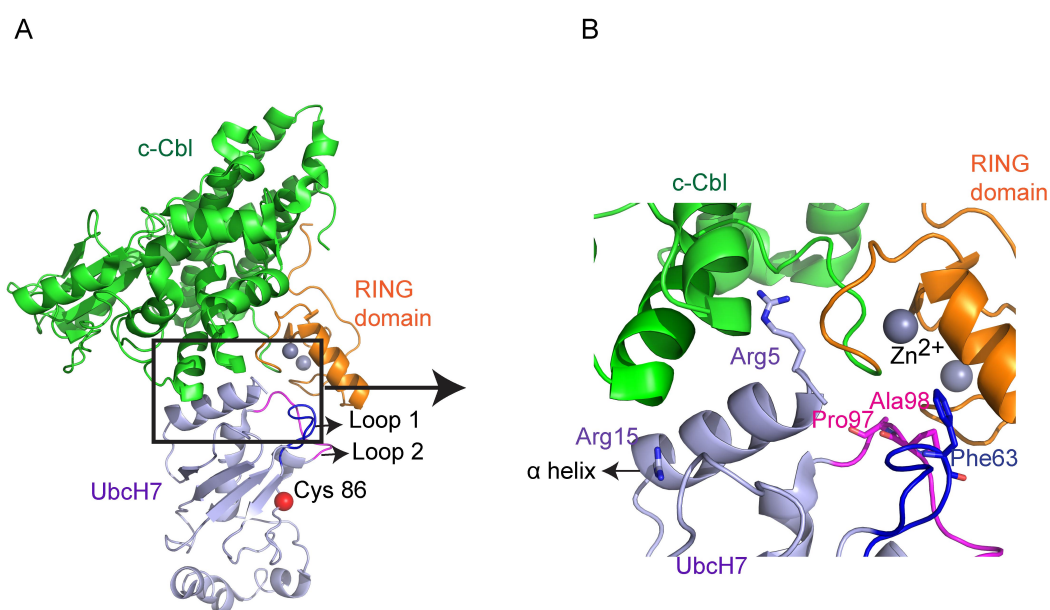


Figure 1-12: Illustration of RING E3-E2 binding. (A) Structure of c-Cbl bound to UbcH7 (PDB ID: 1FBV) [62] with the RING domain coloured in orange and the substrate binding domain in green; the Zn^{2+} -ions are depicted as grey spheres. UbcH7 is coloured light blue. The catalytic Cys of the E2 is shown as a red sphere, and loops 1 and 2 of are coloured in blue and magenta, respectively. (B) Close-up of the interaction between c-Cbl's RING domain and UbcH7. UbcH7's Phe63, Pro97 from loop 1, and Ala98 from loop 2 bind within the groove formed by c-Cbl's Zn^{2+} -ion coordination sites. In addition, Arg5 and Arg15 from UbcH7's α -helix interact with the linker of c-Cbl. These residues are shown as sticks with C atoms coloured as in A, N atoms blue and O atoms red.

A single E2 can bind multiple E3s, suggesting that different residues from E2s can be responsible for binding different E3s [30, 70, 71]. The binding affinity between E3 and E2 is weak ranging from 1.2 μ M to 2 mM range [30, 71]. This low affinity binding is essential since the binding sites for E1 and E3 overlap on E2s. In order to be charged again by E1, E2s first needs to disengage from E3s.

1.6.5 RING E3 activates E2~Ub

RING E3s transfer Ub directly onto a substrate lysine without forming an E3~Ub intermediate. Early RING E3-E2 structures showed that the binding interface is not near E2's active site [62, 70, 71]. In 2005, Ozkan *et al.* identified Ile37 as one of several mutants outside of the E2 active site that causes defects in E3-mediated Ub transfer [28]. Based on these studies, RING E3s were reputed to promote Ub transfer by inducing allosteric changes in E2~Ub. Similar allosteric effects were also shown by E4B binding to UbcH5C and Ubc4. [72]. To gain structural and biochemical insights into how RING E3s stabilise E2~Ub to promote Ub transfer, it was necessary to capture RING E3 bound to E2~Ub. However, in the presence of a RING E3, E2~Ub is unstable and Ub is readily transferred to accessible lysines. Therefore to capture a structure of a RING E3 bound to E2~Ub, Plechanovova *et al.*, (2011) and Dou *et al.* (2012) respectively crystallised complexes of E3s bound to UbcH5A~Ub and UbcH5B~Ub. In these studies, the E2~Ub thioester bond was replaced by mutating E2's active site Cys to Lys in RNF4-UbcH5A~Ub structure and Cys to Ser in Birc7-UbcH5B~Ub structure forming a stable isopeptide and oxyester bond respectively. [66, 67]. Since 2012, many more structures of RING E3 bound to E2~Ub have been published [40, 66, 68, 73, 74]. These E3-E2~Ub and E3-E2 structures showed that there are no major conformational changes in the E2 upon binding E3, regardless of whether it is E2 alone or E2~Ub. However, NMR studies revealed striking differences in the dynamics between 'open' and 'closed' conformations of E2~Ub in the presence of a RING E3 [66-68]. As shown in Figure 1-13A, in the absence of a RING E3, E2~Ub is dynamic and primarily adopts open conformations in which there are no or minimal interactions between E2 and the conjugated Ub. For the UbcH5 family of E2s, the addition of a RING E3 induces E2~Ub to adopt closed conformations. Structural studies revealed that the RING E3 directly contacts the C-terminal tail of E2~Ub to stabilise Ub in a conformation primed for transfer [39, 66, 68, 75].

1.6.5.1 Direct interactions between RING E3 and E2~Ub

The above-mentioned structural studies revealed the presence of a linchpin Arg in RING E3s. This Arg forms hydrogen bonds with Ub and E2, thereby stabilising E2~Ub in the closed conformation [48, 66, 68, 76]. The linching Arg from the RING domain interacts directly with the main chain of Arg72 of Ub and Gln92 of UbcH5B

(Figure 1-13E). For dimeric RING E3s like cIAP1, cIAP2, RNF4, and BIRC7, the C-terminal tail of each subunit contributes to the dimer interface. The C-terminal tail of one RING subunit interacts with other RING subunit and binds the Gly35-surface of Ub to stabilise E2~Ub in a closed conformation (Figure 1-13D) [66, 67, 77]. Arg606 plays a crucial role by pinning Ub^D and UbcH5B together. It stabilizes Ub^D by forming hydrogen bonds with Arg72 and Glu40 of Ub^D. Direct interactions between Arg606 of cIAP1R and Arg72 of Ub^D constrain the C-terminal tail of ubiquitin in a conformation in which the thioester is more reactive. Apart from cIAP1R's Phe616 and Arg606, Ile36 of Ub^D interacts with cIAP1R's C-terminus and RING domain via hydrophobic and hydrophilic interactions (Figure 1-13D). These interactions provide additional stability to RING-Ub^D interactions. These interactions consist of Arg614 at the C-terminus of cIAP1R forming a hydrogen bond with Asp32 of Ub^D, and His588, Ileu604 and Cys592 from cIAP1R's RING domain interacting with Leu8, Ileu36 and Pro37 of Ub^D (Figure 1-13D). Apart from the C-terminal tail of RING E3s, E2s also play an important role in stabilising Ub. Ubiquitin's Ileu44 patch interacts with the α 3-helix of UbcH5B (Figure 1-13E). The interactions between UbcH5B and Ub are stabilized by hydrophobic interactions between Ser108 of UbcH5B and His68 and Val70 of Ub. These interactions were also previously observed in the complex structure of BIRC7 bound to UbcH5B~Ub (Dou *et al.* 2012). Additional interactions are also observed between Lys48, Gln49, and Arg42 of Ub and UbcH5B's Asp112, Leu104, and Lys101 (Figure 1-13E). The C-terminal tail of Ub is extended and lies along the interface between UbcH5B's helices (Figure 1-13C). As shown in the figure, hydrophobic interactions are formed between UbcH5B's Ileu88 and Ub's Leu73. Other interactions shown in figure are between backbone nitrogen of UbcH5B Asp87 and the backbone oxygen of Ub's Arg74 (Figure 1-13C). Most E2s contain a His-Pro-Asn (HPN) motif near the active site that is important for catalysis. Based on numbering from the UbcH5 family of E2s, residues 114-117 comprise a loop near the active site and Asn77 from the HPN motif helps stabilize this loop via interactions with the main chain of Asn114 (Figure 1-13C) [48, 67, 78].

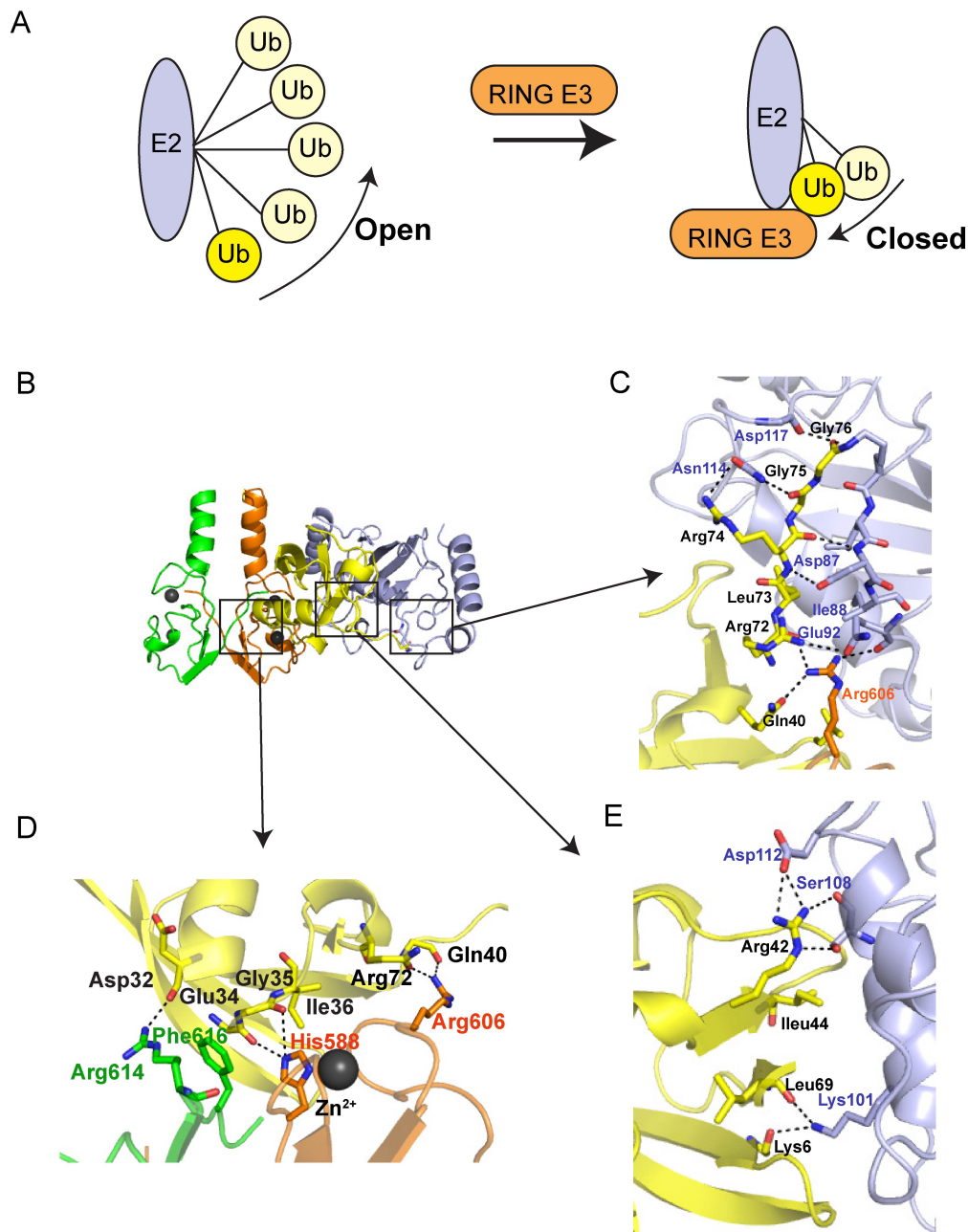


Figure 1-13: Mechanism for stabilizing E2~Ub by RING E3s. (A) E2~Ub is dynamic, shifting between open and closed conformations. Figure on left shows, E2~Ub in open conformations. Figure on right shows stabilized E2~Ub in the closed conformation upon adding E3. (B) cIAP1 bound to Ubch5B~Ub.Zn²⁺ ions are shown as grey spheres, Ubch5B is coloured light blue, Ub in yellow, cIAP-1 RING in orange. (C) Close-up view of the active site of Ubch5B~Ub. Asn77 forms hydrogen bonds with the main chains of Asn114. Asp117 reduces the pKa of substrate lysine [67]. (D) Close-up of view of cIAP1 homodimerisation interface. The C-terminal tail of cIAP1 from one protomer packs against Ub. (E) Close-up view of linchpin Arg interaction network. cIAP1 Arg606 makes contacts with Gln92 of Ubch5B and Glu40 and Arg72 of Ub. This interaction helps to stabilize Ub in the closed conformation.

1.6.5.2 Indirect role of RING E3s for optimal Ub transfer

Several factors contribute to priming E2~Ub for catalysis in addition to direct RING-E2~Ub interactions.

Phosphorylation: Cbl proteins (Cbl-b, c-Cbl and Cbl-c) are a family of RING E3 ligases responsible for targeting receptor tyrosine kinases (RTKs) for degradation by ubiquitination, endocytosis and subsequent lysosomal degradation [79-82]. Using mutational studies, Levkowitz *et al.*, (1999) found that Tyr371 is critical for activating c-Cbl. This was further supported by studies carried out by Kassenbrock *et al.* (2004) in which they also showed the importance of Tyr371 phosphorylation. In contrast, structural studies by Zheng *et al.*, (2000) showed that c-Cbl bound E2 without phosphorylation of Tyr371 and that Tyr371 was buried in a pocket that cannot accommodate a phosphate moiety (Figure 1-14A) [62, 83]. More recent studies have shown that UbcH7 does not work with RING E3s. In 2012, Dou *et al.*, determined the crystal structure of Tyr371-phosphorylated c-Cbl (pc-Cbl) bound to UbcH5B and ZAP70 peptide and showed that Tyr371 phosphorylation induces conformational changes in the linker helix region (LHR) of c-Cbl such that it no longer is in an autoinhibited state (Figure 1-14B). The phosphorylation of a strictly conserved tyrosine in the LHR within the N terminal region of Cbl proteins is important for its activation [84, 85]. The structure of pCbl-b bound to UbcH5B~Ub with ZAP70 peptide (Figure 1-14C) shows that the strictly conserved phosphorylated tyrosine (pTyr363) in the LHR of the N-terminal fragment of Cbl-b forms a hydrogen bond with Thr9 of Ub, thereby stabilising E2~Ub (Figure 1-14D).

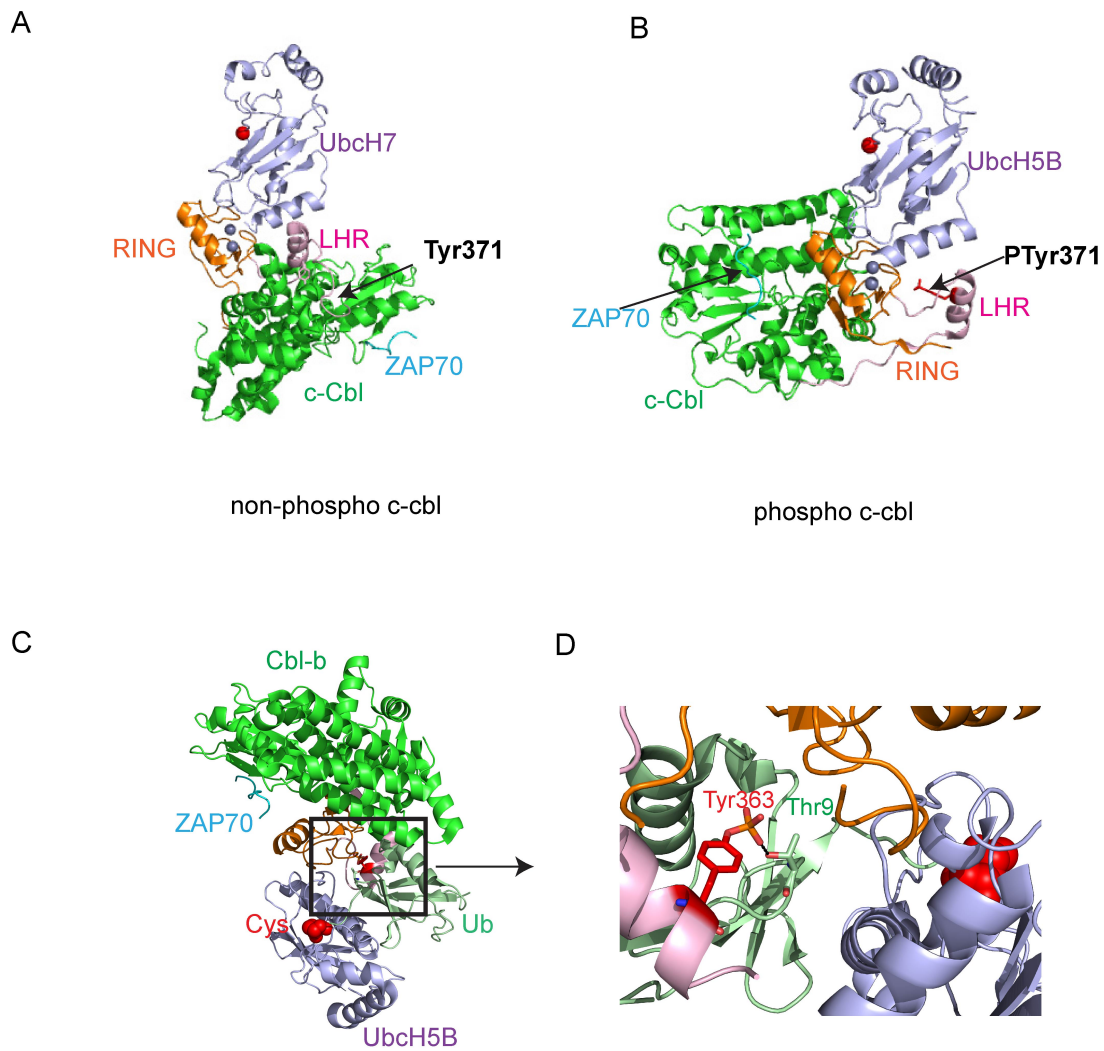


Figure 1-14: Phosphorylation of a conserved tyrosine residue activates Cbl. (A) Structure of c-Cbl bound to Ubch7 and ZAP70 peptide. The substrate binding domain of c-Cbl is coloured in green, the LHR in pink and the RING domain in orange. Zn^{2+} ions are shown as grey spheres and Tyr371 is in red sticks. Ubch7 is in light blue and the catalytic Cys is shown in red spheres. Zap70 peptide is in cyan. (PDB ID: 1FBV) (B) Structure of pc-Cbl bound to Ubch5B and ZAP70 peptide. Coloured as in A (PDB ID: 4A4C). (C) Structure of pCbl-b bound to Ubch5B–Ub and Zap70 peptide, coloured as in A and with Ub in light green (PDB ID: 3ZNI) (D) Close-up of the interaction between the LHR of pCbl-b and Ub, coloured as in A. Key residues from Ub are shown as sticks with C atoms in light green and O atoms in red. C atoms from pTyr363 are shown in red, P atoms in orange and O atoms in red. The dashed line indicates a putative hydrogen bond.

Backside binding to E2s: Some RING E3s have an additional domain that binds to the backside of certain E2s [45, 86, 87]. For example, the RING E3 gp78 binds to the backside of the E2 Ube2g2; this region of gp78 is called G2BR (Figure1-15A). G2BR is a single α -helix that binds perpendicularly to Ube2g2. G2BR binding allosterically stimulates Ube2g2 in two ways: (i) G2BR locks the catalytic cysteine

loop of Ube2g2 and orients it into a closed conformation and (ii) it increases the affinity of Ube2g2 for gp78, which leads to stimulation of ubiquitination. This interaction has very high binding affinity (~21nM), which helps in increased ubiquitylation by Ube2ge and G2BR [45, 86]. Another RING E3, Cue1p, binds to the backside of the E2 Ubc7p via a domain called Ub7BR (Figure 1-15B). The Ubc7p-Ub7BR interaction occurs distal to Ubc7p's active E3-binding sites. Backside binding by Ub7BR does not affect the overall structure of Ubc7p but instead alters loops surrounding the catalytic Cys. When Ub7BR binds to the backside of Ubc7p, loops surrounding Ubc7p's catalytic Cys move away from the active site, making it more accessible to substrate and to E1 for charging for subsequent rounds of ubiquitination. In addition, Ub7BR enhances E3-E2 binding affinity [88, 89].

Another RING E3, Rad18, competes with ubiquitin for non-covalent backside binding to the E2 Rad6 [45, 87]. The Rad18/Rad6 backside interaction promotes substrate monoubiquitination rather than polyubiquitination. Rad18 binds to the backside of Rad6 through its C-terminal domain, called Rad6 binding domain (Rad6BD) (Figure 1-15C). Unlike Ubc7p-Ub7BR binding, Rad18 does not enhance the rate of Rad6~Ub thioester formation; instead it limits the polyubiquitin chain formation by Rad6. NMR studies showed that binding of Rad6BD peptide to Rad6 does not induce any structural changes, except that Rad6BD is in a more compact conformation when bound to Rad6 [87].

Similar to Rad18, another RING E3 called AO7/RNF25 also contains a domain that competes with Ub for non-covalent binding to the backside of the E2 UbcH5B. AO7 binds the backside of UbcH5B via its unique UbcH5B recognition domain called U5BR and a linker, which connects to its RING domain (Figure 1-15D). This acts like a clamp and prevents interactions between UbcH5B's backside and Ub. The binding affinity between U5BR and UbcH5B is very strong, and unlike other E3s, U5BR does not enhance the rate of E2~Ub transfer. This might occur because its primary function is to prevent backside Ub binding; however if the local concentration of E2 bound to backside Ub is low, the U5BR-UbcH5B interaction enhances rate of E2~Ub transfer. Hence the role of AO7-UbcH5B binding is a paradox in that it increases or decreases E3 activity depending on the requirement [90].

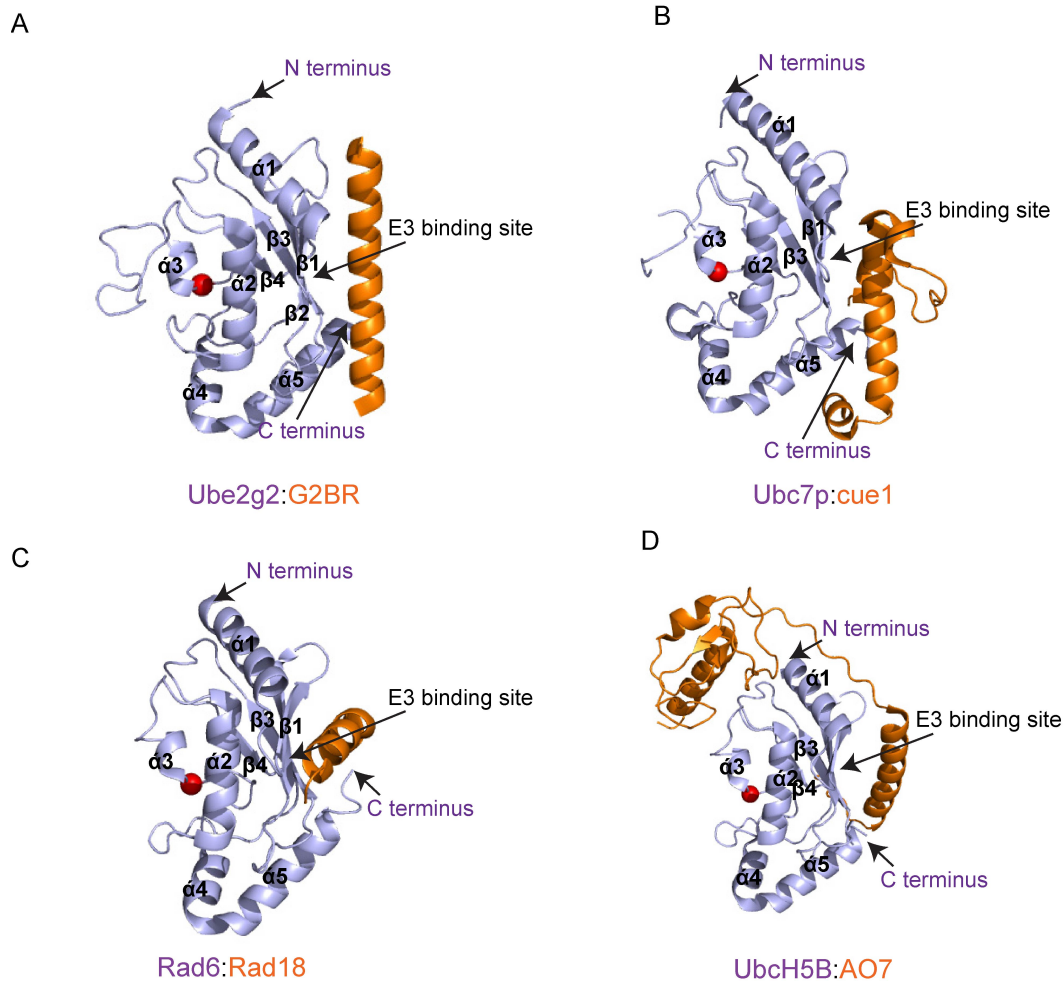


Figure 1-15: E3 binding to E2's backside enhances E2~Ub transfer. (A) Structure of Ube2g2 bound to G2BR (PDB ID: 3H8K). (B) Structure of Ubc7p bound to cue1p (PDB ID: 4JQU) (C) Structure of Rad6 bound to Rad18 (PDB ID: 2YBF). (D) Structure of UbcH5B bound to AO7 (PDB ID: 5D1K).

Apart from non-covalent binding of E3 domains outside of the RING domain to the backside of select E2s as discussed above, Ub also binds the backside of select E2s non-covalently to enhance E2~Ub activity. As discussed earlier in Sections 1.5.2 and 1.5.3, Ub has been shown to bind to the backside of several E2s including the UbcH5, Rad6 and Ube2g2 families [36, 40, 87]. In 2006, Brzovic *et al.* showed for the first time that Ub bound non-covalently to the backside of UbcH5C. The structure revealed that Ub's Ileu44 patch is involved in interacting with the backside surface of UbcH5C centring residue Ser22. They also showed when Ser22 is mutated to Arg, UbcH5C loses its ability to bind Ub. After this many other groups also demonstrated evidence of non-covalent binding of Ub to E2's backside, but they could not explain the relevance *in vivo* based on its low binding affinity to E2 [36, 38, 91, 92]. In 2015, our

lab presented detailed biochemical studies showing that non-covalent Ub binding to the backside of UbcH5B in RING-dependent and RING-independent manners stimulates Ub transfer, with a more prominent effect in RING-dependent transfer. Along with these biochemical studies, we determined crystal structures of complexes of RNF38 bound to UbcH5B–Ub with and without backside Ub (Ub^B). The structures showed a conformational change in the $\alpha 1\beta 1$ loop of UbcH5B in the presence of Ub^B. The $\alpha 1\beta 1$ loop of UbcH5B is more restricted in the presence of Ub^B, which in turn facilitates E2~Ub adopting a closed conformation that is primed for Ub transfer upon binding to the RING domain. When E2~Ub is in the closed conformation, the C-terminal tail of Ub is optimally aligned in E2's active site cleft such that the E2~Ub thioester bond is oriented for nucleophilic attack by a substrate lysine residue [40, 66-68]. SPR results showed that Ub^B enhances RING E3's binding affinity for UbcH5B~Ub by 12-fold and RING E3-E2~Ub complex enhances Ub^B's affinity for the backside of E2 by 20-fold. This explains how a weak Ub^B-E2 interaction ($K_d \sim 300 \mu\text{M}$) could become relevant in cells where Ub concentrations are between 20-85 μM [40].

1.6.6 Substrate targeting by RING E3s

One of the key functions of RING E3s is to bring E2~Ub and substrate lysine into proximity for ubiquitination. Substrate regulation via RING E3s involves two crucial points, substrate identification and substrate ubiquitination. Substrate identification occurs via direct or indirect protein-protein interactions. For example, Cbl has a substrate-binding domain (SBD) that recognises and binds phosphorylated EGFR and targets it for lysosomal degradation. It also binds an additional EGFR-interacting protein GRB2, which helps Cbl to recruit EGFR [48, 81, 93].

1.6.7 Methods to identify RING E3-substrate interactions

E3 ligases are very complex and this makes identification of specific E3 targets difficult. There are several factors responsible for this complexity including the following: (i) Several hundred RING E3 ligases are responsible for targeting thousands of substrates, and within this system, there is redundancy in substrate identification as illustrated in Figure 1-2; (ii) In the presence of RING E3 ligases the transfer of Ub is very rapid, resulting in E3-substrate complexes only having a short lifetime [40, 48, 66-68]; (iii) For some E3 ligases the E3-substrate interaction is very weak, making identification of these E3 targets challenging [94]; (iv) Cellular

concentrations of some substrates are very low [95]. All these factors hinder current methods that have are available to identify substrates [95-97]. Also some RING E3 ligases like Cbls only target their substrates following post-translational modifications, and pathways triggering these post-translational modifications must be activated to isolate such targets. The methods developed to date are not capable of detecting such modifications [8, 48]. Moreover differences in mechanisms among the three E3 ligases classes (HECT, RING and RBR) also contributes difficulties in identifying substrates and validating the role of select E3s in modifying these substrates in cells [98].

In spite of all above challenges, some progress has been made in developing methodologies that can be used to identify specific E3-substrate interactions [98]. Examples include yeast two-hybrid screening (Y2H), phage display, advances in proteomics, and development of antibodies that identify motifs like the diGly (Gly Gly) motif at the C-terminus of Ub and other UbIs and specific polyUb chain linkages etc. [6, 7, 99-101]. Substrate ubiquitination occurs via attachment of Ub onto the side chain of a substrate lysine residue, thereby forming an isopeptide bond. Ub possesses seven lysine residues on its surface, which serve as sites for Ub attachment in the formation of polyUb chains. Specific linkages define the fate of the substrate; examples include degradation via the proteasome or lysosome and, localisation to sites of DNA repair. Studies have shown that all types of linkages co-exist in cells [6, 7, 102]. Post-translational modifications of RING E3s or substrates are the most common modifications that regulate substrate ubiquitination. For example, Cbl is activated by phosphorylation (Section 1.6.4.2). In Cbl, the substrate-binding site is located on a Src Homology 2 (SH2) domain, which recognises tyrosine-phosphorylated proteins for substrate regulation. Similarly dimeric MDM2/MDMX recruits its substrate p53 via regions N-terminal of the RING domain. Multi-component RING E3s like CRLs recruit multiple subunits including a RING domain to bind E2~Ub and a substrate binding receptor domain for substrate recognition. F-box proteins are the best-characterised proteins so far (Figure1-11, Section 1.6.2). There is still a demand for more comprehensive studies to elucidate mechanisms of substrate selection and regulation by RING E3s.

1.7 Cbl proteins

1.7.1 Discovery

Cbl (Casitas B-lineage lymphoma) was first identified as v-Cbl, an oncogenic protein that causes pre-B lymphoma in mice [103, 104]. The cellular form, c-Cbl, is present ubiquitously in mammals, localised within the cytoplasm, and expressed highly in testis and hematopoietic cells [105]. The mammalian Cbl family consists of three homologues: c-Cbl, Cbl-b and Cbl-c.

1.7.2 Domain Organisation

The N-terminal region of Cbl is highly conserved. All three mammalian Cbl homologues (c-Cbl, Cbl-b and Cbl-c) consist of a tyrosine kinase binding domain (TKBD) that only binds tyrosine-phosphorylated polypeptides. This domain is made up of four helical (4H) bundles followed by a calcium binding EF hand and a variant SH2 domain. This region is responsible for binding substrates. The TKBD domain is then followed by a short LHR and a RING domain. The LHR and RING bind E2~Ub [62]. c-Cbl and Cbl-b contain an additional proline rich region that mediates protein-protein interactions. Both Cbl-b and c-Cbl have a Ub associated (UBA) domain at their C-termini known to promote dimerisation in experimental conditions (Figure 1-16) [106, 107].

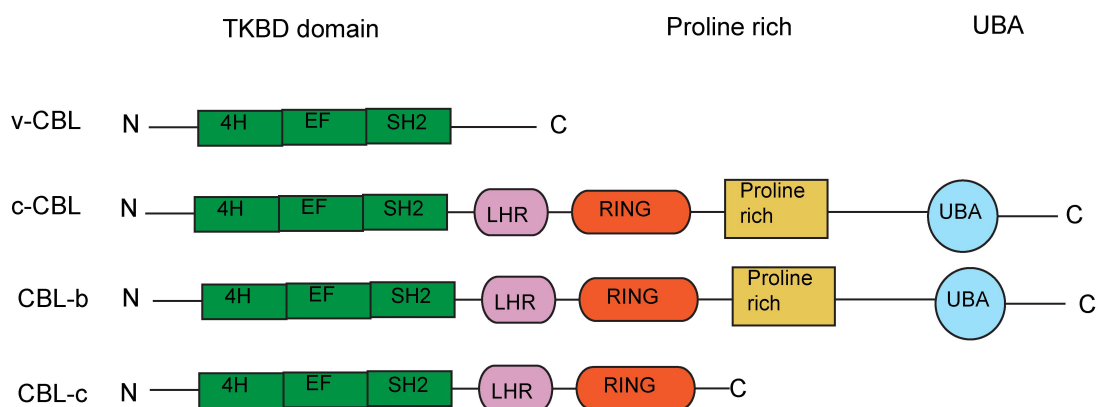


Figure 1-16: Domain Organisation of Cbl family of proteins

1.7.3 Cbl activity and functions

The Cbl family of proteins ubiquitylates and thereby facilitates degradation and downregulation of protein tyrosine kinases (PTKs). EGFR is the best-characterised target of Cbl to date [80, 81]. Auto-phosphorylated EGFR directly binds to the TKBD domain of c-Cbl via its phosphorylated Tyr1045 residue [108, 109]. Alternatively c-Cbl can bind to EGFR indirectly via an adaptor protein called Grb2. Grb2 interacts with EGFR and c-Cbl via its SH2 and SH3 domains respectively [93]. Other SH3 domain containing proteins like CIN85 also bind to c-Cbl via their SH3 domains. Binding to CIN85 indirectly helps in downregulation of EGFR. If the c-Cbl-CIN85 interaction is impaired, it leads to overexpression of EGFR whereas if the binding is sustained it leads to internalisation and ubiquitylation of EGFR [104]. Cbls themselves are negatively regulated by Sprouty2 (Spry2). Spry2 binds to the RING domain and the SH2 domain after being activated by EGFR. This mechanism induces phosphorylation in Spry2, which in turn blocks activated receptors from binding to the SH2 and RING domains of Cbl. Hence Spry2 is responsible for modulating negative regulation of active RTKs by c-Cbl [104]. In addition to EGFR, the Cbl family also downregulates a variety of other PTKs like platelet derived growth factor (PDGF) and colony stimulating factor (CSF-1) [110, 111]. In addition, c-Cbl downregulates a number of non-receptor tyrosine kinases like Syk, Lck, Fyn, Hck, Fgr and c-Abl [112-117].

1.7.4 Cbl as a ubiquitin ligase

The basic functional unit of Cbl required for substrate ubiquitination comprises the TKBD, LHR and RING finger domains. This is also the minimal unit required to ubiquitinate and downregulate activated PTKs in cells [81, 118-120]. The conserved C-terminal regions of c-Cbl and Cbl-b are involved in additional protein-protein interactions [105]. For example, the proline rich regions in c-Cbl and Cbl-b bind Src and are important for Cbl-mediated ubiquitination of Src. [121], even though Src-binding via the TKBD is also observed [122]. In the earliest structural studies performed with the minimal active ligase fragment of c-Cbl, c-Cbl was bound to UbcH7 and ZAP70 peptide. In this complex structure, the E2 is facing away from substrate-binding site and there is a gap of 70 Å between the substrate-binding site

and E2's active site [62]. Later a structure of phosphorylated c-Cbl bound to UbcH5B and ZAP70 peptide showed that this gap is bridged and reduced to 27 Å when c-Cbl's LHR is phosphorylated [85]. When the conserved Tyr (Tyr371 in c-Cbl) in the LHR is phosphorylated, the LHR is detached from the TKBD and becomes more flexible. This allows the RING domain to rotate about a hinge loop connecting the TKBD and LHR, thereby enabling juxtaposition of E2~Ub and the substrate-binding site. Moreover, phosphorylated Tyr371 engages interactions with the RING domain to form a new E2~Ub binding platform to enhance E2~Ub binding affinity. Notably phosphorylated Tyr371 or Tyr363 in Cbl-b directly contacts the donor Ub to stabilise the closed E2~Ub conformation. There are no structures of Cbl bound to intact substrate that illustrate how Cbl mediates Ub transfer to substrate. I have discussed this topic in detail in chapter 5, where I have attempted to capture a complex of Cbl bound to E2~Ub and substrate mimetic.

1.8 Cellular Inhibitor of Apoptosis proteins (cIAPs)

1.8.1 Role of IAPs in signalling pathways

cIAPs act as major regulators of cell death and survival [123] by modulating nuclear factor kappa B (NF-κB) signalling pathways. In unstimulated conditions NF-κB is restrained to the cytoplasm by its inhibitor I kappa B (IκB). Upon stimulation IκB undergoes phosphorylation by the IκB kinase complex (IKK) comprised of IKKα, IKKβ and a regulatory subunit, IKKγ [124]. Activation of NF-κB signalling occurs via one of two pathways: canonical (classical) or non-canonical (alternative) (Figure 1-17). There are many signalling factors responsible for activation of NF-κB including tumour necrosis factor alpha (TNF-α), an inflammatory cytokine [125]. When TNF-α binds to the receptor, tumour necrosis factor-1 (TNF-R1), it triggers activation of the NF-κB signalling pathway. In the canonical pathway, cIAP-1 and cIAP-2 are recruited to the TNF receptors via TNFR-associated factor (TRAF2), TRAF2 mediates formation a complex with the cIAP substrate, receptor interacting protein-1 (RIP-1) [123, 126]. cIAP1 and cIAP2 promote K63-linked polyubiquitination of RIP-1 [127]. Ubiquitinated RIP-1 recruits TAK-1-binding protein (TAB) and TGFβ activated kinase-1 (TAK1), which stimulates activation of IKKβ. This leads to degradation of IκB and translocates two subunits of NF-κB, p50 and transcription factor RELA, to the nucleus [123]. In the non-canonical pathway,

cIAP-1 acts as a negative regulator of NF- κ B signalling by promoting ubiquitylation and proteosomal degradation of NF- κ B-inducing kinase (NIK) as part of a cIAP-TRAF2-TRAF3 complex [128, 129]. Protein levels of NIK are very low in unstimulated cells because of continuous ubiquitination by cIAP-TRAF2-TRAF3 complexes. Binding of various TNF receptors like TWEAK and CD40 to their partners promotes ubiquitination of TRAF2 and TRAF3 and autoubiquitination of cIAPs. This leads to the accumulation of NIK. This in turn leads to phosphorylation and activation of IKK α , which leads to phosphorylation of p100 (also called NF- κ B2). This precursor p100 leads to partial proteosomal processing to generate transcriptionally active p52 [123, 129]. Hence cIAP proteins act as positive and negative regulators of NF- κ B signalling pathways. These contrasting roles illustrate how necessary it is to regulate E3 ligase activity during signalling events.

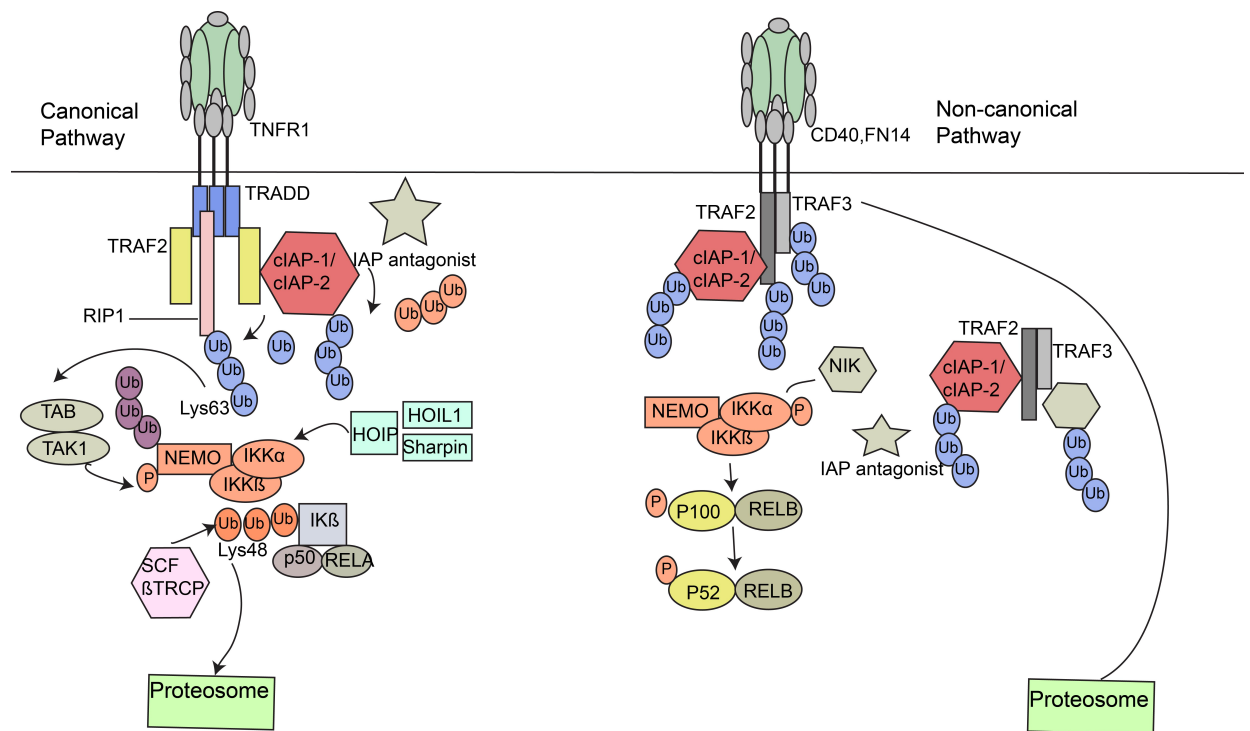


Figure 1-17: Canonical and non-canonical pathways of NF- κ B signalling. cIAPs act as positive regulators of canonical NF- κ B signalling (left) and negative regulators of non-canonical NF- κ B signalling pathways. Figure adapted from Simone Fulda and Domagoj Vucic (2012).

1.8.2 IAPs as ubiquitin ligase

Miller and colleagues first described IAPs in baculoviral genomes about 25 years ago [130-132]. All members of the IAP family possess at least one baculovirus IAP repeat (BIR) domain; BIR domains are characterised by the presence of a Zn^{2+} -binding site and are frequently involved in protein-protein interactions. BIR domains facilitate anti-apoptotic IAP features by interacting with the TRAF-N domain of TNF [128, 133, 134]. A number of IAPs also possess a RING domain that confers RING E3 ligase activity in the form of autoubiquitination and ubiquitination of proteins involved in apoptosis and signalling [123]. cIAP-1, cIAP-2 and XIAP also possess a UBA domain and the cIAPs also have a CARD domain (Figure 1-18)

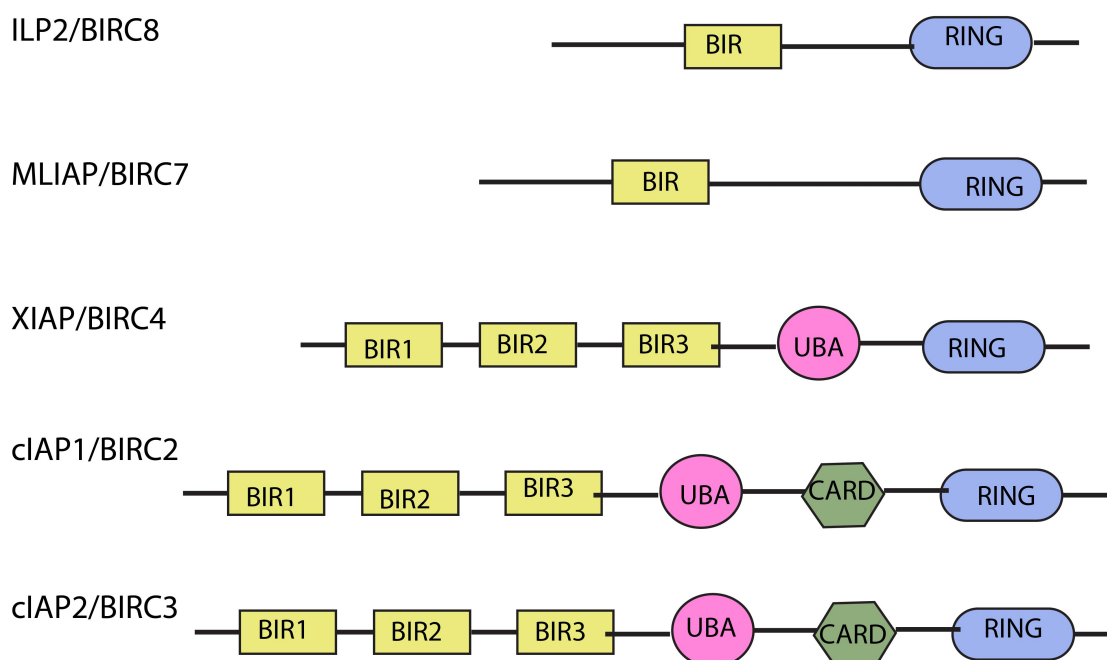


Figure 1-18: Domain organisation of human IAP family of proteins

XIAP, cIAP-1 and cIAP-2 all possess ubiquitin ligase activity that is conferred by the presence of a C-terminal RING domain. cIAP-1 undergoes dimerisation through its RING domain to become an active ligase [135-138]. When unactivated, cIAP-1 exists in a monomeric autoinhibited state in which the RING domain is tucked away through inter-domain interactions between the BIR, CARD and UBA domains. All three of these IAPs inhibit apoptosis by binding caspases and ubiquitinating them, thereby

targeting them for degradation, or by binding caspases and maintaining them in an inactive state. When outer membrane permeabilisation is triggered, a mature form of second mitochondria-derived activator of caspases (SMAC) promotes apoptosis by binding to BIR domains of these IAPs and preventing their interactions with caspases [135, 139]. A peptide Ala-Val-Pro-Ile (AVPI) of the first four residues in SMAC reproduces this effect. Binding of SMAC-peptide *in vitro* disrupts the BIR3-RING interface in autoinhibited cIAP-1, thereby promoting dimerisation and activating auto- and substrate ubiquitination.

1.8.3 Available structures of cIAPs

cIAP-1 and cIAP-2 have similar domain architectures (Figure 1-18). There is no structure available for either full-length cIAP. For cIAP-2, there is a structure of the RING domain alone (PDB ID: 3EB5) and bound to UbcH5B (Figure 1-19 (A)) (PDB ID: 3EB6) [77] and the BIR3 domain alone (PDB ID: 2UVL) [140](Figure 1-19B). In the cIAP-2 structure of the RING alone and with UbcH5B, the C-terminal tail plays an important role in dimerisation. cIAP-2 interacts with its substrates via its BIR domains. To date, there are no structures of either cIAP bound to E2~Ub and/or substrate to illustrate how Ub transfer to substrate is mediated. The closest is a structure of the RING domain of BIRC7 bound to UbcH5B~Ub (Figure 1-19C) (PDB ID: 4AUQ) [66]. A structure of the RING domain of either cIAP bound to E2~Ub will be helpful in understanding how cIAPs mediate Ub transfer and illustrate similarities and differences to other RING E3-E2~Ub complexes.

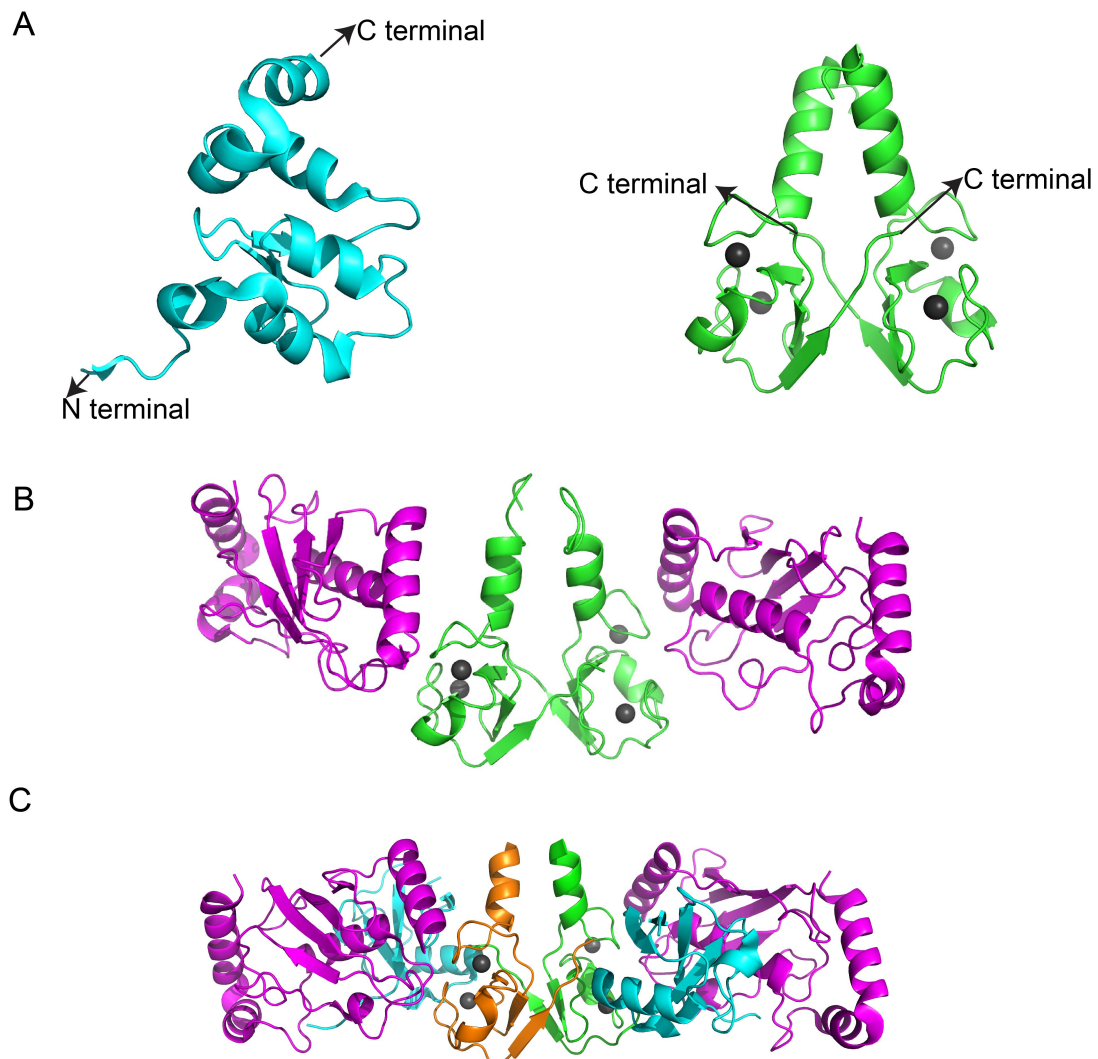


Figure 1-19: Available structures of cIAP2. (A) Left: BIR3 domain of cIAP-2 coloured cyan (PDB ID: 2UVL) [140]. Right: cIAP2 RING dimer coloured green. The dimer was generated using a symmetry mate. Zn^{2+} ions are shown as grey spheres (PDB ID: 3EB5). (B) cIAP2-UbcH5B (PDB ID: 3EB6) [77]. The RING is coloured as in A and the E2 is coloured magenta. (C) BIRC7-UbcH5B~Ub (PDB ID: 4AUQ) [66]. The two subunits of the RING dimer are shown in green and orange, UbcH5B in magenta, Ub in cyan and. Zn^{2+} -ions are shown as grey spheres.

Objectives of the thesis

RING E3s are the biggest family of E3s and are the major focus of my PhD thesis. Recently there has been an increase in the number of structural and biochemical characterisation studies on RING E3 mediated Ub transfer. There are several structures available that illustrate how RING E3s recruit E2~Ub and stabilise the RING domain-E2~Ub complex for optimal Ub transfer. RING E3s also recruit substrate and facilitate transfer of Ub from E2's active site to a lysine residue on substrate. How RING E3s achieve these steps still remains elusive. In addition to the RING domain of RING E3s, there are also other factors that help to stabilise the RING domain-E2~Ub complex. The objectives of my thesis are as follows:

- 1) To use structural and biochemical studies to elucidate the roles of non-covalent Ub in cIAP1-mediated Ub transfer. In 2015, our lab showed for the first time how Ub^B enhances RING-mediated E2~Ub transfer. We used a monomeric RING E3, RNF38, for this study. During my PhD, I aimed to crystallise a complex of cIAP1 bound to UbcH5B~Ub and Ub^B. This study will help us to understand whether the mechanism of non-covalent binding is conserved in other RING E3s and in UbcH5 family of proteins.
- 2) To determine whether non-covalent Ub binding mechanism is conserved in UbcH6. The UBC domain of UbcH6 is very similar to that of the UbcH5 family of E2s, so I aimed to investigate whether the UbcH6 family also exhibits non-covalent binding of Ub to its backside.
- 3) To assemble E3/E2~Ub/substrate complexes to study polyUb chain formation. How RING E3s transfer Ub to a lysine side chain on a substrate is still unknown. In my PhD, I aimed to generate a substrate mimetic to understand how polyUb chain formation occurs.

Chapter 2

Materials and Methods

2.1 Materials

The c-DNA of full-length human c-Cbl and Cbl-b were purchased from Source BioScience. pGEX4T1 and pRSFDuet were purchased from GE Healthcare. Other than Ub fusion peptide, all plasmids were obtained from lab members. DNA polymerase and other cloning buffers and enzymes were purchased from Invitrogen. Dr. Gary Sibbet generated DH5 α and BL21(DE3) competent cells. All expression vectors (pGEX4T1, pRSFDuet) obtained from lab members. GSH sepharose, Nickel agarose and glutathione were purchased from GE Healthcare.

2.2 Methods

2.2.1 Primer design and molecular cloning

All the constructs were generated by standard polymerase chain reaction (PCR) using forward and reverse primers purchased from Integrated DNA Technologies and Pfu Ultra DNA polymerase from Stratagene. QIAquick PCR purification kit and QIAquick gel extraction kit from QIAGEN were used to purify PCR products. PCR product was ligated into appropriate vector by using Quick Ligase from NEB and subsequently transformed into DH5 α competent cells. Positive clones were verified by automated sequencing at the Cancer Research UK Beatson Institute. All constructs and associated primers that I generated for studies in Chapters 3, 4, and 5 are listed in Table 2-1. For generation of Ub fused peptides for Chapter 5, multiple rounds of PCR were formed, where PCR product from each round of PCR was purified and used as the template for the next round of PCR (Figure 2-1). Verified clones were transformed into BL21 (DE3) competent cells for protein expression.

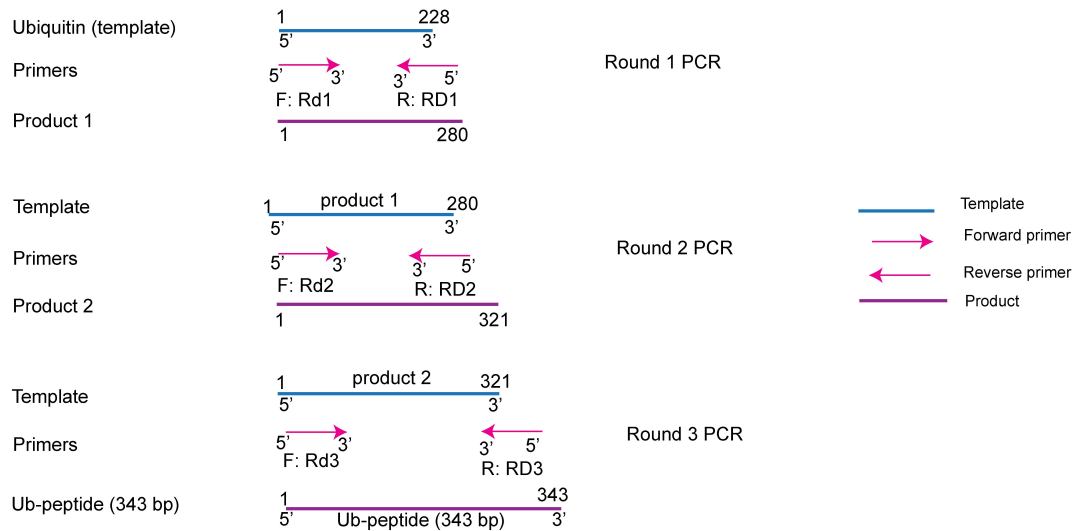


Figure 2-1: Generation of Ub fused peptide (Ub-peptide) using multiple rounds of PCR. F: forward primer, R: reverse primer, Rd1: round1, Rd2: round2 and Rd3: round3

Table 2-1 Generation of protein expression constructs (UbcH5D, cIAP2(255-C) and all Ub-peptide constructs were generated by me. Other people in the lab generated all the other listed constructs)

Construct	Primers (5' to 3')	Restriction site	Vector	Molecular weight (KDa)
cIAP1 (555-C)	F: gaagatctatgcacaaaactgctcccaaag	BglII	pGEX4T1	~42
	R:cggaattcttaagagagaaatgtacgaac agtacc	EcoR1		
UbcH5A	F: catgcatggcgctgaagaggattcag	NCOI	pRSFDuet	~17
	R: cggaattcttacattgcatattctgagtc cattctc	ECOR1		
UbcH5B	F: cgggatccatggctctgaagagaatccac	BamH1	pRSFDuet	~17
	R: cggaattcttacatgcatacttctgagtc	ECOR1		
UbcH5C	F: catgCCATGGcgctgaaacggattaa taag	NCOI	pRSFDuet	~17
	R: cgGAATTCcacatggcatacttctgag tcc	ECOR1		
UbcH5D	F: catgCCATGGcggttaaagcgtatccag aaag	NCOI	pRSFDuet	~17

	R: cgGAATTCttacatagcatatTTTTGGGT ccattc	ECOR1		
UbcH5B _{S22R}	F: ccagcacagtgtcgcgcaggtcctgttg	BamH1	pRSFDuet	~17
	R: caacaggacctgcgcgacactgtgctgg	ECOR1		
UbcH5B _{C85K}	F: cagtaatggcagcattaaactgatattctac gatcac	BamH1	pRSFDuet	~17
	R: gtgatcgtagaatatcaagttaatgctgcca ttactg	ECOR1		
UbcH5B _{C85S}	F: gtaatggcagcatttctcttgatattctacgatc	NCO1	pRSFDuet	~17
	R: gatcgtagaatatcaagagaaatgctgcca ttac	ECOR1		
UbcH5B _{Q20A}	F: gaccctccagcagcgtgttcagcagg	BamH1	pRSFDuet	~17
	R: cctgctgaacacgctgctggagggtc	ECOR1		
UbcH5B _{S108R}	F: ctcttgccatctgtcgtctgtgtgtgatc	BamH1	pRSFDuet	~17
	R: gatcacacaacagacgacagatggacaaga g	ECOR1		
Ubiquitin	F: cgggatccatgcagatttctgtgaaaacc	BamH1	pGEX4T1	~10
	R: ccgctcgagtaaccaccacgaagtctca acac	Xho1		
Ubiquitin I44A	F: cagcagagactggcctttgctggcaag	BamH1	pRSFDuet	~10
	R: cttgccagcaaaggccagtctctgctg	Xho1		
UbcH6 43-C	F: gaagatctaaactctctccaccagcgc	BglII	pRSFDuet	~17
	R: acgctcgacttatgtagcgtatctcttggtcc	Sall		
UbcH6 43-C _{S68R}	F: ccacctaattgccgtgctgggtccaa	BglII	pRSFDuet	~17
	R: ttgggaccagcacggcaattaggtgg	Sall		

cIAP2 (255-C)	F: cgggatcccatgctccccgcttcaagacc	BglIII	pRSFDuet	~42
	R: cggaattctcatgaaagaaatgtacgaactg tacc	ECOR1		
c-Cbl (47-435)	F: cgggatccccgccggggacggtggaca agaag	BamH1	pGEX4T1	~45
	R: ccgctcgagttaatcaaacggatctaccacg atggg	XhoI		
Cbl-b (36-427) _{Y360F}	F: agttacacaggaacaattgaattatattgtga	BglIII	pGEX4T1	~45
	R: tcacaatataattcaaattgttctgtgtaact	XhoI		
SMAC (56-C)	F: catgccatggcggttcctattgcacagaaa tcag	NcoI	pET23d	~25
	R: ccgctcgagatcctcacgcaggtaggcc tcctg	XhoI		
Ub ΔGG	F: cgggatccggtggctctatgcagatttcgtg aaaacc	BamH1	pGEX4T1 2TK	~10
	R: atagtttagcggccgctcaacgaagtctca acacaagatgaag	XhoI		
Ub-ZAP70	F: RD1-3 ctcaggggtgtatccatctgagttgagggtg gccgcacgaagtctcaacacaagatgaag	BamH1	pGEX4T1	~12
	R: RD1 ggtacgctgccgctggccgca cgaagtctcaacacaagatgaag R: RD2 gctcaggggtgtatccatctg agttgagggtagcctgccgctggc R: RD3 cggaattctcagtggatgatgg tgatgtgctggctcaggggtgtatccatctgagtt	EcoRI		
Ub-Src	F: RD1-3 ctcaggggtgtatccatctgagtt gaggtggccgcacgaagtctcaacacaagatg aag	BamH1	pGEX4T1	~12
		EcoRI		

	<p>R: RD1-3 aggcggctgccaccgctac cgccgctgccccggcgcgccacgaagtctca acacaa</p> <p>R: RD2 tgatggccctggcgcgcggtata ttcgttatcttcaatcagggcgctgccaccgc</p> <p>R: RD3 cggaattctcagtgggtga tgatgggtgatggccctggcgcgcggtatattcgt</p>			
Ub-cMET	<p>F: RD1- 3</p> <p>ctcaggggtgtatccatctgagttgagggtg gccgcacgaagtctcaacacaagatgaag</p>	BamH1	pGEX4T1	~12
	<p>R: RD1</p> <p>ttgctgctgccaccgctaccgccgctgcca Cccggggccgcacgaagtctcaacacaa</p> <p>R: RD2</p> <p>ggtgatgttcggaaaggtcgcgcgataa tccacgcttctgtgctgctgccacc</p> <p>R: RD3</p> <p>cggaattctcagtgggtgatgatgggtgatgtt ccggaaaggtcgcgcgataat</p>	EcoR1		
cIAP1 (555-C)	<p>F: gaagatctatgcacaaaactgcctccaaag</p>	BglII	pGEX4T1	~42
	<p>R: cggaattcttaagagagaaatgtacg aacagtacc</p>	EcoR1		
UbcH5A	<p>F: catgccatggcgctgaagaggattcag</p>	NCOI	pRSFDuet	~17
	<p>R: cggaattcttacattgcatatttctgagt ccattctc</p>	ECOR1		
UbcH5B	<p>F: cgggatccatggctctgaagagaatccac</p>	BamH1	pRSFDuet	~17
	<p>R: cggaattcttacatgcatacttctgagtc</p>	ECOR1		
UbcH5C	<p>F: catgCCATGGcgctgaaacggat taataag</p>	NCOI	pRSFDuet	~17

	R: cgGAATTCtcatatggcatacttctg agtcc	ECOR1		
UbcH5D	F: catgCCATGGcgttaaagcgtatcca gaaag	NCOI	pRSFDuet	~17
	R: cgGAATTCttacatagcatatTTTTGGG tccattc	ECOR1		
UbcH5B _{S22R}	F: ccagcacagtgtcgcgcaggtcctgttg	BamH1	pRSFDuet	~17
	R: caacaggacctgcgcgacactgtgctgg	ECOR1		
UbcH5B _{C85K}	F: cagtaatggcagcattaaacttgatattct acgatcac	BamH1	pRSFDuet	~17
	R: gtgatcgtagaatatcaagttaagtctgc cattactg	ECOR1		
UbcH5B _{C85S}	F: gtaatggcagcatttcttctgatattctac gatc	NCOI	pRSFDuet	~17
	R: gatcgtagaatatcaagagaaatgctgcc attac	ECOR1		
UbcH5B _{Q20A}	F: gacctccagcagcgtgttcagcagg	BamH1	pRSFDuet	~17
	R: cctgctgaacacgctgctggagggtc	ECOR1		
UbcH5B _{S108R}	F: ctcttgccatctgctgctgtgtgtgatc	BamH1	pRSFDuet	~17
	R: gatcacacaacagacgacagatggaca agag	ECOR1		
Ubiquitin	F: cgggatccatgcagattttcgtgaaaaccc	BamH1	pGEX4T1	~10
	R: ccgctcgagttaaccaccacgaagtctca acac	XhoI		
Ubiquitin I44A	F: cagcagagactggccttctgtggcaag	BamH1	pRSFDuet	~10
	R: cttgccagcaaaggccagctctgctg	XhoI		
UbcH6 43-C	F: gaagatctaaactctctccaccagcgc	BglIII	pRSFDuet	~17

	R: acgcgtcgacttatgtagcgtatctcttg gtcc	Sall		
UbcH6 43-C _{S68R}	F: ccacctaattgccgtgctgggtcccaa	BglII	pRSFDuet	~17
	R: ttgggaccagcacggcaattaggtgg	Sall		
cIAP2 (255-C)	F: cgggatcccatgctgcccgttcaagacc	BglII	pRSFDuet	~42
	R: cggaattctcatgaaagaaatgtacgaactg tacc	ECOR1		
c-Cbl (47-435)	F: cgggatccccgccggggacggtggacaa gaag	BamH1	pGEX4T1	~45
	R: ccgctcgagttaatcaaacggatctaccac gatggg	Xho1		
Cbl-b (36-427) _{Y360F}	F: agttacacaggaacaattgaattatattgtga	BglII	pGEX4T1	~45
	R: tcacaatataattcaaattgttctgtgtaact	Xho1		
SMAC (56-C)	F: catgccatggcgggttcctattgcacagaaa tcag	Nco1	pET23d	~25
	R: ccgctcgagatcctcacgcaggtaggcct cctg	Xho1		
Ub Δ GG	F: cgggatccggtggctctatgcagatttctg tgaaaacc	BamH1	pGEX4T1 2TK	~10
	R: atagtttagcggccgctcaacgaagtctc aacacaagatgaag	Xho1		

2.2.2 Expression and purification of proteins

Plasmids of protein of interests were transformed into BL21 Gold (DE3) competent cells. Bacterial culture were grown at 37 °C with suitable antibiotics (ampicillin or kanamycin) at 100 mg/L or 50 mg/L, respectively. Cells were induced at an OD $A_{600\text{nm}}$ of 0.8 with 0.2 mM isopropyl β -D-thiogalactopyranoside (IPTG) at 20 °C overnight. Cells were harvested by spinning them at 4000 rpm at 4 °C for 15 minutes. Cells were then resuspended into resuspension buffer (wash buffer used in first step for purification) with 2.5 mM phenylmethylsulphonyl fluoride (PMSF). Before lysing cells, 10 μg DNase I was added to 100 ml lysate to reduce the viscosity of sample and prevents blocking microfluidizer. Cells were lysed using microfluidizer M-110P at 15-18000 psi. Cells were passed twice through the microfluidizer. Lysed cells were then centrifuged twice at 20,000 rpm for 30 minutes at 4 °C in Beckman Ultra high-speed centrifuge. Clear lysates were then purified by either glutathione sepharose (GSH) or Ni^{2+} affinity chromatography depending on the tag used using gravity column. GST or His-tag was subsequently removed by treatment with thrombin or TEV protease and further purified by ion exchange chromatography followed by size exclusion chromatography on AKTA FPLC. Purified protein of interest was then concentrated using Amicon Ultra centrifugal filter units and snap-frozen in liquid nitrogen and stored at -80 °C for future crystallisation and biochemical studies. Protein concentrations were measured by using Bradford assay with bovine serum albumin (BSA) as standard [141]. Concentration of Ubiquitin and Ub-peptide were measured at A_{280} using Denovix DS-11 spectrophotometer

$$\text{Con}(\text{mg/ml}) = \frac{A_{280} * \text{MW}(\text{Da})}{\text{Ext.Co}} \approx \frac{A_{280}}{0.16}$$

Buffers used in for affinity purification and gel filtration chromatography:

Chromatography	Buffers
GSH-affinity	Wash buffer: 50 mM Tris-HCl 7.6, 0.2 M NaCl, 1 mM DTT Elution buffer: 50 mM Tris-HCl 8.0, 0.2 M NaCl, 5 mM DTT and 10 mM GSH
Ni ²⁺ affinity	Wash buffer: 50 mM Tris-HCl 7.6, 0.15 M NaCl, 15 mM imidazole and 5 mM BME
Size exclusion	50 mM Tris-HCl 7.6, 0.15 M NaCl and 1 mM DTT

The list of proteins purified is listed below in Table 2-2. The table describes which protein is purified and their contributors. Those proteins that I purified are described in details below.

Table 2-2: List of proteins purified

Protein	Contributors
cIAP1(555-C)	See Section 3.2.1
UbcH5A, UbcH5C, UbcH5D	See Section 2.6
UbcH5B	See Section 2.5
UbcH6 WT and S68R	See Section 4.2.1
UbcH5BC85K-Ub,UbcH5BS22R-Ub, UbcH5BC85-S,N77A	See Section 2.7
<i>Arabidopsis thaliana</i> Uba1	See Section 2.4
Ub-peptide (Ub-ZAP70, Ub-cMet, Ub-Src)	See Section 5.2.4
Pc-Cbl, and pCbl-b	See Section 2.3
cIAP2(255-C)	See Section 2.8
cIAP1(260-C)	Purified by Mads Gabrielsen
UbcH5B variants S108R and Q20A	Purified by Lori Buetow and Hao Dou
Ubiquitin variant (I44A) and Ub Δ GG	Purified by Lori Buetow and Hao Dou
SMAC (56-C)	Purified by Lori Buetow

2.3 Purification of ubiquitin

Histidine tagged ubiquitin was cloned into RSFDuet vector with TEV cleavage site. Cells were grown harvested and lysed as mentioned in Section 2.2.2. Lysed cells were purified onto 30ml Ni²⁺ beads on gravity column. Buffers used for purification are mentioned below:

Wash buffer	50mM Tris-HCl pH 7.6, 0.2M NaCl, 20mM imidazole pH8.0 and 5mM β -mercaptoethanol
Elution buffer	50mM Tris pH 7.6, 0.2M NaCl, 200mM imidazole pH8.0 and 5mM β -mercaptoethanol

Eluted protein was mixed with TEV protease at 1:50 protein ratio (TEV: protein) to remove His tag, The mixture was dialysed against 50 mM Tris-HCl pH 7.6, 0.15 M NaCl and 5 mM β -mercaptoethanol at room temperature overnight. Next day, protein was passed back onto 10ml Ni²⁺ beads to remove uncleaved protein and was further purified by gel filtration column (S75 16/60). Eluted fractions was concentrated and snap frozen at -80°C.

2.4 Protein purification of pc-Cbl and pCbl-b

c-Cbl₄₇₋₄₃₅ Y368F was previously cloned into pGEX4T1 His-GST vector with a thrombin cleavage site by my colleague. It was co-transformed into BL21 Gold (DE3) with mouse Src₈₄₋₅₂₆, which was cloned into pRSFDuet with a N-terminal His-MBP tag. A single colony was used to inoculate 200 mL of LB media containing 100 mg/L ampicillin and 25 mg/L kanamycin and the culture was grown at 37 °C overnight. Next day, the overnight culture was used to inoculate 60 litres of LB media containing 100 mg/l ampicillin and 25 mg/l kanamycin and the culture was grown at 37 °C and induced as described in the method above. Before lysing cells 2 mM sodium orthovanadate (Sigma) was added to inhibit protein phosphotyrosyl phosphatases and prevent dephosphorylation. pCbl was purified using Ni²⁺ affinity chromatography using 25 ml Ni²⁺ beads on a gravity column. Eluted protein was then stirred with GSH-sepharose beads for one hour and then washed and eluted. Protein was then treated overnight with thrombin protease in 1:100 thrombin:protein ratio (mg ratio) in presence of 10 mM CaCl₂ at 4 °C overnight (Figure 2-2A). Next day, cleaved protein

was passed through 25 ml Ni²⁺ beads column to get rid off His-GST tag and subsequently applied on an anion exchange chromatography (20 mL Source Q column) to separate phosphorylated c-Cbl from non-phosphorylated c-Cbl (Figure 2-2B). Buffers used for Source Q column are mentioned below. Phosphorylated c-CBL was pooled, concentrated using Amicon Ultra centrifuge and further passed through size exclusion chromatography S75 10/300 for final buffer exchange (Figure 2-2D). Fractions containing pure pCbl were pooled and concentration was determined. Then pCbl was aliquoted in small volume, snap-frozen and then stored at -80 °C for crystallisation (Figure 2-2).

Chromatography	Buffers
20 ml Source Q	Buffer A: 50 mM Tris-HCl pH 8.5 and 1 mM DTT
	Buffer B: 50mM Tris-HCl pH 8.5, 1 M NaCl and 1 mM DTT
Size exclusion chromatography S75 10/300	50 mM Tris-HCl pH 7.6, 0.15 M NaCl and 1 mM DTT

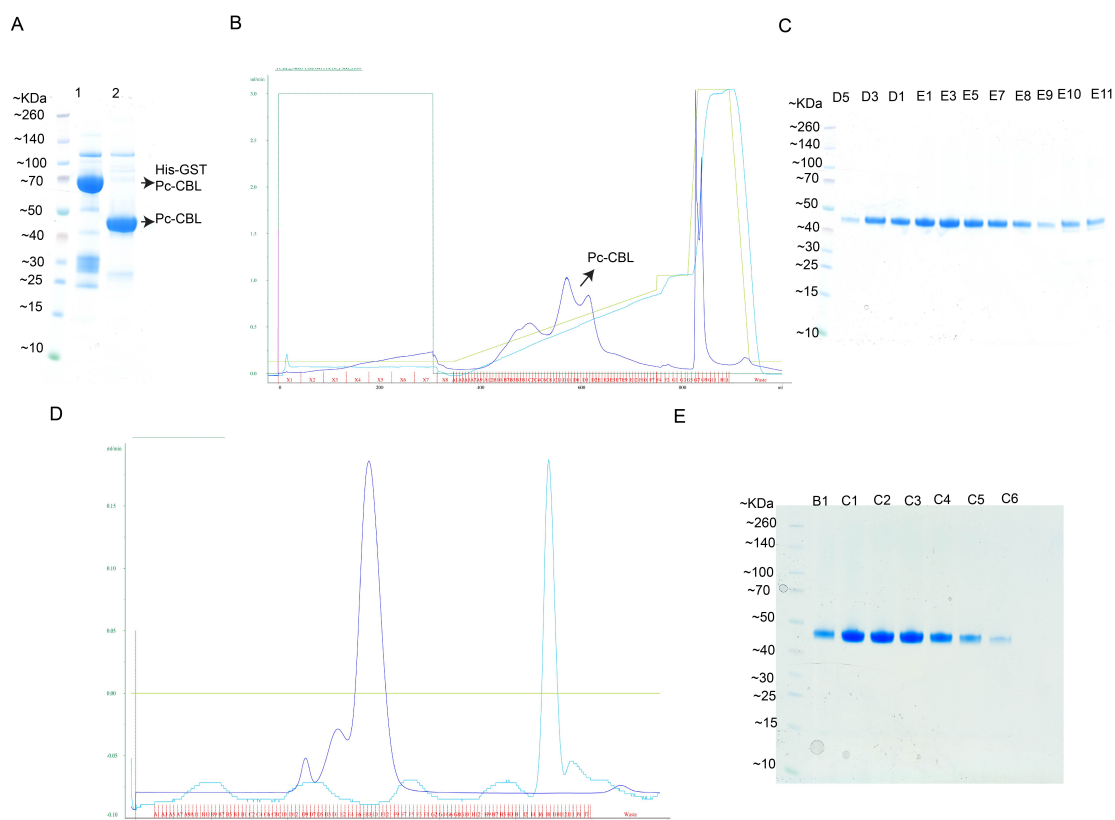


Figure 2-2: Purification steps of pCbl. (A) Gel run after thrombin cleavage. Lane 1 shows sample after Ni²⁺ and GSH-sepharose affinity purification and lane 2 shows sample in lane 1 treated with thrombin overnight followed by Ni²⁺ pass back. This sample was applied onto 20 mL Source Q column. (B) Chromatogram showing elution profile of pCbl on 20 ml source Q column chromatography. (C) SDS-PAGE showing the purity of fractions from (B). Fractions containing pure pCbl were pooled, concentrated and applied on a SD75 gel filtration column. (D) Chromatogram showing elution profile of pCbl on SD75 gel filtration chromatography. (E) SDS-PAGE showing the purity of fractions from (D). Single band equivalent of pCbl size can be seen. Fractions B1-C5 were pooled and concentrated and then aliquoted, snap-frozen and stored at -80 °C.

2.5 Purification of *Arabidopsis thaliana* Uba1 (developed by Danny Huang)

Untagged *Arabidopsis thaliana* Uba1 was cloned in pET23d vector. 24 litres of *E. coli* culture was grown at 37 °C LB media with 100 mg/l ampicillin. Cells were induced, harvested and lysed as described in the methods above. GST tagged Ub was cloned into pGEX4T1 vector was also expressed similarly as mentioned above. Lysates from both Uba1 and GST tagged Ub were mixed together along with 2.5 mM MgCl₂ and 2.5 mM ATP. The mixture of lysate was stirred for two hours at 4 °C. Uba1~GST-Ub was purified using GSH-sepharose affinity column and Uba1 was released from GSH-sepharose column by incubating with wash buffer containing 20

mM DTT. Uba1 was further purified by anion exchange chromatography (20ml Source Q column). Protein eluted from Source Q was pooled, aliquoted, snap-frozen and stored at -80 °C in buffer containing 50 mM Tris-HCl pH 7.6, 0.15 M NaCl and 1 mM DTT (Figure 2-3).

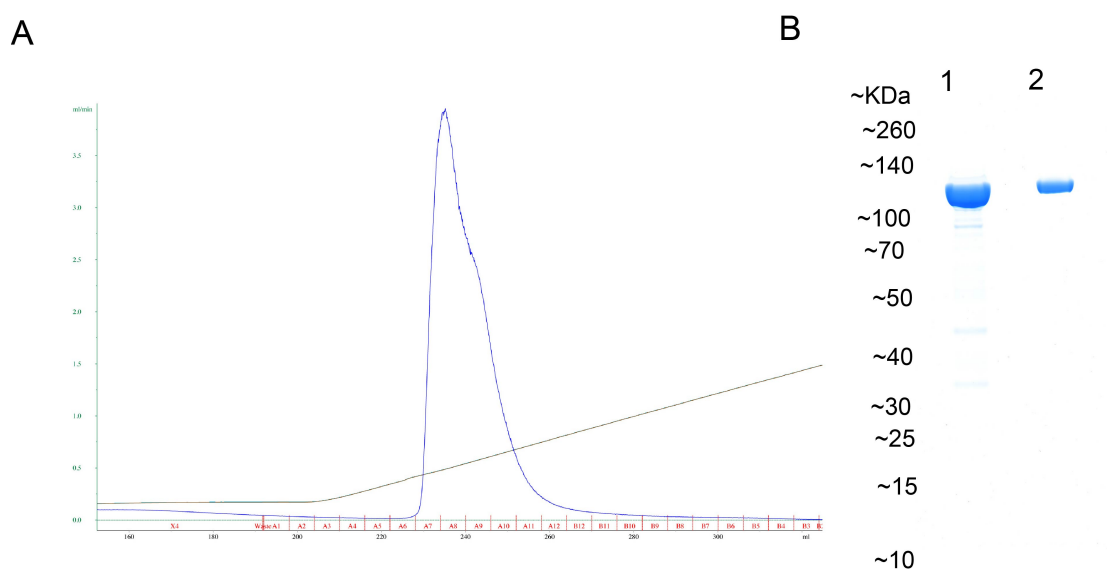


Figure 2-3: Purification of Uba1. (A) Chromatogram of Uba1 after 20 ml Source Q column. (B) SDS-PAGE showing the purity of Uba1. Lane 1 is after elution from GSH-sepharose column and Lane 2 is from the peak fraction in 20 mL source Q column.

2.6 Purification of UbcH5B

Untagged UbcH5B was transformed and expressed into BL21 DE3 *E. Coli* cells. Cells were grown and harvested and lysed as mentioned in above section 2.2.2. Lysate was then diluted with 50mM MES buffer pH 6.5 with 1mM DTT, the lysate turned milky on dilution. Now the lysate was loaded on 20ml sulphopropyl (SP) sepharose beads on gravity column. After loading the lysate, column was washed with 50mM MES pH 6.5, 50mM NaCl and 1mM DTT. Protein was eluted with 50mM MES pH 6.5, 0.2 M NaCl and 1 mM DTT. Eluted protein was then diluted with 50mM MES pH 6.5 and 1mM DTT to dilute the salt concentration. Now, diluted protein was loaded onto 20 ml Source S column. Buffers used for Source S column are mentioned below. Eluted protein was then concentrated with 50mM Tris 7.6, 0.2M NaCl and 1mM DTT, since UbcH5B is unstable at low salt concentration. Concentrated protein was then loaded onto size exclusion S75 column. Buffer used for gel filtration is mentioned in Section

2.3. The eluted protein was snap frozen and stored at -80°C (see Figure 2-4 for purification).

Chromatography	Buffers
20 ml Source S	Buffer A: 50 mM MES pH 6.5, 1mM DTT
	Buffer B: 50mM MES pH6.5, 0.2M NaCl, 1mM DTT
Size exclusion chromatography S75 10/300	50 mM Tris-HCl pH 7.6, 0.15 M NaCl and 1 mM DTT

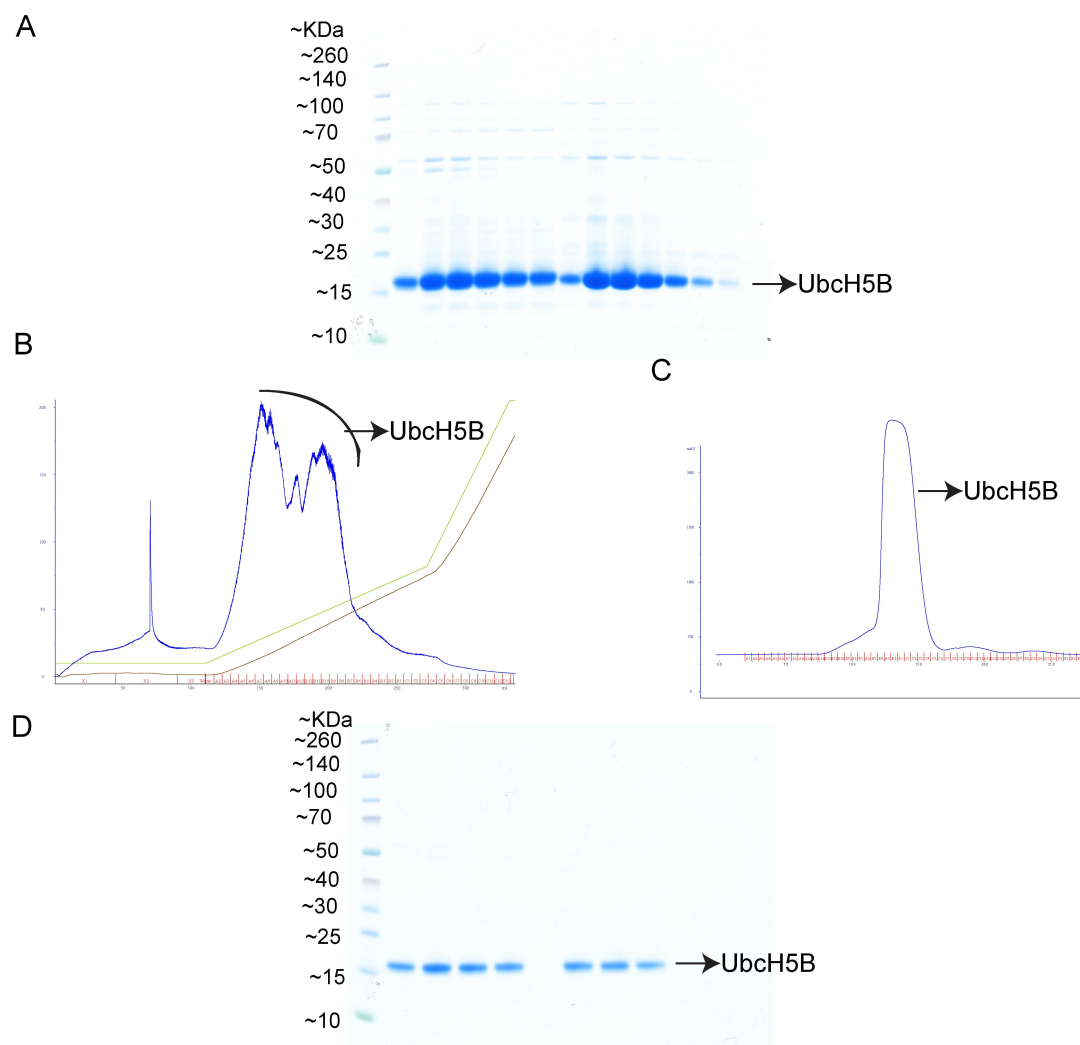


Figure 2-4: Protein purification of Ubch5B WT. (A) SDS gel after 20ml SP sepharose gravity column (B) chromatogram showing elution after 20ml Source S column (C) chromatogram after gel filtration SD75 column (D) SDS gel for fractions eluted after SD75 gel filtration column.

2.7 Purification of Ubch5A, Ubch5C and Ubch5D

Untagged Ubch5A, C and D were cloned into pRSFDuet vector. They were then transformed and expressed into BL21 DE3 *E.Coli.* cells. Method for growth, expression, harvesting and lysing cells is same as described in Section 2.2. Lysate was purified using 20ml SP sepharose beads on gravity column. Buffers used were same as that used in purification of Ubch5B. Eluted protein was then purified using on 20 ml Source S column using cation exchange chromatography followed by gel filtration chromatography using S75 column. Buffers used for Source S and S75 column were same as that used in Ubch5B WT. Protein eluted from S75 column were concentrated and run on SDS gel to check purity (Figure 2-5).

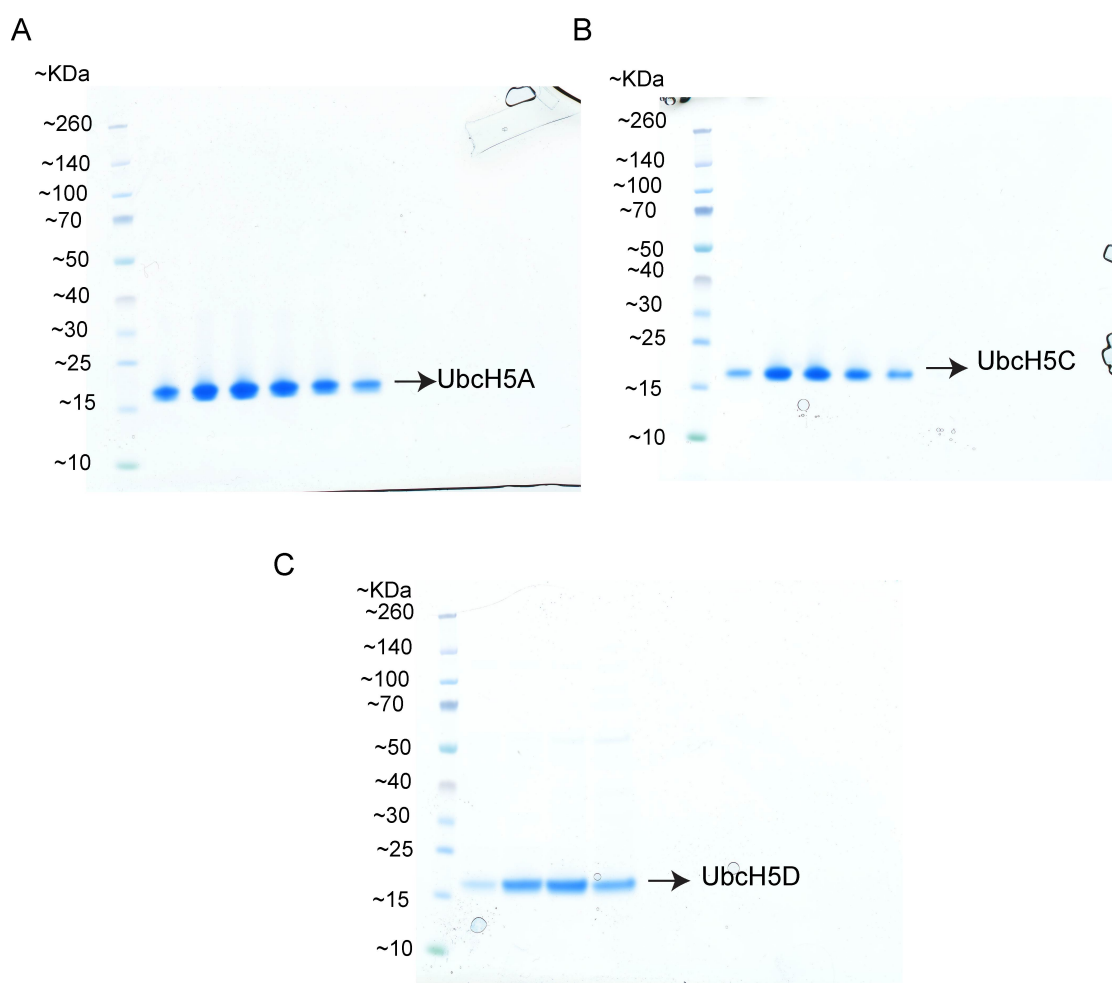


Figure 2-5: Protein purification of Ubch5A, Ubch5C and Ubch5D. (A) SDS gel for fractions eluted from S75 column for Ubch5A (B) SDS gel for fractions eluted from SD75 column for Ubch5C (C) SDS gel for fractions eluted from SD75 column for Ubch5C

2.8 Purification of UbcH5B~Ub

UbcH5B~Ub thioester linkage is not very stable and rapidly dissociates into E2 and Ub in presence of E3s. To generate stable UbcH5B~Ub linkage, our lab has mutated UbcH5B's catalytic Cys85 to Lys (C85K) to generate stable isopeptide linkage or (C85S) to generate stable oxy-ester linkage [66]. During my PhD, I used the method developed in lab to generate UbcH5B~Ub variants (UbcH5B_{C85K}~Ub, UbcH5B_{S22R}~Ub, UbcH5B_{C85S,N77A}~Ub). Below (section 2.5.1) I have described method of purifying UbcH5B_{C85K}~Ub in detail. Other UbcH5B~Ub variants were purified in similar manner.

2.8.1 Purification of UbcH5B_{C85K}~Ub

Untagged UbcH5B_{C85K}, His tagged Ub and untagged Uba1 were purified separately as explained in method section. Individual protein was thawed and centrifuged at 13000 rpm for 10 minutes at 4° C. Charging reaction was setup as follow. I charged approximately 120 μM of untagged UbcH5B_{C85K} by adding 2 molar excess of His-Ub compared to UbcH5B_{C85K}. To this, I added 0.1M Tris pH 9.0 followed by 5-6 μM of Arabidopsis Uba1 for every 6 mg of UbcH5B_{C85K} and 10mM MgCl₂. The reaction was started by adding 10mM ATP pH ~7-8. The reaction was allowed to sit at 30 °C for 12-16 hrs. Charging reaction was analysed by SDS-PAGE (Figure 2-6A). The reaction was stopped by adding 5 mM β-mercaptoethanol and then purified by Ni²⁺-affinity column. Eluted fractions were pooled (Figure 2-6B) and mixed with TEV protease at 1:50 protein ratio (TEV: protein) to remove His tag, The mixture was dialysed against 25 mM Tris-HCl pH 7.6, 0.15 M NaCl and 5 mM β-mercaptoethanol at 4 °C overnight. Next day, TEV cleavage was analysed by SDS-PAGE (Figure 2-6C).

The cleaved protein was passed back onto 10 ml Ni²⁺ gravity column to remove uncleaved protein. Flow through was collected and diluted with 50 mM MES, pH 6.0, 1 mM DTT to bring down the pH of buffer and then further purified using 20 ml Source S column (Figure 2-6D). Fractions A7-B7 containing UbcH5B_{C85K}~Ub were pooled (Figure 2-6E) and concentrated using method as explained in method section 2.2.2 for concentrating proteins. Concentrated protein was centrifuged at 13000 rpm at 4 °C for 10 minutes to spun down any pellet/aggregate after concentrating protein. Concentrated protein was then purified using 10/300 SD75 gel filtration column in

buffer containing 50 mM HEPES, pH 8.0, 0.15 M NaCl and 1 mM DTT. Fractions containing pure UbcH5B_{C85K}-Ub were pooled, concentrated, aliquoted, snap-frozen and stored at -80 °C.

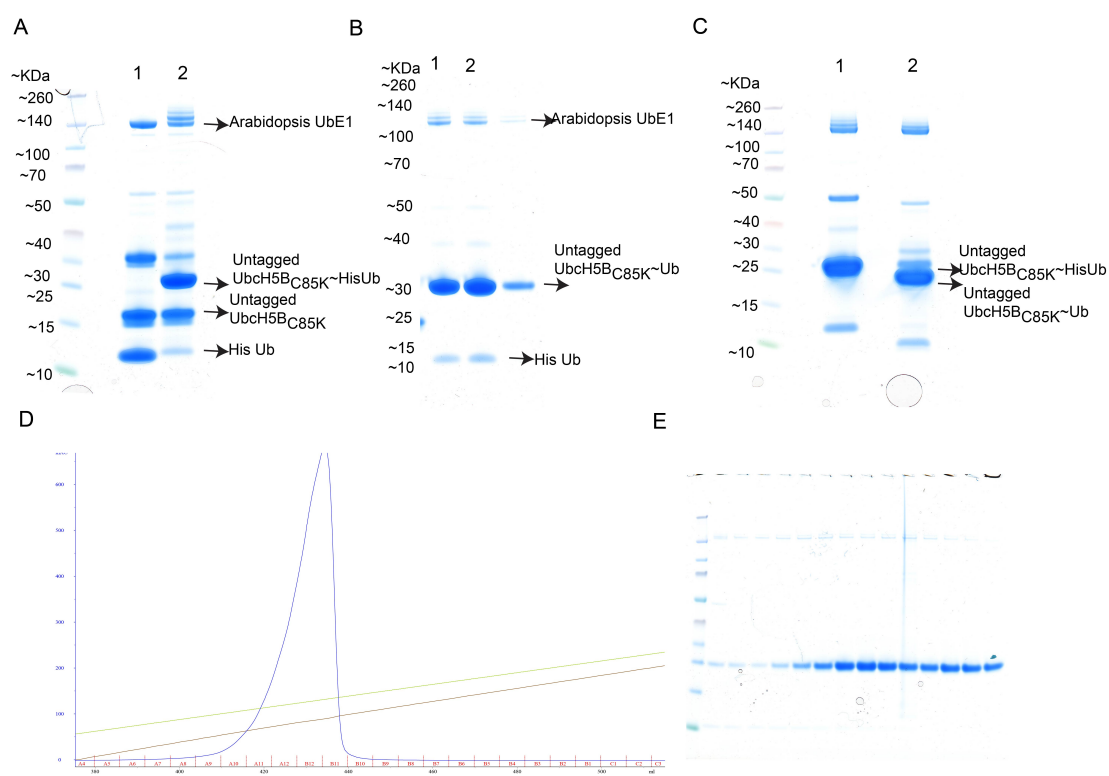


Figure 2-6: Protein purification steps of UbcH5B_{C85K}-Ub. (A) SDS gel showing before (lane 1) and after (16-20 hrs; lane 2) setting up the reaction to charge UbcH5B_{C85K} with His-Ub. (B) SDS-gel showing Ni²⁺ pull down of UbcH5B_{C85K}~His-Ub. Lane 1, 2 and 3 are fractions 1, 2 and 3 of 10ml each after eluting from 10ml Ni²⁺ gravity column. Only His-Ub and UbcH5B_{C85K}~His-Ub was retained with some trace amount of Uba1. (C) SDS gel showing UbcH5B_{C85K}~His-Ub before (lane 1) and after (lane 2) TEV treatment. (D) 20 ml Source S chromatography of UbcH5B_{C85K}~Ub. Chromatogram showing a single peak of eluted protein. (E) SDS gel showing proteins from fractions A3 to B10 in (D).

2.9 Protein purification of cIAP2 (255-C)

cIAP2(255-C) construct was cloned into pGEX4T1 His-GST vector with TEV cleavage site (vector modified and designed by Lori Buetow). Cells were grown harvested and lysed as mentioned in Section 2.2.2. Lysed cells were purified onto 20ml GSH sepharose beads on gravity column. Buffers used are mentioned in Section 2.2.2. Eluted protein was mixed with TEV protease at 1:50 protein ratio (TEV: protein) to remove His-GST tag, The mixture was dialysed against 25 mM Tris-HCl pH 7.6, 0.15 M NaCl and 5 mM β-mercaptoethanol at 4 °C overnight. Next day,

protein was passed back onto 10ml Ni²⁺ beads to remove uncleaved protein and was further purified by gel filtration column (S75 16/60). Eluted fractions was concentrated and snap freezed at -80°C (Figure 2-7).

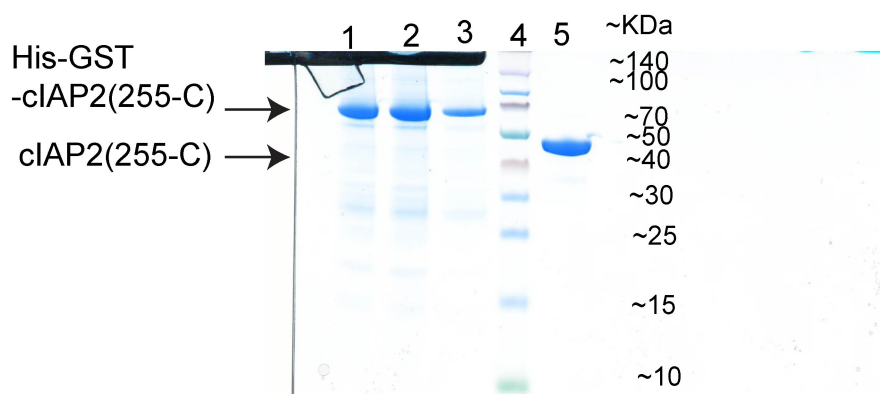


Figure 2-7: Protein purification of cIAP2(255-C). Lanes 1,2 and 3 are protein fractions run after GST pull down. Lane 4 is protein marker and lane 5 is concentrated protein after TEV cleavage, Ni²⁺ pass back and gel filtration run

2.10 Crystallisation

2.10.1 cIAP1R-UbcH5B_{C85K}-Ub-Ub^B complex

cIAP1R-UbcH5B_{C85K}-Ub-Ub^B complex was assembled by mixing cIAP1R (8.5 mg/ml) UbcH5B_{C85K}-Ub (20mg/ml) and Ub (100mg/ml) at 1:1:1.2 molar ratio. Initial crystallisation screen was performed using sitting drop vapour diffusion technique with screens from crystallisation kits JCSG+, PEGs, Proplex, Index, Morpheus, Ammonium Sulphate, PACT (bought from Molecular Dimensions, Hampton Research and Qiagen) at 19 °C where each drop contains equal volume (200 µL) of protein and reservoir solution. Crystals was obtained and optimised in condition containing 0.2M ammonium fluoride and 15% (w/v) PEG 3350. The crystals were harvested and flash frozen in 0.2 M ammonium fluoride, 18% (w/v) PEG 3350 and 20% (v/v) ethylene glycol.

2.10.2 Data collection and processing

Data were collected at beamlines I03 at Diamond Light Source (DLS) and processed using xia2 pipeline [142]. The data were integrated with automated XDS (Kabsch, 2010) including POINTLESS (Evans, 2006), AIMLESS (Evans and Murshudov, 2013), CCP4 (Winn et al., 2011). Initial phases of cIAP1R-UbcH5B_{C85K}-Ub-Ub^B complex were obtained by molecular replacement with PHASER using UbcH5B and Ub from PDB 3ZNI and cIAP2 RING from PDB 3EB6 . All models were built in COOT (Emsley and Cowtan, 2004) and refined using PHENIX (Adams et al., 2002). cIAP1R-UbcH5B_{C85K}-Ub-Ub^B complex was refined to resolution of 1.7 Å. The final model contains one copy of cIAP1R (chain A, residues 556-C), one copy of UbcH5B_{C85K} (chain C residues 1-147), one copy of Ub^B (chain B residues 1-72) and one copy of Ub^D (chain D, residues 1-76). All figure models were generated using PYMOL.

2.11 Lysine discharge assays

Lysine discharge assays were performed to monitor rate of E2~Ub transfer in the presence and absence of excess of UbΔGG (UbΔGG lacks C terminal diglycine tail, and therefore cannot be charged by E1). In a typical lysine discharge assay E2 is charged with equimolar Ub with reaction mixture containing E1 and Ub for about 15-20 minutes (depending on which E2 is used) at 23 °C. The charging is then stopped by adding mixture of EDTA and apyrase. The reaction is initiated by adding mixture of E3 and lysine, with or without excess of UbΔGG and is then stopped at specific time points by mixing with SDS loading buffer. Assays performed using radio labelled Ub was processed and visualised using autoradiography, whereas non-labelled Ub were run on SDS gel and visualised using coomassie stain. The graphical view of what happens in lysine discharge assay is illustrated below in Figure 2-8.

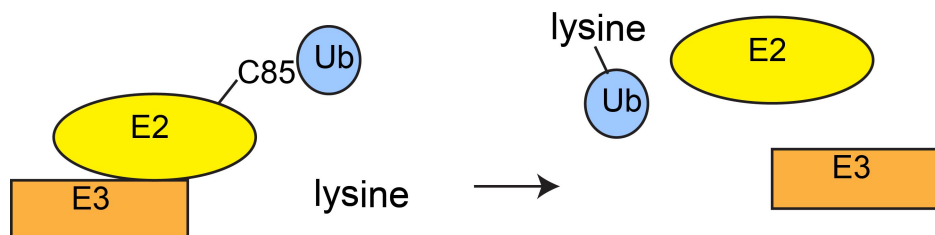


Figure 2-8: Lysine discharge assay. E2 is charged with equimolar of Ub for 15 minutes. The charge is then stopped by adding EDTA and apyrase. A mixture containing lysine and E3 was then added to initiate E2~Ub discharge reaction. Discharge is monitored by the disappearance of E2~Ub band on SDS-PAGE. When Ub is labelled with ^{32}P , the gel is dried and analysed by autoradiogram.

Labelling Ub with radioactive ^{32}P

2TK-Ub was used for labelling, which was expressed and purified by Lori Buetow. Radiolabelled 2TK Ub was generated using method as described [143]. The reaction mixture used for labelling Ub contained 10x buffer made up of 500 mM Tris 7.6, 50 mM ATP pH 7-8, 50mM MgCl_2 ; 2TK Ub (I usually made a stock of 200 μM Ub); [$\gamma\text{-}^{32}\text{P}$]-ATP (NEG502Z250UC; Perkin Elmer); 0.5 μl of 2,500 U/ml protein kinase A (PKA) enzyme and water. This reaction mixture is allowed to incubate for 2 hours at room temperature before using it in the assays.

2.11.1 Lysine discharge assays with UbcH5B~Ub

For ^{32}P -Ub assays shown in Section 3.2.2, Figure 3-3, UbcH5 variants (12.5 μM) were charged with Arabidopsis Uba1 (1 μM) and ^{32}P -Ub (12.5 μM) for 15 min at 23 $^\circ\text{C}$ as described previously (Buetow et al., 2016) including BSA (1mg/ml). Charging was stopped by incubating the reaction with 0.01 U/ml apyrase and 50 mM EDTA at 23 $^\circ\text{C}$. The ^{32}P -Ub lysine discharge assays were initiated by addition of reaction mixture containing 50 mM Tris-HCl, pH 7.6, 150 mM NaCl, 1 mg/ml BSA, 20 mM L-lysine (in presence of E3) and 500 nM cIAP1R in presence of Ub ΔGG (300 μM). Reactions were stopped with SDS loading buffer at specified time points and resolved by SDS-PAGE. Reactions were dried and visualised by autoradiography.

2.11.2 Lysine discharge assays with UbcH6 (43-C)~Ub

For lysine discharge assays shown in Figure 4-6, UbcH6 (43-C) variants (WT and S68R) were charged equimolar with ^{32}P -Ub as described above for 20 min at 23 $^\circ\text{C}$. The reaction was initiated with different concentration of Ub ΔGG (0, 20 μM , 300 μM and 1mM Ub ΔGG) in presence of reaction mixture containing 50mM Tris -HCl

pH 7.6, 150 mM NaCl, 1mg/ml BSA, 20 mM L-lysine and 500 nM cIAP1R. Reactions were stopped with SDS loading buffer at specified time points and resolved by SDS-PAGE. Reactions were dried and visualised by autoradiography.

2.11.3 Lysine discharge assay with UbcH6(43-C)~Ub using ubiquitinated cIAP1

For lysine discharge assay using ubiquitinated cIAP1 (260-C) shown in Figure 4-8, first reaction was set up for autoubiquitination of cIAP1. This reaction mixture contained 0.5 μ M of cIAP1 (260-C), 5 μ M Ub, 50 mM Tris-HCl pH 7.6, 50 mM NaCl, 5 mM MgCl₂, 5 mM ATP, 1mM DTT, 0.3 U/ml inorganic pyrophosphatase, 0.3 U/ml creatine kinase and 5 mM creatine phosphate. The reaction was incubated at 23°C for 2.5 hours. Adding 30 mM EDTA and 0.01 U/mL of apyrase stopped reactions. This reaction was then used to initiate lysine discharge assays. UbcH6 (43-c) WT and S68R was charged similarly as described above, and discharge assay was initiated with ubiquitinated cIAP1. Reactions were stopped with SDS loading buffer at specified time points and resolved by SDS-PAGE. Reactions were dried and visualised by autoradiography.

2.11.4 Non-radioactive lysine discharge assays

For the non-radioactive lysine discharge assays shown in Figures 3-6 to 3-10 and 3-12, assays were performed using wild-type non-radiolabelled Ub. UbcH5 variants (12.5 μ M). For Figure 3-12, UbcH5A, B, C and D were charged with Arabidopsis Uba1 (1 μ M) and Ub (12.5 μ M) for 15 min at 23 °C as described previously in above section including BSA (1mg/ml). Charging was stopped by incubating the reaction with 0.01 U/ml apyrase and 50 mM EDTA at 23 °C. The lysine discharge assays were initiated by addition of reaction mixture containing 50 mM Tris-HCl, pH 7.6, 150 mM NaCl, 1 mg/ml BSA, 20 mM L-lysine and 500 nM cIAP1R in presence and absence of 300 μ M Ub Δ GG. . Whereas Figures 3-6 to 3-9 are lysine discharge assays of UbcH5B, cIAP1R and Ub variants performed under similar conditions as mentioned above, all in presence of Ub Δ GG. For Figure 3-9, UbcH5B Q20A mutant was charged and assay was performed with and without excess of Ub. Gels were visualised and stained with InstantBlue (Expedeon).

2.12 Ubiquitination assays

Ubiquitination assays were carried out using radiolabelled ^{32}P 2TKUb as mentioned earlier in Section 2.7. The labelling of Ub and charging of E2 was exactly same as mentioned above in Section 2.7 and 2.7.2. I performed autoubiquitination of cIAP1 and cIAP2 shown in Figure 4-6A,B and Figure 4-8 respectively. Similarly, I performed SMAC substrate ubiquitination, shown in Figure 4-6C. In autoubiquitination assay charged E2~Ub transfer Ub onto E3's lysine sites and form polyUb chains, whereas in substrate ubiquitination Ub is transferred from charged E2~Ub onto substrate's lysine sites. Graphical view of what happens in a typical autoubiquitination and substrate ubiquitination assay is shown in figure below.

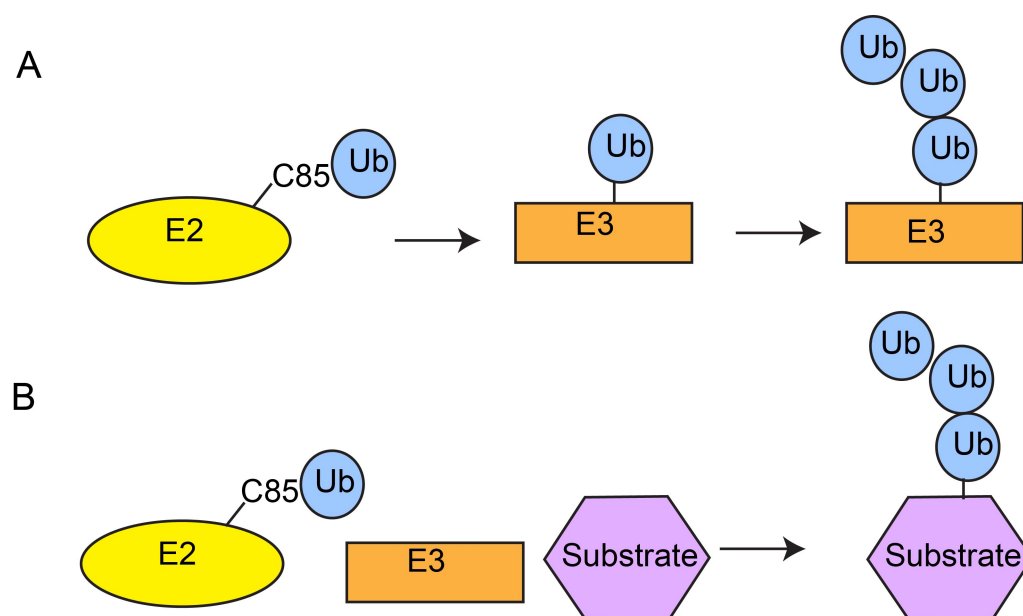


Figure 2-9: Ubiquitination assay. (A) Autoubiquitination of E3s. Charged E2 would transfer Ub onto lysine site on E3 and form polyUb chain on E3. (B) Substrate ubiquitination. Charged E2 in presence of E3 would transfer Ub to substrate preferentially forming polyUb chain on substrate.

2.12.1 Autoubiquitination of cIAP1 and cIAP2

Autoubiquitination of cIAP1 (260-C) and cIAP2 (255-C) as shown in Figure 4-7A,B and 4-9A,B respectively were performed in presence of 50 mM Tris-HCl, pH 7.6, 50 mM NaCl, 5 mM MgCl₂, 5 mM ATP, 1mM DTT, 0.3 U/ml inorganic pyrophosphatase, 0.3 U/ml creatine kinase and 5 mM creatine phosphate, 1 μM *Arabidopsis* Uba1, 5 μM UbcH6 variants, 50 μM ^{32}P -Ub and 2.5 μM E3. Before adding E3s, the reaction mixture was allowed to charge for 20 minutes at 23°C. The

reactions were stopped with 2X loading buffer, resolved by SDS-PAGE, dried and visualised by autoradiography.

2.12.2 SMAC substrate ubiquitination by cIAP1

SMAC substrate ubiquitination shown in Figure 4-7C was performed in presence of 50 mM Tris-HCl, pH 7.6, 50 mM NaCl, 5 mM MgCl₂, 5 mM ATP, 1mM DTT, 0.3 U/ml inorganic pyrophosphatase, 0.3 U/ml creatine kinase and 5 mM creatine phosphate, 1 μM *Arabidopsis* Uba1, 5 μM UbcH6 variants, 50 μM ³²P-Ub, 2.5 μM cIAP1 and 5 μM SMAC. As discussed in Section 2.8.1, UbcH6 was precharged for 20 minutes at 23°C before adding mixture of SMAC and cIAP1. The reactions were stopped with 2X loading buffer, resolved by SDS-PAGE, dried and visualised by autoradiography.

2.12.3 Ub-peptide substrate ubiquitination

Ub-peptide substrate ubiquitination shown in Figures 5-9 and 5-10 were performed in presence of 50 mM Tris-HCl, pH 7.6, 50 mM NaCl, 5 mM MgCl₂, 5 mM ATP, 1mM DTT, 0.3 U/ml inorganic pyrophosphatase, 0.3 U/ml creatine kinase and 5 mM creatine phosphate, 0.1 μM *Arabidopsis* Uba1, 2 μM UbcH5B, 0.5 μM pc-Cbl and 50 μM Ub-peptide. The reactions were stopped with 2X loading buffer and 1mM DTT. Gels were visualised and stained with InstantBlue (Expedeon).

2.13 Surface plasmon resonance (SPR)

Binding of Ub^B to UbcH5B and UbcH5B-Ub in presence and absence of cIAP1R was analysed by SPR (See section 3.2.2). SPR is a method of determining biomolecular interactions (protein-protein, protein-ligand, DNA-protein etc.) [144]. In SPR, the sensor surface forms floor of a small flow cell, through which solution passes under continuous flow. To detect interaction one molecule (ligand) is immobilised onto the sensor surface. A thin layer of gold on the chip facilitates conductivity. Its binding partner (the analyte) is injected into sample buffer through the flow cell (Figure 2-10). In our lab, we use Biacore T200 instrument from GE healthcare for SPR analysis. The instrument uses detection system from Biacore T200 control software and is controlled by a PC. The anti-GST sensor chip used in the experiments were also purchased from GE healthcare. Buffer used during experiment contained 25mM Tris-

HCl pH 7.6, 150mM NaCl, 0.005% tween 20 and 1mM DTT. In the performed experiments GST tagged cIAP1R was immobilised on the chip and UbcH5B variants (WT and S22R), UbcH5B–Ub variants (UbcH5B_{C85K}–Ub and UbcH5B_{S22R}–Ub) with and without excess of Ub were flown as analyte to measure the binding. SPR experiments shown in chapter 3 were performed by Dr. Gary Sibbet, whereas experiments shown in chapter 4 were performed by me.

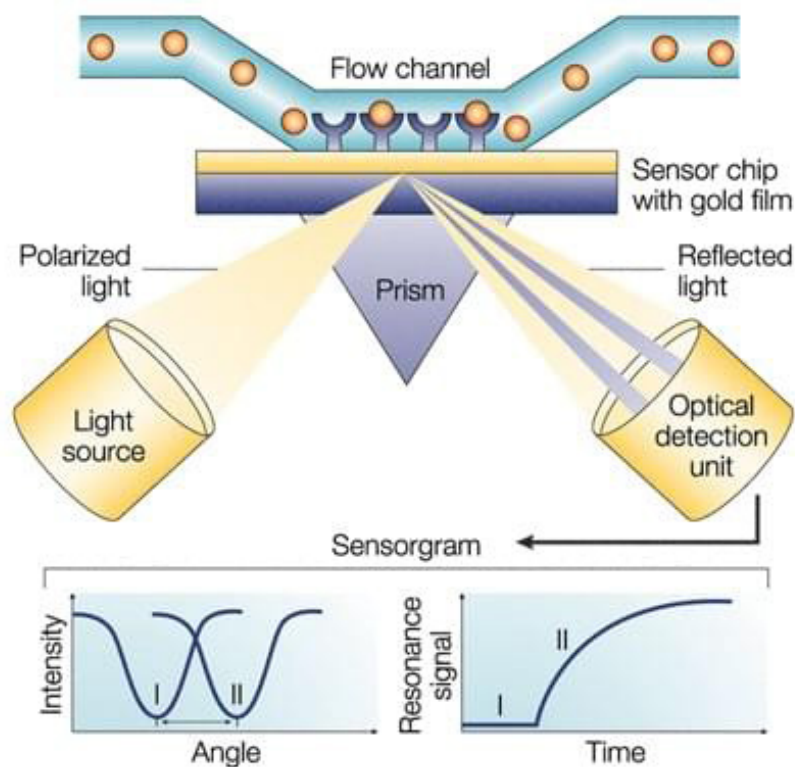


Figure 2-10: SPR experimental set up. SPR helps in detecting variations in refractive index in the near proximity of the sensor chip surface. It is observed as shadow in the light reflected from the surface. Change in angle is determined by mass of surface. Figure adapted from Cooper (2002).

2.14 Nuclear Magnetic Resonance (NMR)

Nuclear magnetic resonance (NMR) is a powerful technique to study protein-protein interactions and mapping protein-binding surface in solution. Apart from X-ray crystallography, NMR has been used extensively in the past two decades to understand protein structures and its interactions. Earlier solving protein structure using NMR was limited due to low sensitivity of NMR spectrum and complex size of biomolecules. But with recent advancement in spectrometer design, data collection and analysis, it has emerged as a powerful technique in solving protein structures.

Apart from determining protein structures it has many advantages over other techniques to study protein-protein interactions. The biggest advantage of using NMR is that one can study biomolecules under natural physiological conditions [145]. I have used NMR technique to study interaction between Ub and UbcH6's backside surface. My colleague, Mark Nakasone performed all NMR experiments.

All NMR experiments were performed at 23°C on Bruker Avance III 600 spectrometer equipped with three channel ceypocrobe. All the samples were in 25mM sodium phosphate buffer pH 7.0, 100mM NaCl containing 0.02% NaN₃ and 5% D₂O. The data was processed using TopSpin v2.1 (Bruker Biospin Inc) and analysed using in-house software.

Resonance frequencies of ¹H_N, ¹⁵N in proteins can trace perturbations, and hence is used universally to analyse protein-protein interactions and to determine protein binding interface Differences between ¹H_N-¹⁵N NMR spectra were quantified as chemical shift perturbations (CSPs), defined as: $CSP = [(d_{HA} - d_{HB})^2 + ((d_{NA} - d_{NB})/5)^2]^{1/2}$. Here d_H and d_N are chemical shifts of ¹H and ¹⁵N, respectively, for a given backbone N-H group. Titration experiments monitoring chemical shift changes occurring upon ¹⁵N Ub binding to UbcH5B/UbcH6 was performed by sequential addition of unlabelled UbcH5B/UbcH6 to ~0.3mM ¹⁵N Ub. 1H-15N NMR recorded at each titration step monitored the binding.

Chapter 3

Role of non-covalent ubiquitin in cIAP1- mediated ubiquitin transfer

3.1 Aims and Objectives

There are several structures of RING E3s in complex with E2~Ub that show how RING E3s restrain E2~Ub in a closed conformation thereby making the E2~Ub thioester bond optimal for Ub transfer [40, 67, 68, 73, 146]. Structural and biochemical studies show that RING E3s stabilise donor Ub in a closed conformation together with E2, such that residues in E2's active site clamp Ub's C-terminal tail and position the thioester for nucleophilic attack. These structures show that in addition to the RING domain, other factors also contribute to the increase the processivity of Ub transfer. Several RING E3s contain a domain or motif outside the RING domain that assists the RING domain in stabilising the closed donor Ub (Ub^D) conformation; examples include the phosphorylated tyrosine in the linker helix region (LHR) of Cbl proteins and the C-terminal tail of RING dimers such as BIRC7 and RNF4 [66, 67, 73]. E2's active site residues play an important role in creating an environment that favours catalysis; for example, the asparagine from the conserved His-Pro-Asn motif helps to stabilise the oxyanion intermediate in the transition state, and an aspartate on a loop near the active site cysteine reduces the pK_a of the incoming substrate lysine [28, 29, 78, 147, 148]. Some RING E3s have an additional E2-binding motif that binds to the backside of E2s. In the case of the RING E3 gp78, its G2BR domain binds selectively to the E2 Ube2g2's backside resulting in enhanced ubiquitylation [86]. Furthermore, Ub has been shown to bind the backside of some of E2s like UbcH5, UbcH6, Rad6 and Ube2g2 families and promote polyUb chain formation [36, 87, 149, 150]. This non-covalent binding of Ub to the backside of UbcH5 family has been shown to increase the processivity of polyUb chain but the mechanism remains elusive [36, 38, 39].

At the start of my PhD, our lab was investigating the mechanism by which non-covalent Ub-binding to the backside of the UbcH5 family of E2s (this backside bound Ub is referred to as Ub^B) increases the processivity of polyUb formation. Our lab showed that Ub^B stimulates UbcH5B-catalyzed Ub transfer in both RING-dependent and RING-independent manners, but with a more prominent effect in RING-dependent transfer. We showed that Ub^B enhances the affinity of RING E3s for UbcH5B~Ub [40]. In this study we used a monomeric RING E3, RNF38, for structural analyses and found that Ub^B stabilises UbcH5B's $\alpha 1$ and $\alpha 1\beta 1$ loop conformations to enhance RING E3's affinity for UbcH5B~Ub. To assess whether the

mechanism of Ub^B stimulation is conserved for other RING E3s, I have determined the structure of a dimeric RING E3, cIAP1, bound to UbcH5B–Ub and Ub^B. In this chapter, I will discuss how cIAP1 activates E2–Ub for transfer and how Ub^B influences cIAP1-UbcH5B–Ub complex to stimulate ubiquitination. I also present biochemical analyses to validate the structure and to characterise the Ub^B stimulatory effect.

3.2 Results

3.2.1 Purification of His-GST cIAP1 RING (cIAP1R) domain with TEV cleavage site

The His-GST-TEV cIAP1 RING domain (cIAP1R; 556-616) construct was cloned by a former graduate student in the lab (Julia). She did the first step of protein purification with Ni²⁺ pull down and stored the protein (approx. 100mgs in 35ml) at -80° C. I performed the later steps of protein purification. First, I concentrated protein to 5 ml and then purified using 10 ml GSH sepharose beads on gravity column (see Methods Section 2.2.2). Eluted protein was then incubated with TEV overnight and dialysed against a buffer containing 50 mM Tris-HCl 7.6, 0.2 M NaCl and 1 mM DTT. Next day, the cleaved protein was passed back onto the GSH sepharose beads to remove His-GST-tag. Protein obtained after pass back was then purified using size exclusion chromatography (SD75 1660). Eluted protein was run on a SDS gel and marked bands were pooled (Figure 3-1), concentrated to 8.5 mg/ml, and stored at -80° C.

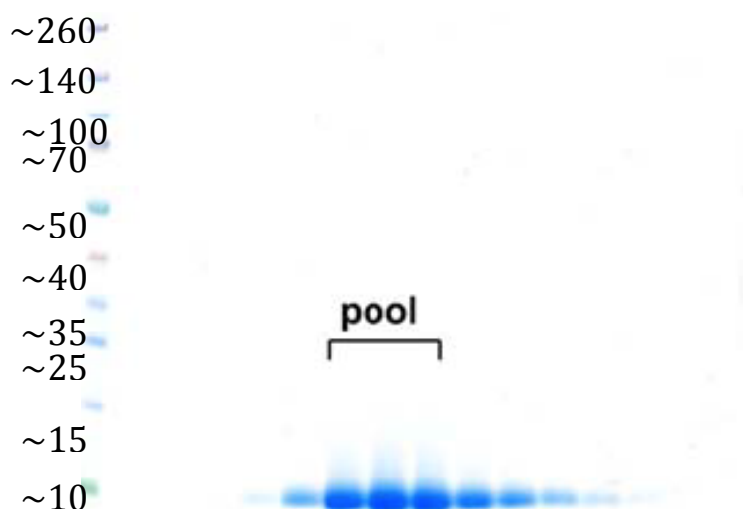


Figure 3-1: SD75/1660 elution profile of cIAP1R. Marked fractions were pooled and concentrated.

3.2.2 Ub^B enhances cIAP1's affinity for UbcH5B~Ub

Our lab has previously developed a method for measuring RING E3's affinity for E2~Ub by using Surface Plasmon Resonance (SPR) analyses (see Methods). Briefly, GST-tag cIAP1R was captured on a CM5 chip that was coupled with anti-GST antibody and binding was measured for a range of UbcH5B~Ub concentrations. To assess the effect of Ub^B on RING E3's affinity for UbcH5B~Ub, a fixed, saturated Ub concentration was included with all UbcH5B~Ub concentrations tested. My colleague, Gary Sibbet, performed all of the SPR experiments. We generated a stable UbcH5B~Ub complex by mutating UbcH5B's catalytic cysteine (Cys85) to lysine, thereby forming a stable amide linkage that mimics the thioester linkage (hereafter UbcH5B C85K~Ub is referred to as UbcH5B~Ub; [73]). GST-cIAP1R exhibited ~85-fold higher binding affinity for UbcH5B~Ub than UbcH5B. Addition of excess of Ub (0.6 mM; K_d for Ub^B-UbcH5B is ~300 μ M; [40]) further enhanced GST-cIAP1R's binding affinity for UbcH5B~Ub by ~10 fold (Table 3-1) (Figure 3-2). As a control we measured GST-cIAP1R's binding affinity for UbcH5B S22R~Ub (the S22R substitution abrogates backside Ub binding; [36]) and found that GST-cIAP1R displayed a similar affinity for UbcH5B S22R~Ub as for UbcH5B~Ub, but there was no improvement in binding upon adding excess Ub, suggesting that interaction between UbcH5B's backside and free Ub is necessary for Ub^B to exert its stimulatory effect. These observations were consistent with our prior study with other RING/U-box domains such as RNF38, UBE4B and BIRC4 [40]. Together my data showed that Ub^B enhances cIAP1R's affinity for UbcH5B~Ub.

Table: 3-1: Dissociation constants (K_d) for interactions between cIAP1R, UbcH5B, UbcH5B~Ub with and without excess Ub

Ligand	Analyte	K_d (μ M)
GST-cIAP1R	UbcH5B	223 \pm 29
GST-cIAP1R	UbcH5B~Ub	2.7 \pm 0.7
GST-cIAP1R	UbcH5B~Ub + 0.6 mM Ub	0.49 \pm 0.14
GST-cIAP1R	UbcH5B S22R~Ub	2.7 \pm 0.7
GST-cIAP1R	UbcH5B S22R~Ub + 0.6 mM Ub	2.7 \pm 0.6
GST-Ub	UbcH5B~Ub + cIAP1R	13 \pm 2

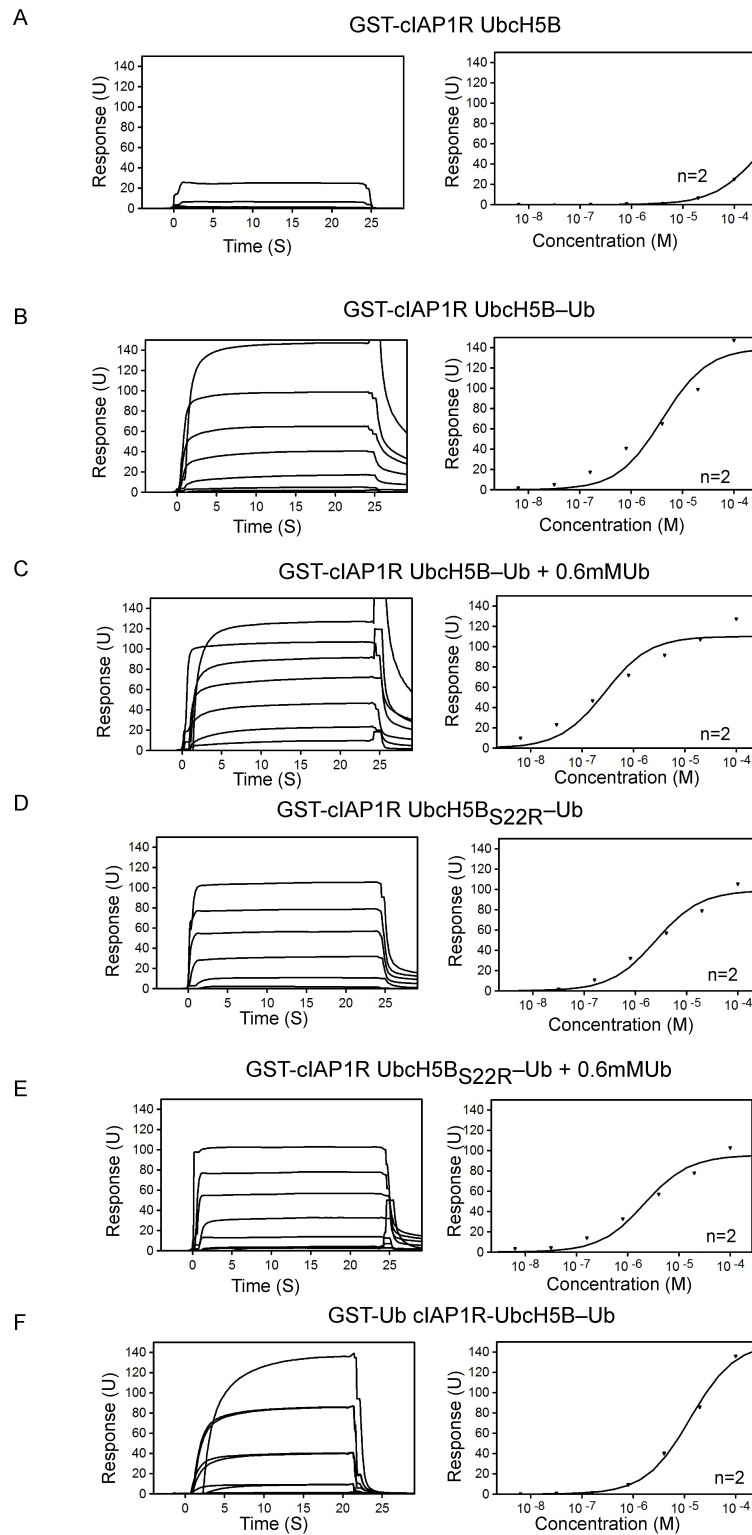


Figure 3-2: SPR binding data showing representative sensograms (left) and binding curves (right). (A) Sensogram and binding curve for UbcH5B and GST-cIAP1R. (B) Sensogram and binding curve for UbcH5B-Ub and GST-cIAP1R. (C) Sensogram and binding curve for UbcH5B-Ub + 0.6 mM Ub and GST-cIAP1R. (D) Sensogram and binding curve for UbcH5B S22R-Ub and GST-cIAP1R. (E) Sensogram and binding curve for UbcH5B S22R-Ub and GST-cIAP1R. (F) Sensogram and binding curve for GST-Ub and UbcH5B-Ub in the presence of cIAP1R.

3.2.3 Ub^B stimulates cIAP1R-catalysed Ub transfer

To assess the effect of Ub^B on cIAP1R-catalysed Ub transfer, I performed *in vitro* single turnover UbcH5B~Ub discharge assays using wild-type (WT) UbcH5B (Figure 3-3A) and UbcH5B S22R (Figure 3-3B). UbcH5B WT and S22R were precharged with equimolar concentrations of ³²P-Ub and then chased by adding cIAP1R alone and in the presence of Ub Δ GG. Ub Δ GG lacks the C-terminal Gly-Gly motif and cannot be charged by E1, but can still bind to the backside of UbcH5B WT. Addition of Ub Δ GG stimulated discharge of UbcH5B~Ub but had no effect on UbcH5B S22R~Ub (Figure 3-3). Thus, Ub^B stimulates cIAP1R-catalysed Ub transfer.

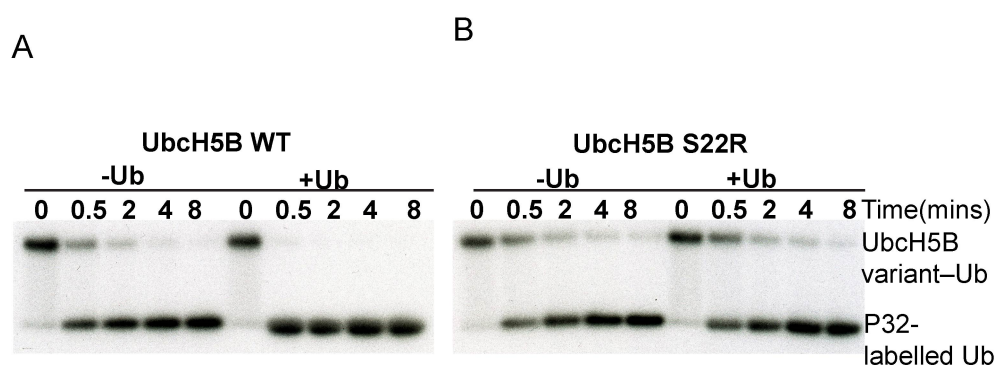


Figure 3-3: Lysine discharge assays of UbcH5B WT and S22R. (A) Non-reduced autoradiogram of lysine discharge assays of UbcH5B WT (B) Non-reduced autoradiogram of lysine discharge assays of UbcH5B S22R. Significant disappearance of UbcH5B~³²P-Ub in presence of cIAP-1R and with and without excess Ub.

3.2.4 Crystallisation of cIAP1R-UbcH5B-Ub-Ub^B complex

The SPR analyses showed that cIAP1R binds UbcH5B~Ub with a K_d of $\sim 0.4 \mu\text{M}$ in the presence of excess Ub. To obtain cIAP1R-UbcH5B~Ub-Ub^B complex, cIAP1R (8.5 mg/ml), UbcH5B~Ub (20 mg/ml) and Ub (100 mg/ml) were mixed at 1:1:1.2 molar ratio such that final concentration of cIAP1R was $\sim 5.5\text{-}6 \text{ mg/ml}$. I screened the complex in 1000 different crystallisation conditions. Crystals were obtained in conditions containing PEG3350 from the initial screen and subsequently optimised. To confirm if the crystals contained all components in the complex, crystals were washed and separated on an SDS gel (Figure 3-4B). The SDS gel showed that UbcH5B~Ub and an additional band that corresponds in size to both Ub and cIAP1R was present. Since both cIAP1R and Ub have a similar molecular weight, whether both components were present was unclear. Nonetheless, I collected data at Diamond

Light Source and determined the structure by molecular replacement (see Section 2.6.2). I found that UbcH5B–Ub, cIAP1R and Ub^B were all present.

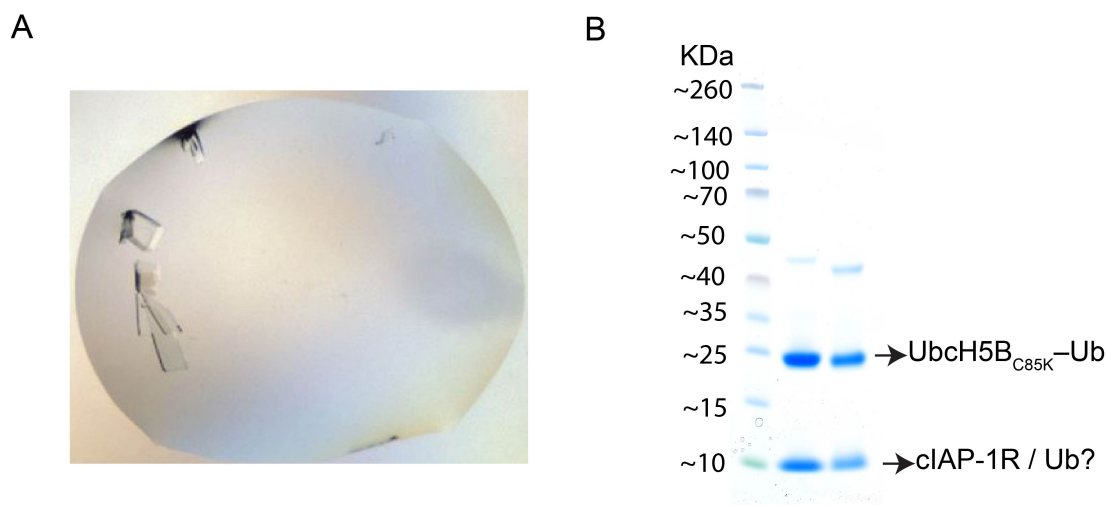


Figure 3-4: Crystallisation of cIAP1R-UbcH5B-Ub-Ub^B complex. (A) Crystals of cIAP1R-UbcH5B-Ub-Ub^B complex. (B) SDS gel showing protein components in the protein crystals from (A). A mixture of complex (lane 1) was run as the control. Lane 2 contains the components in the protein crystals. cIAP1R and Ub have a similar molecular weight of ~10 kDa.

3.2.5 Structure of cIAP1R-UbcH5B-Ub-Ub^B complex

The cIAP1R-UbcH5B-Ub-Ub^B complex crystals belong to space group C121 with one copy of cIAP1R-UbcH5B-Ub-Ub^B complex in the asymmetric unit. The structure was refined to a resolution of 1.7 Å (Table 3-2). Since cIAP1 exists as biological homodimer via the RING domain [136-138], I used crystallographic symmetry to generate a symmetry mate to form a dimeric cIAP1R-UbcH5B-Ub-Ub^B complex. (Figure 3-5). The structure shows that cIAP1R dimerises via the RING domain, the C-terminal tail, and a helix that precedes the RING domain. This arrangement is similar to that observed in other IAP family RING E3s such as cIAP2, XIAP and BIRC7 [66, 77, 151]. cIAP1R's RING domain binds both UbcH5B and Ub^D and arranges UbcH5B-Ub complex in a closed conformation. Additionally, the C-terminal tail of the second subunit in the cIAP1R dimer also packs against Ub^D to stabilise the closed UbcH5B-Ub conformation. The closed UbcH5B-Ub conformation observed here is similar to that observed in other structures of RING E3-E2-Ub complexes [40, 66-68, 73, 146]. In the structure, Ub^B binds to the backside of UbcH5B centring on the Ser22

surface as reported previously [36, 40]. In the following sections, I will explain how cIAP1R binds and activates UbcH5B–Ub and how Ub^B stimulates the activity.

Table 3-2: Diffraction and refinement statistics cIAP1R-UbcH5B–Ub-Ub^B complex

Data Collection

Space group	C 1 2 1
Cell dimensions	
a, b, c (Å)	79.19 53.60 78.54
α , β , γ (°)	90, 107.57, 90
Resolution (Å)	23.67-1.70
Rmerge	0.051 (0.029-0.474)
I/ σ	13.8 (41.3-2.0)
Completeness (%)	98.8 (94.8-94.7)
Redundancy	3.29
Wilson B factor	47.18

Refinement

Resolution (Å)	(23.52-1.70)*
No. Reflections	34206
Rfree/Rwork	0.23/0.20
No. atoms	
Protein	2777
Ions	2
Water	217
R.m.s. deviations	
Bond length (Å)	0.007
Bond angles (°)	1.20

* values indicates highest-resolution shell

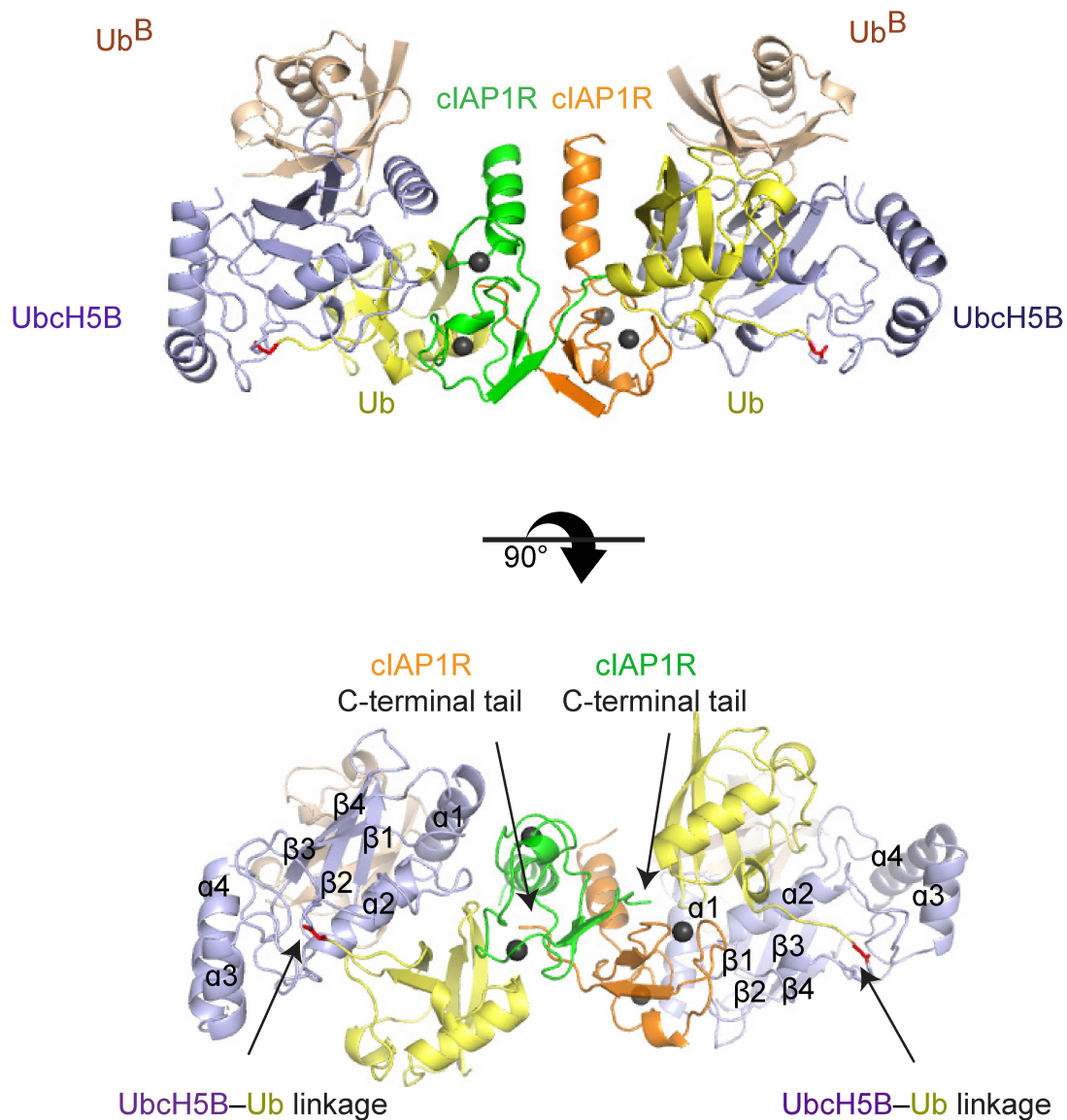


Figure 3-5: Crystal structure of cIAP1R-UbcH5B-Ub-Ub^B (A) cartoon representation of dimeric cIAP1R bound to UbcH5B-Ub and Ub^B. One subunit of cIAP1R is in pink and the other is in orange. UbcH5B is in light blue; Ub^D is in pale green; and Ub^B is in wheat. Zn²⁺ ions are shown as grey spheres. UbcH5B-Ub linkage is highlighted in red. (B) 90° rotation of complex in A. cIAP1R subunits are coloured in orange and green, UbcH5B in light blue, Ub^D in yellow and Ub^B is coloured in wheat.

3.2.6 Interactions important for the closed E2–Ub conformation

There are two key interactions that are crucial for the observed closed E2–Ub conformation in my structure: (I) the RING domain and C-terminal tail of cIAP1R with Ub^D and (II) UbcH5B and Ub^D interaction.

(I) cIAP1R-Ub^D : The structure shows that the C-terminal tail of cIAP1R of one protomer packs against Ub^D that is bound to cIAP1R in the second protomer: Arg614 and Phe616 from the C-terminal tail of one subunit pack against Ub's Gly35 surface (Figure 3-6A). The interaction between a hydrophobic tail residue from the RING E3 and Ub^D was observed in our prior structure of BIRC7-UbcH5B–Ub complex and in other complexes of dimeric RING E3s such as RNF4 and MDM2/MDM4 bound to E2–Ub [66, 67, 74]. In all cases, substitution of Phe or Tyr at this position on these RING E3s to a histidine or alanine disrupted the ligase activity. Previous studies have also shown that Phe616 also plays an important role in RING E3 dimerisation [66, 77]. To determine the importance of this residue, I mutated cIAP1R's Phe616 to His and performed lysine discharge assays to assess the effect on Ub transfer. I found that the F616H mutant was defective in discharging UbcH5B~Ub (Figure 3.6D), suggesting that this interaction is important in stabilising the closed UbcH5B–Ub conformation. Consistent with my finding, an earlier study showed that substitution of cIAP1's Phe616 to His abrogated its activity [152].

In the RING domain of cIAP1R, Arg606 plays a crucial role by pinning Ub^D and UbcH5B together. It stabilises Ub^D by forming hydrogen bonds with Arg72 and Glu40 of Ub^D (Figure 3-6A). Direct interactions between Arg606 of cIAP1R and Arg72 of Ub^D constrains the C-terminal tail of ubiquitin in a conformation in which the thioester is more reactive (Figure 3-6B). This interaction has been previously observed in other RING-E2–Ub structures [48, 66, 76], and is consistent with Arg606's assigned function as a linchpin that stabilises Ub^D for optimal transfer. To assess the important of it in my structure, I mutated Arg606 to Ala and performed lysine discharge assays. The mutant (R606A) was defective in UbcH5B~Ub transfer (Figure 3-6E)). Hence, the function of this Arg as a linchpin in RING-mediated Ub transfer is conserved in cIAP1R.

Apart from cIAP1R's Phe616 and Arg606, Ile36 of Ub^D interacts with cIAP1R's C-terminus and RING domain via hydrophobic and hydrophilic interactions (Figure 3-6A). These interactions provide additional stability to RING-Ub^D interactions. These

interactions consist of Arg614 at the C-terminus of cIAP1R forming a hydrogen bond with Asp32 of Ub^D, and His588, Ileu604 and Cys592 from cIAP1R's RING domain interacting with Leu8, Ileu36 and Pro37 of Ub^D. Again, to determine the role of Ile36 in RING-mediated Ub transfer, I mutated Ile36 to Ala and performed lysine discharge assays to visualise its effects. Ub Ile36A does not charge complete [40, 66], to make the results comparable I charged WT Ub similar to Ub I36A. My results showed that the mutant is defective in UbcH5B~Ub discharge. (Figure 3-6F).

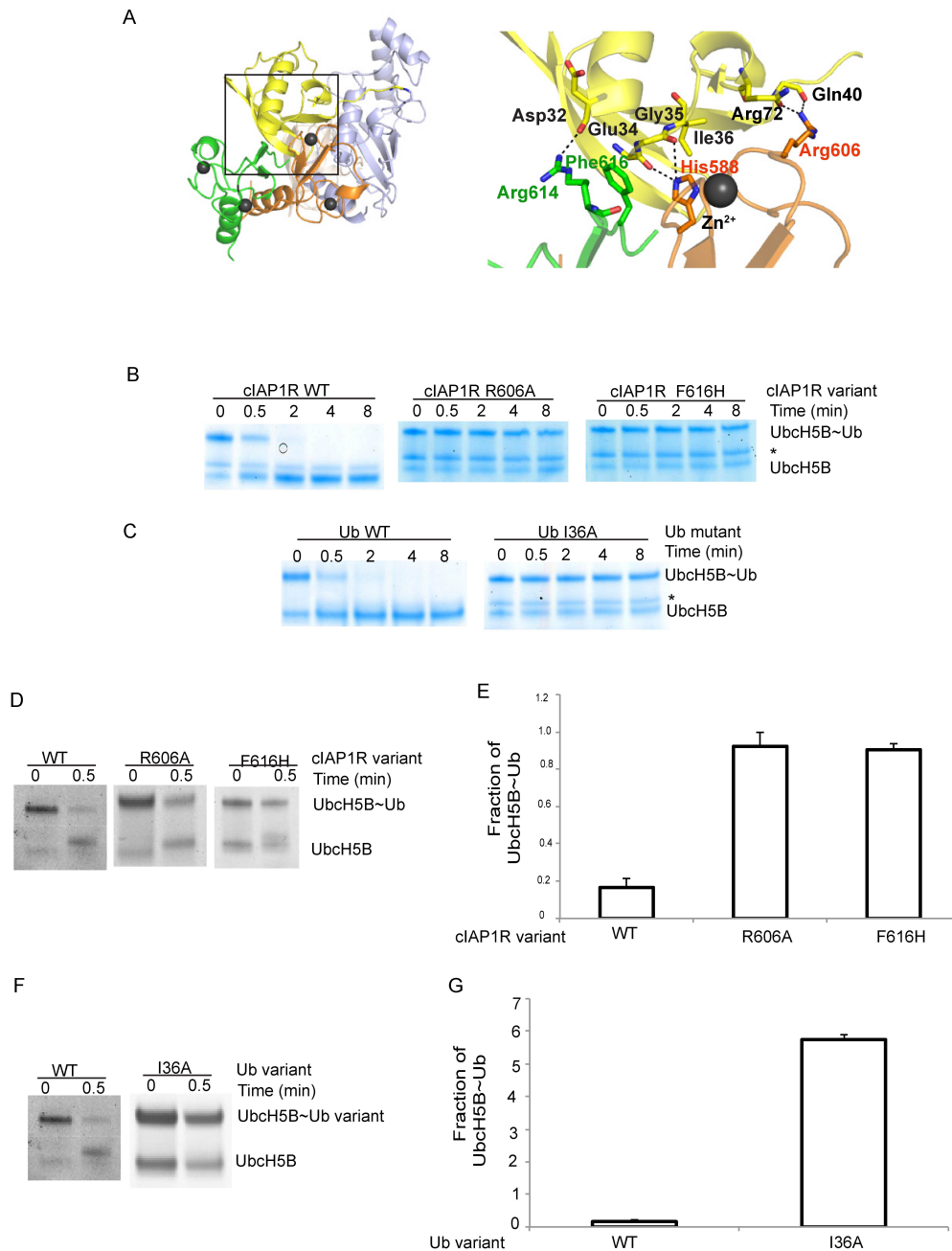


Figure 3-6: Interactions of cIAP-1R C-terminal tail. (A) Close-up cartoon representation of interactions between Ub^D and the RING domain and C-terminal tail of cIAP1R. Colouring is as described in Figure 3-5. Interacting residues are shown in stick with putative hydrogen bonds shown with dashes. (B) Non-reduced SDS gels of lysine discharge assays of cIAP1R WT, cIAP1R R606A and F616H. * indicates impurity. (C) Non-reduced SDS gels of lysine discharge assays of Ub WT and Ub I36A. * indicates impurity. (D) A representative SDS gel showing the effects of cIAP1R mutants in discharging Ubch5B~Ub to L-lysine in presence of 300 μM Ub in 0.5 minutes. (E) A bar graph showing fraction of Ubch5B~Ub left in (D). (F) A representative SDS gel showing the effects of Ub mutant in discharging Ubch5B~Ub to L-lysine in presence of 300 μM Ub in 0.5 minutes. (G) A bar graph showing fraction of Ubch5B~Ub left in (F).

(II) UbcH5B and Ub^D interactions: cIAP1R binds UbcH5B–Ub such that it restrains UbcH5B–Ub in a closed configuration. This closed UbcH5B–Ub interaction is further stabilised by interactions between Ub^D and UbcH5B. Ubiquitin's Ileu44 patch interacts with the α 3-helix of UbcH5B (Figure 3-7A). The interactions between UbcH5B and Ub are stabilised by hydrophobic interactions between Ser108 of UbcH5B and His68 and Val70 of Ub. These interactions were also previously observed in the complex structure of BIRC7 bound to UbcH5B~Ub (Dou *et al.* 2012). Additional interactions are also observed between Lys48, Gln49, and Arg42 of Ub and UbcH5B's Asp112, Leu104, and Lys101 (Figure 3-7A).

To investigate the importance of these interactions, I performed single-turnover lysine discharge assays using Ub in which Ile44 was substituted to Ala or UbcH5B in which Ser108 was substituted to Arg. In both cases, RING-mediated ubiquitin transfer was impaired (Figure 3-7B).

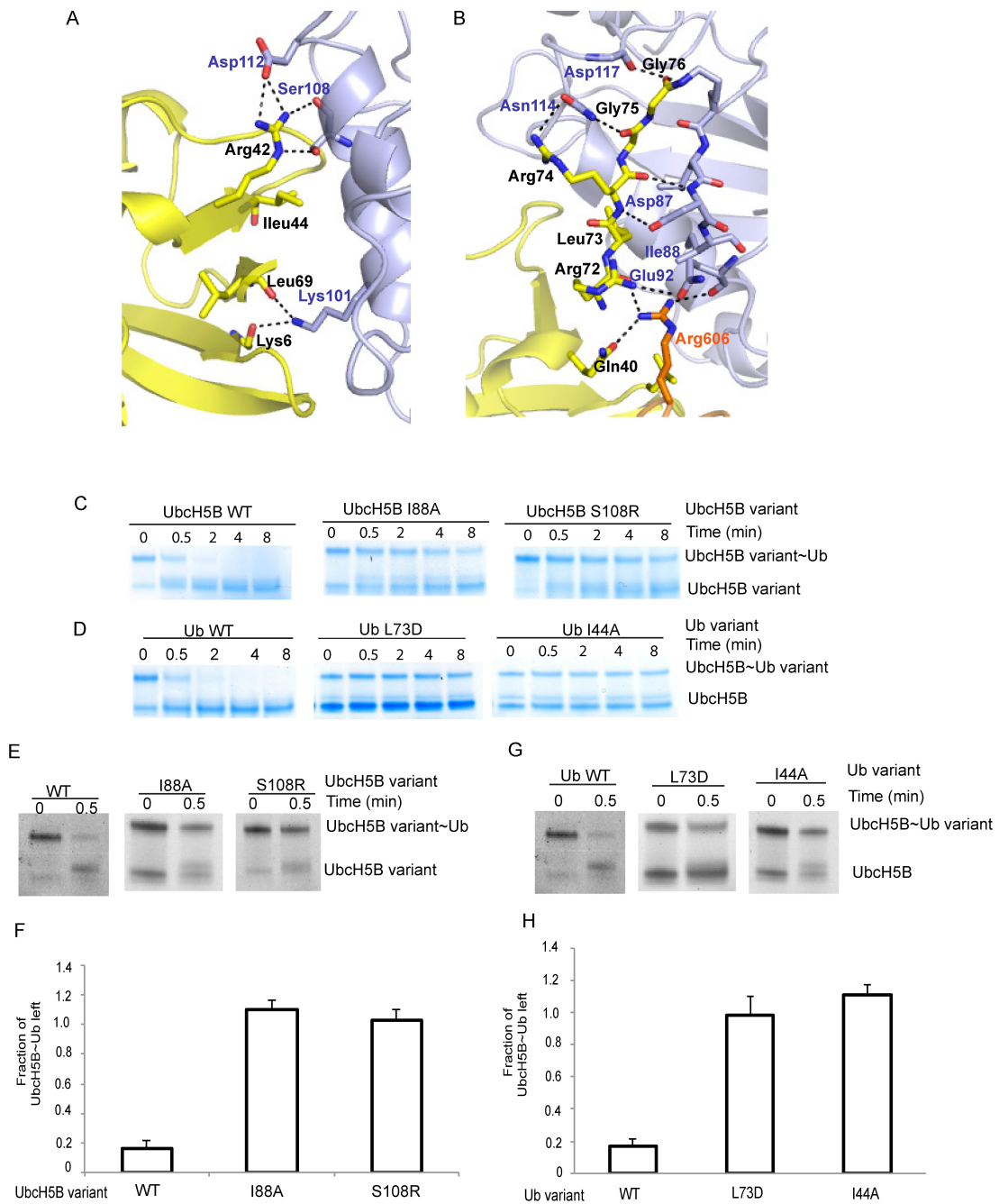


Figure 3-7: Interactions between UbD and UbcH5B (A) Close up of boxed region shown on left showing interactions between the Ile44 patch of Ub^D and UbcH5B. (B) Close up of interactions between UbcH5B's α 2-helix and the tail of Ub (C) Non-reduced SDS gels of single turnover lysine discharge assays of UbcH5B WT, S108R and I88A. (D) Non-reduced SDS gels of single turnover lysine discharge assays of Ub WT, I44A and L73D. (E) A representative SDS gel showing the effects of UbcH5B mutants in discharging UbcH5B~Ub to L-lysine in presence of 300 μ M Ub in 0.5 minutes. (F) A bar graph showing fraction of UbcH5B variant~Ub left in (E). (G) A representative SDS gel showing the effects of Ub mutants in discharging UbcH5B~Ub to L-lysine in presence of 300 μ M Ub in 0.5 minutes. (H) A bar graph showing fraction of UbcH5B variant~Ub left in (G).

The C-terminal tail of Ub is extended and lies along the interface between UbcH5B's helices (Figure 3-7B). As shown in the figure, hydrophobic interactions are formed between UbcH5B's Ileu88 and Ub's Leu73. Other interactions shown in figure are between backbone nitrogen of UbcH5B Asp87 and the backbone oxygen of Ub's Arg74. To validate the effect of important residues between UbcH5B and Ub tail, I mutated Ub's Leu73 to Asp (L73D) and performed lysine discharge assay with the mutant. Results showed that the mutant was defective in UbcH5B~Ub discharge. Similarly, I tested residue from UbcH5B's α_2 helix by mutating Ileu88 to Ala (I88A) and performed lysine discharge assays with it. The mutant was found to be defective in UbcH5B~Ub discharge (Figure 3-7C). It has been previously shown Ub mutants L73D and I44A does not charge complete [66].

3.2.7 Comparison between cIAP1 and cIAP2 to understand ubiquitin transfer

The RING domains of cIAP1 and cIAP2 have conserved structures and sequences (Figure 3-8A,B). My structure is the only structure at present of either of these two RING domains bound to a Ub-conjugated E2. Mace *et al.* (2008) solved the first structure of dimeric cIAP2 RING alone and with UbcH5B and demonstrated that the RING domain undergoes structural changes on binding to E2. However, there was no structural information on the RING mediates ubiquitin transfer. Superposition of the structures of cIAP2 bound to UbcH5B with our cIAP1R bound to UbcH5B~Ub structure (r.m.s.d. of 0.914 Å) revealed that Arg606 in cIAP-1 is rotated by 7Å compared to the equivalent of Arg in cIAP-2 (Arg592, Figure 3-8C). This rotation of Arg606 enables the RING domain of cIAP-1 to interact with Arg72 and Gln40 of UbcH5B and Ub^D. This observation and the Ub-RING tail interactions discussed above provide additional insights into the mechanism of ubiquitin transfer in IAP RING E3 ligases. In the cIAP2R-UbcH5B structure, Arg592 forms hydrogen bond with UbcH5B's Gln92. Furthermore there is a slight rotation in UbcH5B relative to the RING domain (Figure 3-8C). These differences show that the presence of Ub^D could influence how RING E3 interacts with E2.

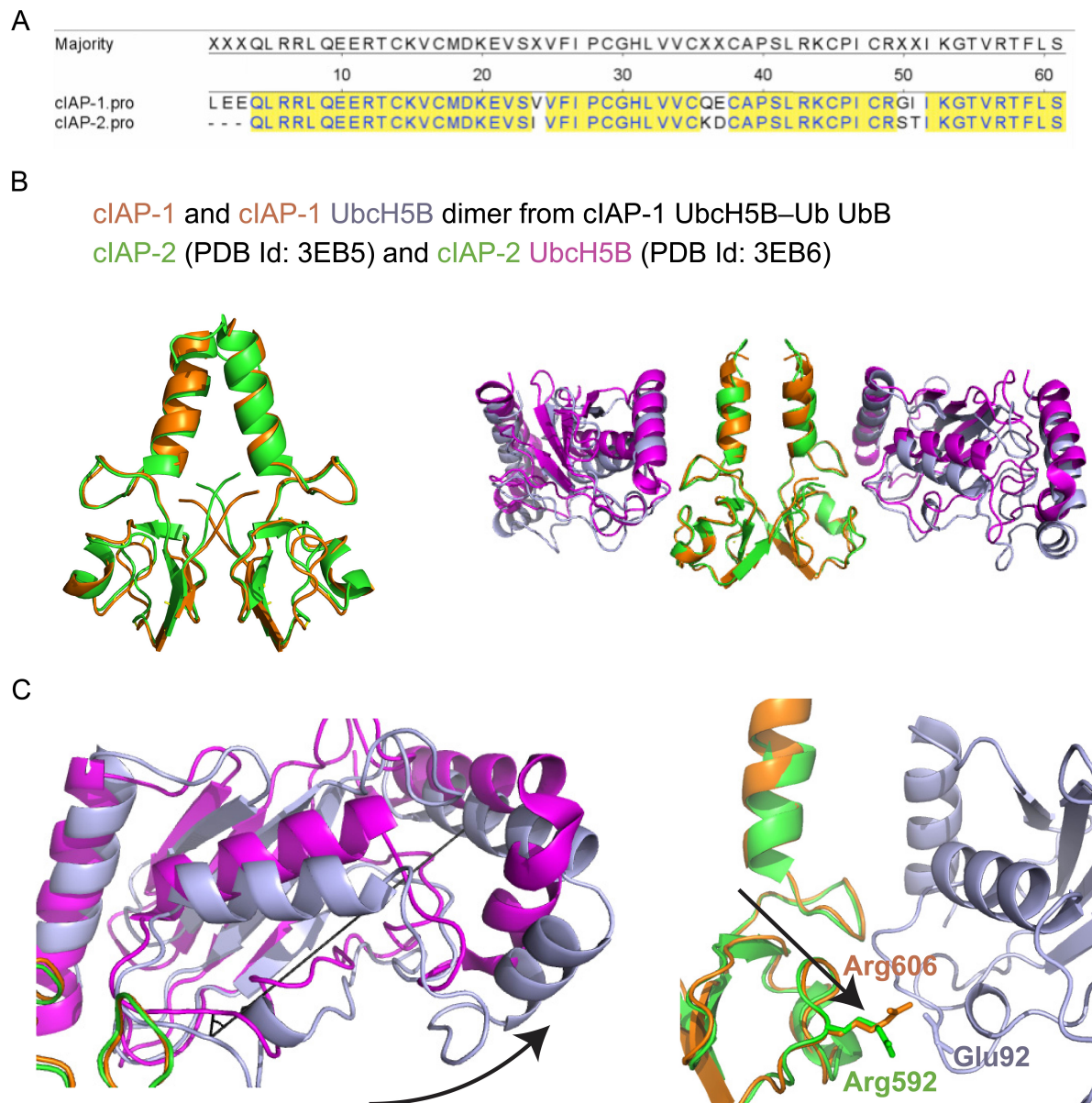


Figure 3-8: Structural comparison of clAP1R-UbcH5B-Ub and clAP-2R-UbcH5B (A) Sequence alignment of clAP1R(556-C) domain with clAP-2R domain (541-C) using MegAlign from DNASTar. Matched residues are shaded in yellow. (B) On left clAP-1R(orange) superposed with clAP-2R(green)(PDB ID: 3EB5). On right, clAP-1R-UbcH5B (orange and light blue, respectively) superposed with clAP-2R-UbcH5B (PDB ID: 3EB6)(green and magenta, respectively) (c) On left, superposed UbcH5B from clAP-1R(light blue) and clAP-2R(magenta). On right, Arg606 from clAP-1R (orange) superposed with Arg592 from clAP-2R(green) to show interactions with Glu92 of UbcH5B in light blue.

3.2.8 Ub^B as an allosteric activator of cIAP1 mediated Ub transfer

Ub^B binds UbcH5B via the Ile44 hydrophobic patch on Ub^B and UbcH5B's backside β 1-3 surface around Ser22. This binding mode resembles other available structures of UbcH5 family E2s bound to Ub^B [36, 38, 40, 153]. In my structure, Ub^B does not contact cIAP1R or Ub^D. In addition to UbcH5B's Ser22 surface, Ub^B also contacts UbcH5B's α 1 β 1 loop, which in turn packs against Ub^D (Figure 3-9A). Here, Ub^B's Lys6 and His68 form hydrogen bonds with carbonyl oxygens of UbcH5B's Pro17 and Pro18, respectively, and Leu8 packs against UbcH5B's Gln20 thereby placing Gln20 within hydrogen bonding distance of the backbone amide of Ub^D's Gly47 (Figure 3-9B). To test the importance of Gln20, I used mutant UbcH5B Q20A (expressed and purified by Lori and Mads) to perform cIAP1R-mediated lysine discharge assays. The rate of UbcH5B Q20A~Ub discharge in the presence and absence of excess of Ub remained the same, suggesting that Gln20 plays an important role in Ub^B-mediated stimulation of Ub transfer (Figure 3-9E). Our lab has previously determined the structures of a monomeric RING E3, RNF38, bound to UbcH5B~Ub alone and in complex with Ub^B [40]. When I compared the α 1 β 1 loop in my structure to UbcH5B~Ub~RNF38 (where there is no Ub^B), I observed that Gln20 is shifted in my structure (Figure 3-9C). This shift was also present in the comparison of Ub^B-UbcH5B~Ub~RNF38 to UbcH5B~Ub~RNF38. Consistent with this earlier study, my structure showed that Ub^B packs against UbcH5B's α 1 β 1 loop to further stabilise Ub^D in the closed conformation (Figure 3-9D).

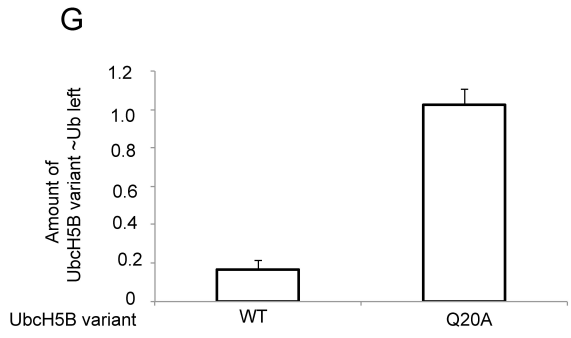
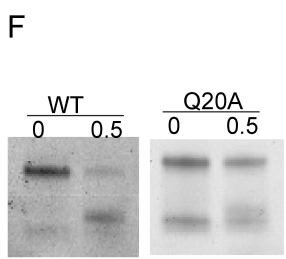
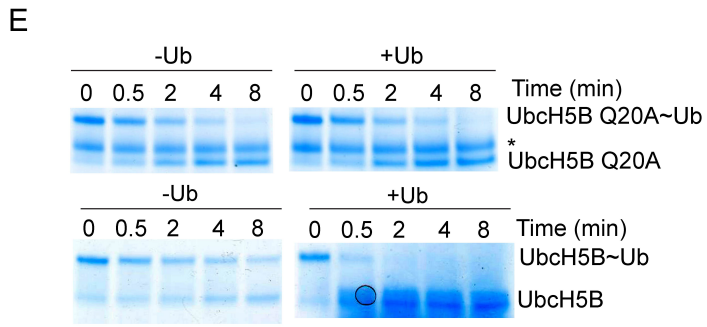
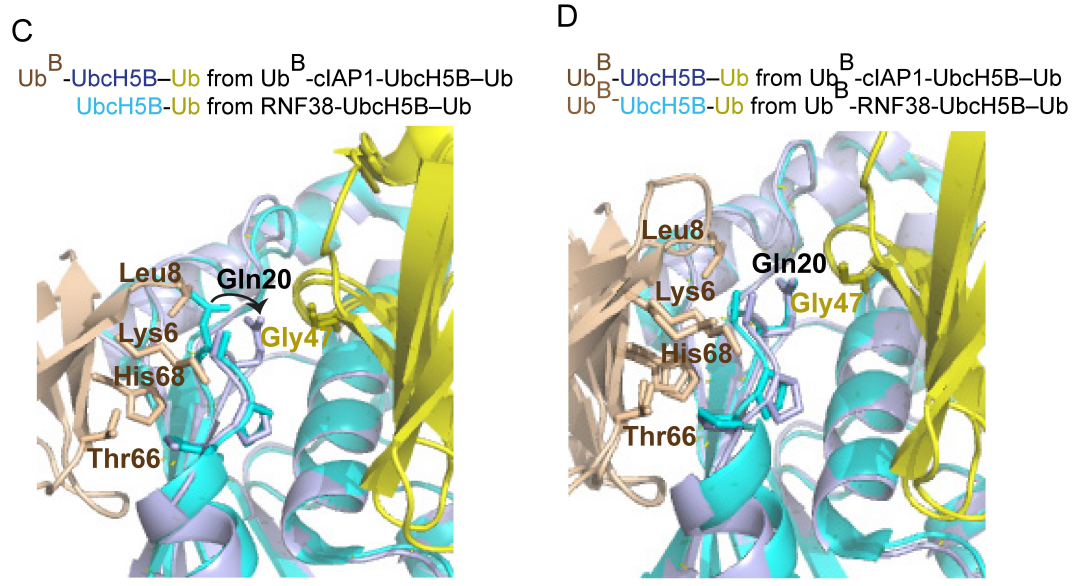
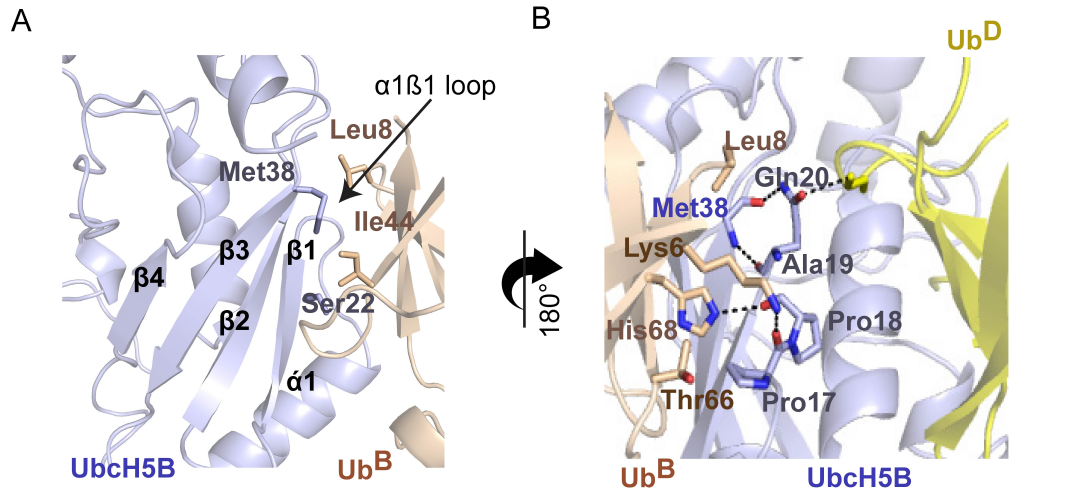
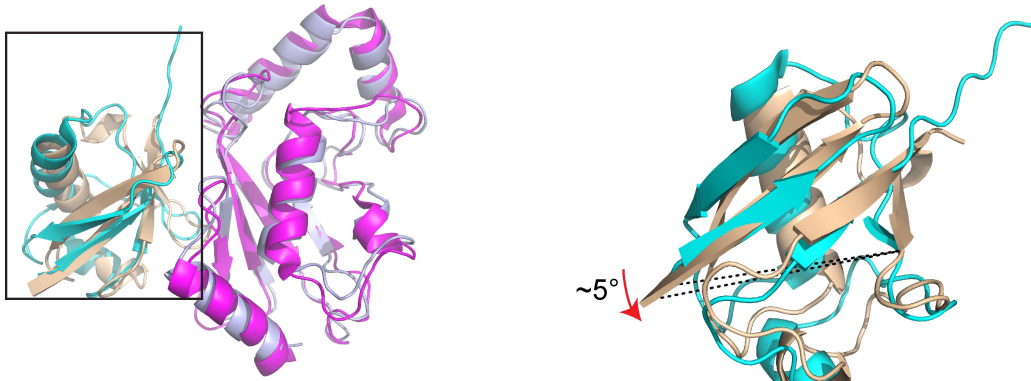


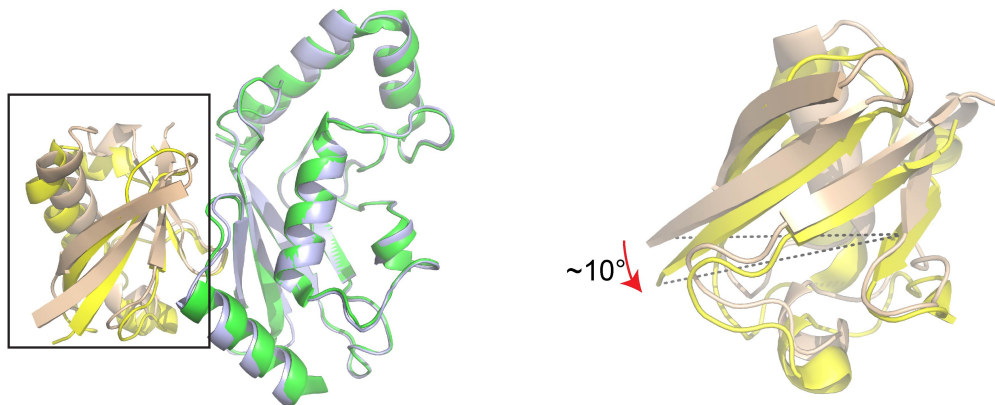
Figure 3-9: Mechanistic aspects of Ub^B-stimulation (A) Close-up view of Ub^B in wheat colour interacting with UbcH5B's α 1 β 1 loop coloured in light blue. Binding to the backside of UbcH5B occurs via the Ile44 hydrophobic patch of Ub^B. (B) close-up of interactions of residues from UbcH5B and Ub^B are shown in sticks. Putative hydrogen bonds are shown in dashed lines (C) Close-up view of UbcH5B's α 1 β 1 loop from the overlaid structures of RNF38-UbcH5B-Ub (PDB ID: 4V3K; UbcH5B is in green) and Ub^B-UbcH5B-Ub-cIAP1R(unpublished; UbcH5B is in light blue) complexes (D) Close-up view of UbcH5B's α 1 β 1 loop from the overlaid structures of Ub^B-UbcH5B-Ub-RNF38 (UbcH5B is in green and Ub^B in yellow) and Ub^B-UbcH5B-Ub-cIAP1R (UbcH5B is in light blue and Ub^B is in wheat) complexes (E) Non-reducing SDS-PAGE showing the disappearance of UbcH5B WT and Q20A~Ub over time catalysed by cIAP1R in the presence and absence of excess Ub. (F) A representative SDS gel showing the effects of UbcH5B mutants in discharging UbcH5B~Ub to L-lysine in presence of 300 μ M Ub in 0.5 minutes.(G) A bar graph showing fraction of UbcH5B variant ~Ub left in (F).

There are several structures of Ub^B bound to E2. Superimposition of the existing Ub^B-E2 structures from Ub^B-UbcH5C (PDB ID: 2FUH)[36] and Ub^B-UbcH5B-Ub-RNF38 (PDB ID: 4V3L)[40] onto my structure by overlaying the E2 structures showed a slight rotation in the Ub^B conformation relative to the E2 (Figure 3-10C). In comparison with Ub^B-UbcH5C and Ub^B-UbcH5B-Ub-RNF38 structures, Ub^B in my structure has rotated by $\sim 5^\circ$ and 10° , respectively (Figure 3-10A,B). Despite these differences, Ub^B still makes contacts with UbcH5's α 1 β 1 loop in all three structures. Notably, the conformation of UbcH5's α 1 β 1 loop is identical in both Ub^B-UbcH5B-Ub-RNF38 complex and Ub^B-UbcH5B-Ub-cIAP1R complex structures (Figure 3-9D). In all other UbcH5B-containing structures, this loop adopts various conformations (Figure 3-9C). Thus, my results showed that irrespective of the oligomeric state of the RING E3, Ub^B functions to stabilise UbcH5's α 1 β 1 loop, which in turn packs against Ub^D to further stabilise the closed UbcH5B-Ub conformation to stimulate RING E3-catalysed Ub transfer.

A **Ub^B UbcH5B** from cIAP-1 UbcH5B-Ub Ub^B
Ub^B UbcH5B from UbcH5C UbB (PDB Id: 2FUH)



B **Ub^B UbcH5B** from cIAP-1 UbcH5B-Ub Ub^B
Ub^B UbcH5B from RNF38 UbcH5B-Ub Ub^B (PDB Id: 4V3L)



C **Ub^B UbcH5B** from cIAP-1 UbcH5B-Ub Ub^B
Ub^B UbcH5B from UbcH5C UbB (PDB Id: 2FUH)
Ub^B UbcH5B from RNF38 UbcH5B-Ub Ub^B (PDB Id: 4V3L)

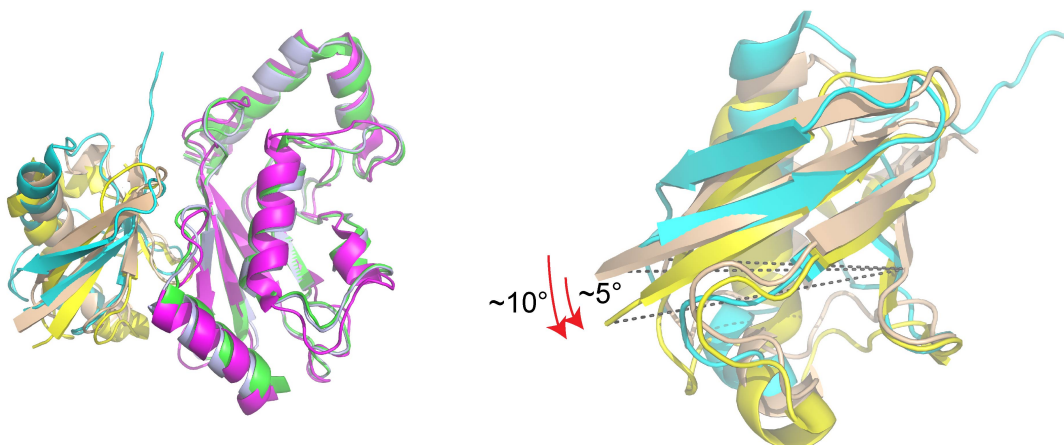


Figure 3-10: Comparing Ub^B from cIAP1R-UbcH5B-Ub-Ub^B with RNF38-UbcH5B-Ub-Ub^B (PDB ID: 4V3L) and UbcH5C-Ub^B (PDB ID: 2FUH) (A) Superimposition of Ub^B-UbcH5B portion of structure from cIAP1R-UbcH5B-Ub-Ub^B complex (UbcH5B is in light blue and Ub^B is in wheat) onto Ub^B-UbcH5C complex (PDBID 2FUH; UbcH5C is magenta and Ub^B is cyan) by aligning the E2 structures. Left and right panels show the overlaid Ub^B-E2 complex and Ub^B, respectively. A red arrow indicates Ub^B rotation. (B) Superimposition of Ub^B-UbcH5B portion of structure from cIAP1R-UbcH5B-Ub-Ub^B complex (coloured as in A) onto Ub^B-UbcH5B portion of structure from RNF38-UbcH5B-Ub-Ub^B complex (PDB ID: 4V3L; UbcH5B is in green and Ub^B is in yellow) by aligning the E2 structures. Left and right panels show the overlaid Ub^B-UbcH5B complex and Ub^B, respectively. A red arrow indicates Ub^B rotation. (C) Overlaid structures of Ub^B-E2 portion of structures from RNF38 UbcH5B-Ub-Ub^B (PDB ID: 4V3L; coloured as in B) and cIAP1R-UbcH5B-Ub-Ub^B (coloured as in A) complexes and Ub^B-UbcH5C (PDB ID: 2FUH; coloured as in A). Left and right panels show the overlaid Ub^B-E2 complexes and Ub^B, respectively. A red arrow indicates Ub^B rotation.

3.2.9 Ub^B stimulating mechanism observed across UbcH5 family

The UbcH5 family of E2s are evolutionarily conserved and widely expressed in humans [34]. This group of E2s consists of four genes known as UbcH5A, UbcH5B, UbcH5C and UbcH5D, amongst which the most commonly studied are UbcH5A-C. These human proteins have at least 88% sequence identity and 95% sequence similarity to each other (Figure 3-11A) [36]. Structures of UbcH5A-C reveal that their UBC domain is conserved and additional studies have shown similar functionality *in vitro* and *in vivo* (Figure 3-11B) [34].

Although there is lot of structural and functional information available about the UbcH5A-C families, not much is known about UbcH5D. Studies on UbcH5A and UbcH5C show that the Ub^B-E2 interaction is important for processivity of polyUb chain formation as S22R substitution in both E2s reduced substrate ubiquitination [36, 67]. To assess whether Ub^B also stimulates RING E3-catalysed Ub transfer with the UbcH5 family E2s, I performed single turnover Ub transfer assays. I precharged E2 with Ub and then stopped and chased with cIAP1R and 20 mM lysine as the Ub acceptor in the presence and absence of 300 μM K0UbΔGG. Addition of 300 μM K0UbΔGG increased the rate of UbcH5~Ub discharge for all UbcH5 family E2s (Figure 3-11C). Thus, my results showed that Ub^B was able stimulate cIAP1R-catalysed Ub transfer for the entire UbcH5 family of E2s.

A

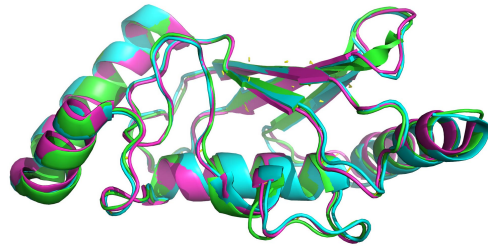
```

MALKRI QKELSDLXRDPPAQCSAGPVGDDXFWHGATI MGPNDSPYQGGVFFLTI HFPTDYPPFKPKVAFITXI YHP
      10      20      30      40      50      60      70
UbcH5A MALKRI QKELSDLQRDPPAHCSAGPVGDDLFWHGATI MGPNDSPYQGGVFFLTVHFPTDYPPFKPKI AFTTKI YHP
UbcH5B MALKRI QKELTDLQRDPPAQCSAGPVGDDLFWHGATI MGPNDSPYQGGVFFLTI HFPTDYPPFKPKVAFITTKI YHP
UbcH5C MALKRI NKELSDLARDPPAQCSAGPVGDDMFWHGATI MGPNDSPYQGGVFFLTI HFPTDYPPFKPKVAFITRI YHP
UbcH5D MALKRI HKELNDLARDPPAQCSAGPVGDDMFWHGATI MGPNDSPYQGGVFFLTI HFPTDYPPFKPKVAFITRI YHP

NGSI CLDI LRSQWSPALTXSKVLLSI CSLLCDPNPDDPLVPEI ARI YKTDREKYNRI AREWTQKYAM
      90      100     110     120     130     140
UbcH5ANGSI CLDI LRSQWSPALTVSKVLLSI CSLLCDPNPDDPLVPEI AQI YKSDKEKYNRHAREWTQKYAM
UbcH5BNGSI CLDI LRSQWSPALTVSKVLLSI CSLLCDPNPDDPLVPEI AHTYKADREKYNRLAREWTQKYAM
UbcH5CNGSI CLDI LRSQWSPALTI SKVLLSI CSLLCDPNPDDPLVPEI ARI YKTDREKYNRI SREWTQKYAM
UbcH5DNGSI CLDI LRSQWSPALTI SKVLLSI CSLLCDPNPDDPLVPEI ARI YKTDREKYNRI AREWTQKYAM

```

B



C

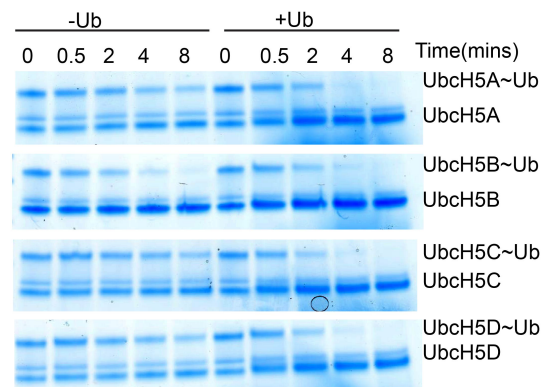


Figure 3-11: Ub^B-stimulation is conserved across the UbcH5 family (A) Sequence alignment of UbcH5 family of E2s (UbcH5A–D) using clustalW method using MegAlign software. Strictly conserved residues are highlighted in yellow. (B) Cartoon representation of superimposed structures of UbcH5A (PDB ID: 2C4P; green), UbcH5B (PDB ID: 3TGD; cyan) and UbcH5C (PDB ID: 1X23; magenta). (C) SDS-PAGE showing disappearance of UbcH5~Ub over time in lysine discharge reactions catalysed by cIAP1R in the absence (left) and presence (right) of K0UbΔGG for the UbcH5 family of E2s (indicated on the right).

3.3 Discussion

The structure of cIAP1R-UbcH5B-Ub-Ub^B reported here is the first structure of a dimeric RING E3 bound to E2-Ub and Ub^B. Also this is the first structure of cIAP1 bound to E2-Ub. The previous structure of cIAP2 bound to UbcH5B did not reveal the mechanism of Ub transfer as it lacked donor Ub [77]. However, a closely related IAP family E3, BIRC7, bound to UbcH5B-Ub provided insights into how the IAP family RING E3s activate E2~Ub complex for catalysis [66]. Consistent with these BIRC7 findings, I showed that cIAP1 activates Ub for transfer by restraining UbcH5B-Ub into the closed conformation that favours catalysis. This mechanism is also observed in several other RING E3-E2~Ub complexes.

Similar to other RING E3-E2~Ub complexes, the closed E2~Ub conformation is stabilised by RING-E2, RING-Ub^D and Ub^D-E2 interactions. Crucially, a linchpin Arg (Arg606 in cIAP1) makes hydrogen bonds with carbonyl oxygens of Glu92 of UbcH5B and Arg72 of Ub^D and Gln40 side chain of Ub^D (Figure 3-5B). This interaction network is conserved in several structures of RING E3-E2~Ub complexes. I showed that substitution of this Arg in cIAP1 reduced ligase activity, consistent with earlier findings. Moreover, studies showed that Arg substitutions at this position influence the RING E3's ability to populate E2~Ub in the closed conformation [66-68, 76], highlighting the importance of this residue.

In addition to the RING domain, cIAP1 contains a C-terminal tail that binds and stabilises Ub^D in a manner similar to that observed in the structures of BIRC7 and RNF4 bound to E2-Ub. My data showed that C-terminal tail of cIAP1 plays important roles in RING domain dimerisation and stabilisation of Ub^D in the closed conformation, thereby enhancing ligase activity (see section 3.2.5). The tail-Ub^D interaction occurs *in trans*, where the C-terminal tail of one of the RING domains from one subunit of the dimer binds Ub^D that is bound to the RING domain in the second subunit. This arrangement explains the importance of the RING domain dimerisation in regulating ligase activity.

In 2006 Brzovic *et al.*, showed that Ub^B binding to the backside of UbcH5C enhances the processivity of polyUb chain formation. How Ub^B enhances polyUb chain formation was not well understood until our lab published a structure of RNF38-UbcH5B-Ub-Ub^B and characterised its mechanism of action [40]. We showed that Ub^B improved RING E3's affinity for UbcH5B~Ub and RING E3-UbcH5B~Ub

complex enhances Ub^B's affinity for UbcH5B. This synergism results in the enhancement of the catalytic efficiency of RING E3-mediated Ub transfer, thereby enabling processive polyUb chain formation. We showed that Ub^B stimulates RING E3-UbcH5B~Ub complex by binding to UbcH5B's $\alpha 1\beta 1$ loop, which in turn pack against Ub^D to further stabilise Ub^D in the closed conformation.

In the work described in this chapter, I wanted to understand whether this mechanism of Ub^B-stimulation is conserved for other RING E3s. Given that our previous structural work was performed with a monomeric RING E3, RNF38, I decided to investigate this mechanism using a dimeric RING E3, namely cIAP1. Comparison of the structures of cIAP1-UbcH5B-Ub-Ub^B with RNF38-UbcH5B-Ub-Ub^B suggested that Ub^B stimulates Ub transfer in dimeric RING E3-mediated catalysis via a similar mechanism as observed earlier for monomeric RING E3s by Buetow *et al.* (2015) (Figure 3-9D). The $\alpha 1\beta 1$ loop of UbcH5B makes extensive contacts with Ub^D in presence of Ub^B. Gln20 of UbcH5B interacts with backbone amide of Gly47 of Ub^D. In addition, Lys6 of Ub^B contacts the backbone carbonyl oxygen of Pro17 of UbcH5B, which was not evident in the structure of RNF38-UbcH5B-Ub-Ub^B complex. Despite the slight differences in how Ub^B interacts with UbcH5B's $\alpha 1\beta 1$ loop and the orientation of Ub^B relative to UbcH5B, the conformation of UbcH5B's $\alpha 1\beta 1$ loop and its interaction with Ub^D are identical in both structures. Thus my structure and data presented here further reinforced our proposed mechanism that Ub^B activates RING E3-UbcH5B-Ub complex by binding to UbcH5B's $\alpha 1\beta 1$ loop, which in turn stabilises the closed Ub^D conformation.

Finally, I studied whether the mechanism of Ub^B stimulation is conserved in the UbcH5 family of E2s. The sequences of UbcH5 family E2s are highly conserved (section 3.2.11, Figure 3-11A). There is no crystal structure available for UbcH5D, but its sequence is similar to that of UbcH5B. To probe the Ub^B mechanism, I performed lysine discharge assays with UbcH5A, B, C and D. I found that Ub^B stimulates cIAP1R-mediated Ub transfer with all members of the UbcH5 family of E2s (Figure 3-11C). The $\alpha 1\beta 1$ loop sequence of UbcH5A is different from other members of UbcH5 family. Gln20 is substituted with His in the $\alpha 1\beta 1$ loop. It is unclear how His at this position influences interactions with Ub^D. Presumably the aromatic side chain of His could pack against Ub^D. Further studies are required to dissect how sequence variations in the $\alpha 1\beta 1$ loop influence Ub^B stimulation.

Moreover, it is possible that there are other elements contributing to Ub^B-mediated stimulation that remains to be investigated.

The SPR data showed that addition of excess Ub enhances cIAP1's binding affinity for UbcH5B~Ub by ~10 fold. Likewise cIAP1R-UbcH5B~Ub complex enhances the binding affinity for Ub^B such the K_d is now ~13 μ M (Table 3-1). This explains how a weak Ub^B-UbcH5B interaction (K_d of ~300 μ M) could become relevant in cells where Ub concentration is between 20-85 μ M. Collectively, this finding is consistent with our previous observation with the monomeric RING E3, RNF38 [40].

Chapter 4

Study of UbcH6's backside binding mechanism

4.1 Aims and Objectives

Several recent studies have shown the crucial role of interactions between E2 UBC domains and non-covalent ubiquitin in Ub transfer [36, 38, 40, 91]. These studies prompted me to investigate whether non-covalent Ub binding affects other E2s as well. To investigate this, I decided to study the core/UBC domain of UbcH6 (residues 43-C). This E2 is also known as UbcH6 and hereafter this construct is referred to as UbcH6^{core}. Previous work done by Schumacher and *et al.* in 2013 has shown that the UbcH5 and UbcH6 families of E2s both promote multi-mono and polyubiquitination of cIAP2. They also showed that non-covalent Ub does not interact with UbcH6, as substitution of a serine residue (Ser68; corresponding to UbcH5B's Ser22) in the backside of UbcH6 did not hinder Ub transfer as observed in UbcH5 family E2s [43]. Since there is strong structural and sequence similarity between UbcH6 and UbcH5 family E2s (see Section 1.5.3, Figure 1-8), I set out to investigate the relevance of Ub^B in regulating UbcH6-mediated Ub transfer.

To investigate the UbcH6 backside mechanism, I performed ubiquitination and lysine discharge assays on UbcH6 WT and S68R using cIAP1. The cIAP1 construct used in these assays comprises the BIR3 (baculovirus inhibitor of apoptosis repeat 3), ubiquitin-associated (UBA), CARD and RING domains (residues 260-C; hereafter referred to as cIAP1(B3-C)). I selected this construct because it is equivalent to the construct of cIAP2 used by [41] to investigate the effect of Ub^B on UbcH6. In this chapter, I show that UbcH6 has a weak binding affinity for Ub^B and Ub^B stimulation can only be achieved by adding at least 1 mM of free Ub. However, when cIAP1 is modified with polyUb chains, the Ub moieties from the polyUb chains can function as Ub^B *in cis* to overcome the high Ub concentration requirement to stimulate cIAP1-catalysed UbcH6-mediated Ub transfer. Collectively my results showed that UbcH6 relies on ubiquitin molecules from E3s or substrate modified with polyUb chains to serve as the source of Ub^B. E3-bound polyUb can greatly increase the local concentration of Ub to compensate for the weak backside Ub-binding affinity. Thus, UbcH6 utilises a distinct Ub^B-stimulation mechanism that is somewhat different to the UbcH5 family of E2s.

4.2 Results

4.2.1 Purification of UbcH6^{core} wild-type (WT) and S68R

UbcH6^{core} WT and S68R mutant were cloned in pRSFDuet vector containing an N-terminal His-tag followed by a TEV cleavage site. Protein purification method for both the proteins was same. Below I have shown method for purifying UbcH6^{core} WT. His-tagged UbcH6^{core} WT was purified using 30 mL Ni²⁺ beads on a gravity column. Protein was eluted (for buffers used see Section 2.2.2) and run on a SDS gel to check for purity (Figure 4-1A). Fractions were pooled together and dialysed against buffer containing 50 mM Tris-HCl 7.6, 0.2 M NaCl and 5 mM β -mercaptoethanol with TEV (see section 2.5.1) overnight at 4 °C. The next day, the completeness of the TEV cleavage was assessed on an SDS gel (Figure 4-1B). The cleaved protein was passed back onto Ni²⁺ beads to remove any uncleaved protein. The cleaved protein was collected in the flow through and assessed by SDS-PAGE (Figure 4-1C). Subsequently protein was purified using cation exchange chromatography. Protein from Ni²⁺ pass back was diluted with buffer containing 50 mM MES 6.5 and 1 mM DTT to bring down the pH of the protein solution. The diluted protein was then loaded onto a 20 mL Source S column (buffers see section 2.2.2). A representative chromatogram for the elution from a Source S column is shown in Figure 4-1D. Peak fractions containing the protein were pooled and concentrated using Amicon ultra centrifugal filters. During concentration, protein was buffer exchanged to a buffer containing 50 mM Tris 7.6, 0.2 M NaCl and 1 mM DTT as UbcH6^{core} is less stable in low NaCl and pH conditions (UbcH6^{core} was eluted at 50 mM NaCl). After concentration, protein was loaded onto a gel filtration column (S75 10/300) (Figure 4-1E). Peak fractions were analysed by SDS-PAGE (Figure 4-1F). All fractions shown in Figure 4-1F were pooled, aliquoted, snap frozen in liquid nitrogen and stored at -80 °C.

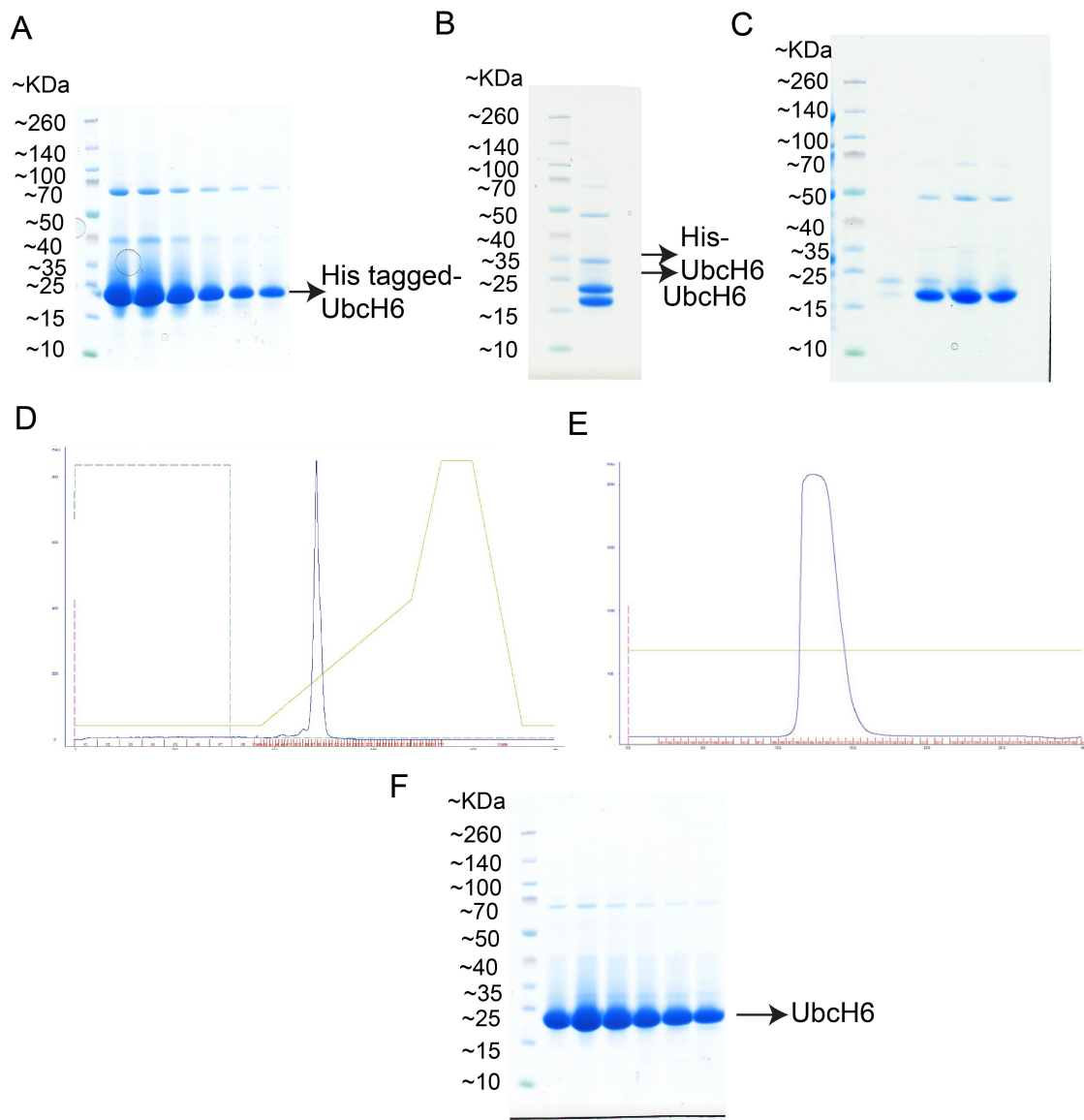


Figure 4-1: Purification of UbchH6^{core} WT (A) SDS gel after Ni²⁺ pull down of UbchH6^{core}. (B) SDS gel showing UbchH6^{core} before and after TEV cleavage. (C) SDS gel showing UbchH6^{core} after Ni²⁺-agarose pass back. (D) Chromatogram showing the elution profile of UbchH6^{core} from a 20 mL Source S column. The biggest peak fraction contains UbchH6^{core}. (E) SD75 gel filtration chromatography elution profile. The peak fraction contains UbchH6^{core}. (F) SDS gel showing fractions eluted from the peak shown in (E).

4.2.2 Non-covalent Ub binds to UbchH6^{core} weakly

To analyse the binding between Ub and UbchH6^{core}, my lab colleague, Mark Nakasone, performed NMR experiments with ¹⁵N-labelled Ub and UbchH6^{core} WT. Here, we titrated different concentrations of UbchH6^{core} (from ~0.3 mM to ~2 mM) against ¹⁵N-labelled Ub (~0.305 mM). As a control, we titrated UbchH5B WT to ¹⁵N-labelled Ub. We used NMR chemical shift perturbation (CSP) mapping to record signals of UbchH5B and UbchH6^{core} bound to Ub. In Figure 4-2, I have shown CSP

plots for UbcH5B bound to ^{15}N -labelled Ub (Figure 4-2A) and UbcH6^{core} bound to ^{15}N -labelled Ub (Figure 4-2B). The CSP plots (Figure 4-2A and B) show signals indicating interactions with Ub for both E2s. Despite weak CSP signals for UbcH6^{core} (Figure 4-2B) as compared to that of UbcH5B (Figure 4-2A), the Ub residues that undergo CSPs upon binding to UbcH5B and UbcH6^{core} were similar. Figures 4-2B and 4-3 show that Ub's Thr7, Ile13, ALA46, Lys48 and Leu71 undergo significant CSPs upon binding to UbcH6^{core}.

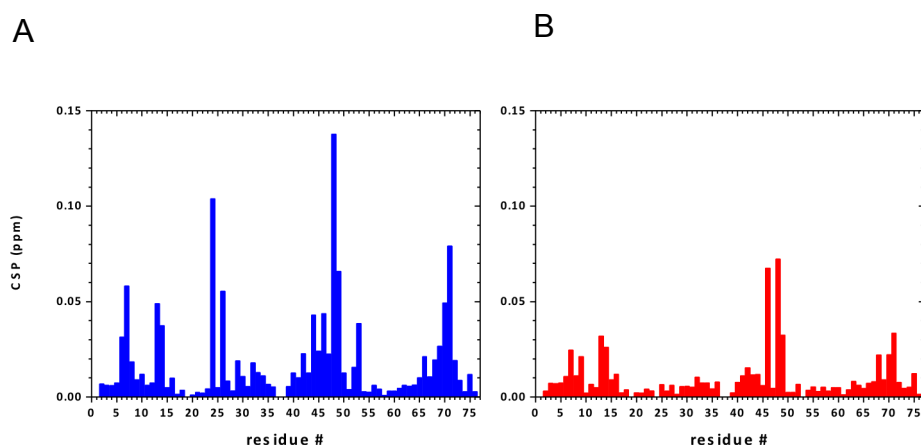


Figure 4-2: Chemical perturbation shifts (CSP) plots of Ub bound to UbcH5B and UbcH6^{core}. (A) CSP plot in blue to show signals observed when ^{15}N -labelled Ub binds to UbcH5B. On x-axis is the Ub residue number and y-axis indicates chemical shift perturbation. (B) CSP plot in red to show signals observed on ^{15}N -labelled Ub binding to UbcH6^{core}. On x-axis is the Ub residue number and y-axis indicates chemical shift perturbation

Previous studies showed that the binding affinity between UbcH5 family E2s and Ub is between 200-300 μM [36, 40]. To measure the binding affinity between UbcH6^{core} and Ub, we titrated UbcH6^{core} to ^{15}N -labelled Ub. Unfortunately, we could not saturate the binding even at 2 mM UbcH6^{core}, indicating a very weak interaction. Together, these results suggest that UbcH6^{core} contain a weak non-covalent binding surface for Ub and the interaction likely occurs via UbcH6^{core}'s backside surface.

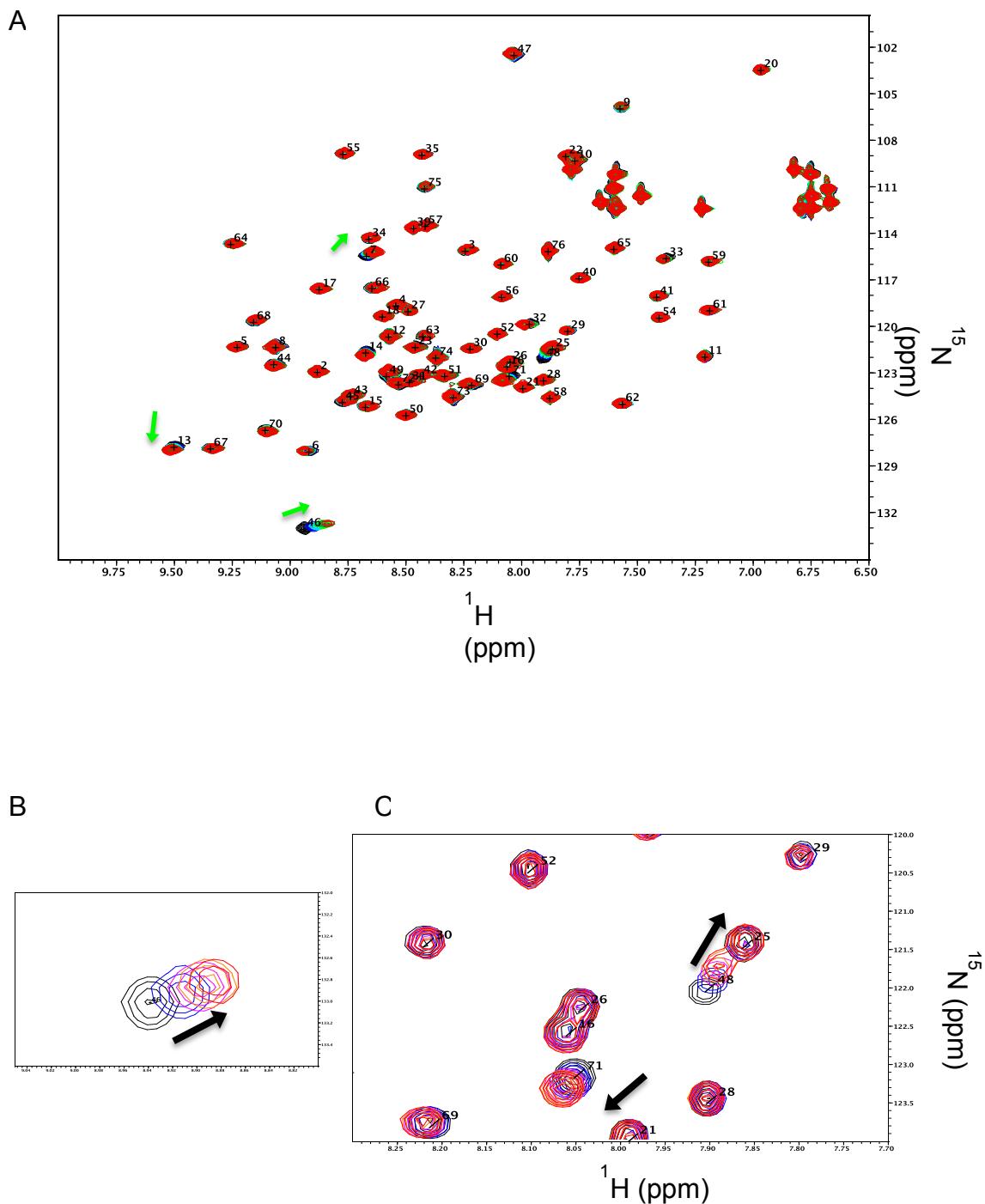


Figure 4-3: Chemical shift perturbation data for UbH6^{core} interactions with Ub. (A) ¹H-¹⁵N HSQC spectra for ¹⁵N-labelled Ub alone (black) and titrated with increasing concentrations of UbH6^{core} (0.3 mM is in blue, 1 mM is in pink and 2 mM is in red). (B) Lys 48 of labelled Ub overlaid with five different points of concentration shown in different colour, with red be the highest concentration. (C) Chemical shifts shown for Lys 48, Lue71.

Since, peaks obtained from UbcH5B and UbcH6 were from similar residues, I mapped CSPs from ^{15}N -Ub-UbcH6 spectra on Ub (Figure 4-4A) and Ub^{B} -UbcH5B from Ub^{B} -UbcH5B-Ub-cIAP1 structure (unpublished, chapter 3)(Figure 4-4B). From the figure it is evident that the mapped residues are interacting with UbcH5B's backside. Therefore, it seems likely that Ub residues undergoing CSP when interacting with UbcH6 is due to non-covalent binding to UbcH6's backside.

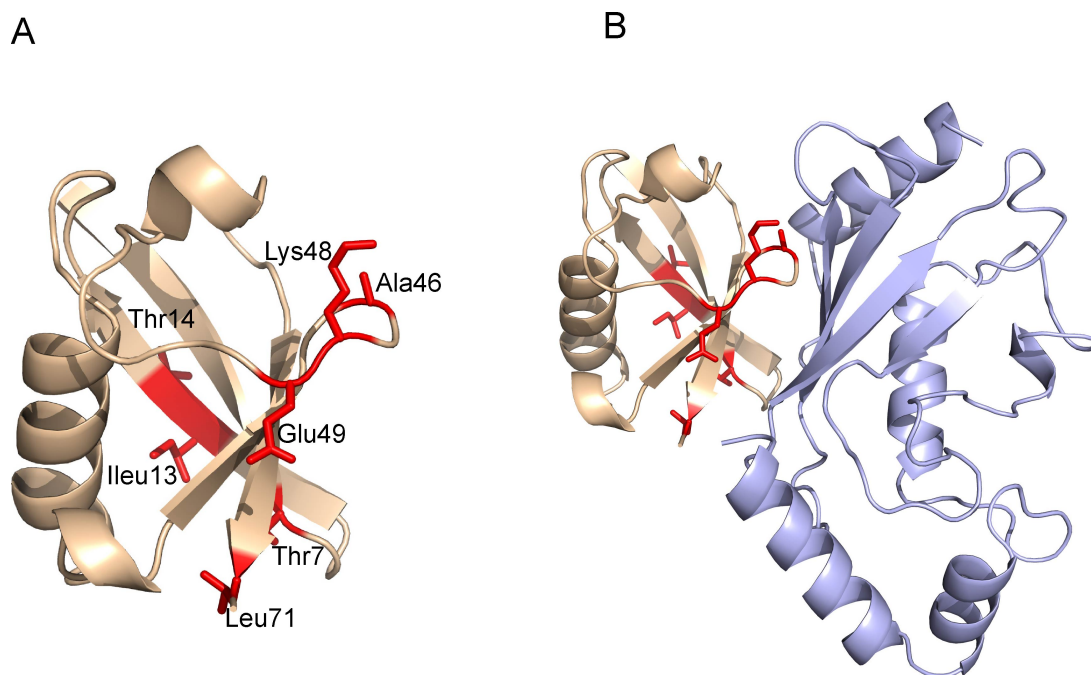


Figure 4-4: CSPs mapped on Ub's surface. (A) CSPs from figure 4-2 mapped onto Ub's surface in red. (B) Mapped CSPs on Ub^{B} -UbcH5B structure from Ub^{B} -UbcH5B-Ub-cIAP1 structure (unpublished, Chapter 3). Ub^{B} is coloured in wheat, UbcH5B in light blue.

4.2.3. SPR analysis also showed weak UbcH6-Ub binding

Since NMR did not give me exact K_d for UbcH6-Ub binding, I went on and performed SPR experiment to measure the binding affinity. I captured GST-tag Ub on a CM5 chip that was coupled with anti-GST antibody and binding was measured for range of UbcH6 concentrations, with 1mM as the highest and 0.2 μM as the lowest concentration. Sensogram and binding curve is shown in below Figure 4-5. Unfortunately, even at 1mM concentration, I could not saturate UbcH6 and hence did not get proper binding curve. Therefore, comparable with my NMR results, the binding affinity between UbcH6 and Ub is expected to be greater than 1mM.

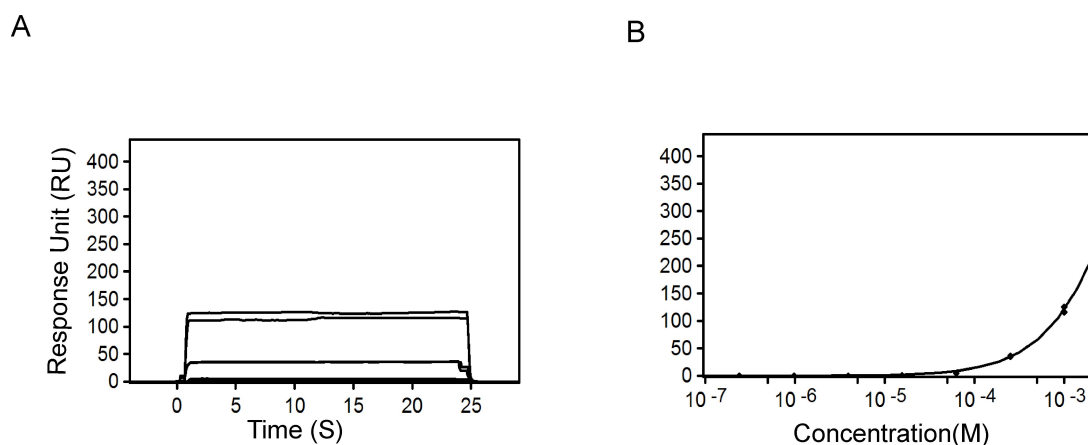


Figure 4-5: SPR binding data showing representative sensograms. (A) Sensogram for UbchH6 and GST Ub. (B) Binding curve for UbchH6 and GST Ub.

4.2.4 Stimulation by Ub^B of RING-catalysed UbchH6-mediated Ub transfer occurs at high Ub concentrations

Previous studies showed that UbchH6^{core} S68R had no effect on cIAP2 autoubiquitination as compared with UbchH6^{core} WT[41] whereas the corresponding S22R substitution in the UbchH5 family of E2s hindered RING E3-catalysed polyubiquitination [36, 38, 40, 91]. It is noteworthy that Schumacher *et al.*, in 2013 performed autoubiquitination assays in the presence of 50 μ M of Ub. My NMR and SPR results showed that the K_d for the Ub^B-UbchH6 interaction is likely greater than 1 mM. Thus, it seems likely that higher Ub concentrations may be required to observe the effect of Ub^B in UbchH6-mediated Ub transfer. To assess whether Ub can stimulate UbchH6-mediated reactions, I performed lysine discharge assays in the presence of varying Ub Δ GG (deleted Gly-Gly motif at the C terminus of Ub, so that it cannot be charged by E1) concentrations. Detailed methodology for lysine discharge assay is shown in Methods section (See section 2.7). Briefly, I precharged both UbchH6^{core} WT and S68R with ³²P-Ub and then chased with a cocktail containing cIAP1(B3-C), lysine and varying concentrations of Ub Δ GG. Samples were removed to monitor the disappearance of UbchH6^{core}~³²P-Ub bands over time. Figure 4-6 shows that the rates of the disappearance of UbchH6^{core} WT~Ub band were similar in the presence of 0, 20 and 300 μ M Ub. However, in the presence of 1 mM Ub Δ GG, UbchH6^{core} WT~Ub band disappeared faster than in the absence of Ub Δ GG indicating Ub-mediated stimulation (Figure 4-6). Moreover, incorporation of an S68R substitution in UbchH6 abrogated Ub-mediated stimulation, suggesting UbchH6's

backside interaction with Ub is important for enhanced activity. Together my results showed that Ub^B stimulates cIAP1-UbcH6-catalysed reactions provided that excess Ub concentrations are high enough to at least partially saturate UbcH6's backside.

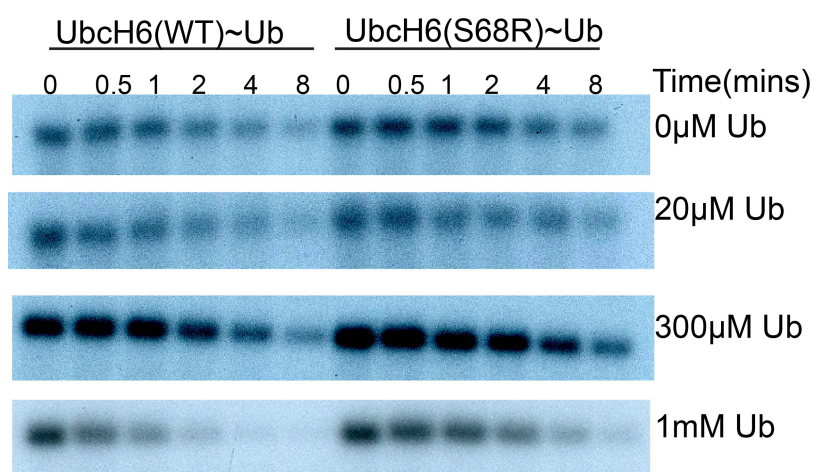


Figure 4-6: Lysine discharge of UbcH6 WT and S68R with and without Ub Δ GG at indicated concentrations

4.2.5 Assessing the effects of Ub^B on cIAP1-UbcH6-catalysed autoubiquitination

Schumacher *et al.*, in 2013 showed that, UbcH6^{core} S68R had no effect on cIAP2 autoubiquitination as compared with UbcH6^{core} WT. In their assay, they only used 50 μ M Ub. Low Ub concentrations might explain their observation since I only saw Ub^B-stimulation at 1 mM Ub. To further investigate these activity differences, I performed an autoubiquitination assay under similar conditions but for using cIAP1(B3-C) and *Arabidopsis* Uba1. cIAP1(B3-C) is comparable to the cIAP2 construct that was used by [41]. My reaction conditions were similar to those in the Frances-Rose study (2013), but I used a higher E1 concentration to ensure that UbcH6^{core} is constantly recharged with Ub during the reaction and precharged the E2 prior to adding E3. In contrast to the aforementioned study, I found that UbcH6^{core} WT catalysed cIAP1 autoubiquitination faster than UbcH6^{core} S68R (Figure 4-7A and B; see Section 2.11 for detailed method of autoubiquitination assay). Since the total concentration of Ub in cells is in the low μ M range [154, 155], I also performed autoubiquitination assay with 10 μ M ³²P-Ub (Figure 4-7A). Even at low Ub concentrations, autoubiquitination of cIAP1(B3-C) is faster with UbcH6^{core} WT than UbcH6^{core} S68R. I further went ahead and quantified the gel. I performed three (n=3) independent autoubiquitination

assays of cIAP1 with UbcH6 WT and S68R under same conditions as mentioned above with 10 μ M Ub. Results from quantification were analysed on Image lab from Biorad. (Figure 4-7C and D). The error bars in Figure 4-7D indicate standard deviation.

In cells, substrate binding helps to stabilise some E3s by preventing their autoubiquitination and degradation [40, 156]. Since mature SMAC is the substrate for IAPs, I next examined how Ub^B-binding on UbcH6 affects cIAP1(B3-C)-mediated ubiquitination of mature SMAC (Figure 4-7C). The reactions were performed similarly to cIAP1 autoubiquitination where UbcH6^{core} WT and S68R were precharged with ³²P-Ub and then cIAP1 (B3-C) and 5 μ M matured SMAC were added. Figure 4-7C shows that SMAC ubiquitination was faster in the presence of UbcH6^{core} WT than UbcH6^{core} S68R.

It is unclear why Frances-Rose et al. did not observe the backside effect for UbcH6. It is speculative that the E1 concentration that they used was too low and hence it was not sufficient to recharge UbcH6 fast enough, thereby causing the E1-E2 reaction to become the rate-limiting step. We found that UbcH6 charging was not as efficient as UbcH5B charging. In my assays, it was surprising that 10 μ M Ub was sufficient to observe Ub^B-stimulation in the autoubiquitination assays but not the lysine discharge assays. In the latter, I only observed Ub^B stimulation when an excess of 1 mM Ub was present. The major difference between the two assays is that in the autoubiquitination assays, cIAP1(B3-C) is modified with polyUb, whereas in the lysine discharge assay, Ub is discharged to lysine and hence cIAP1(B3-C) is not modified. This raises the question whether polyUb modified on cIAP1(B3-C) can function as the source of Ub^B. If so, this would enable polyUb to reach UbcH6's backside in a *cis* arrangement thereby greatly increasing the local Ub concentration and overcoming the high Ub concentration requirement.

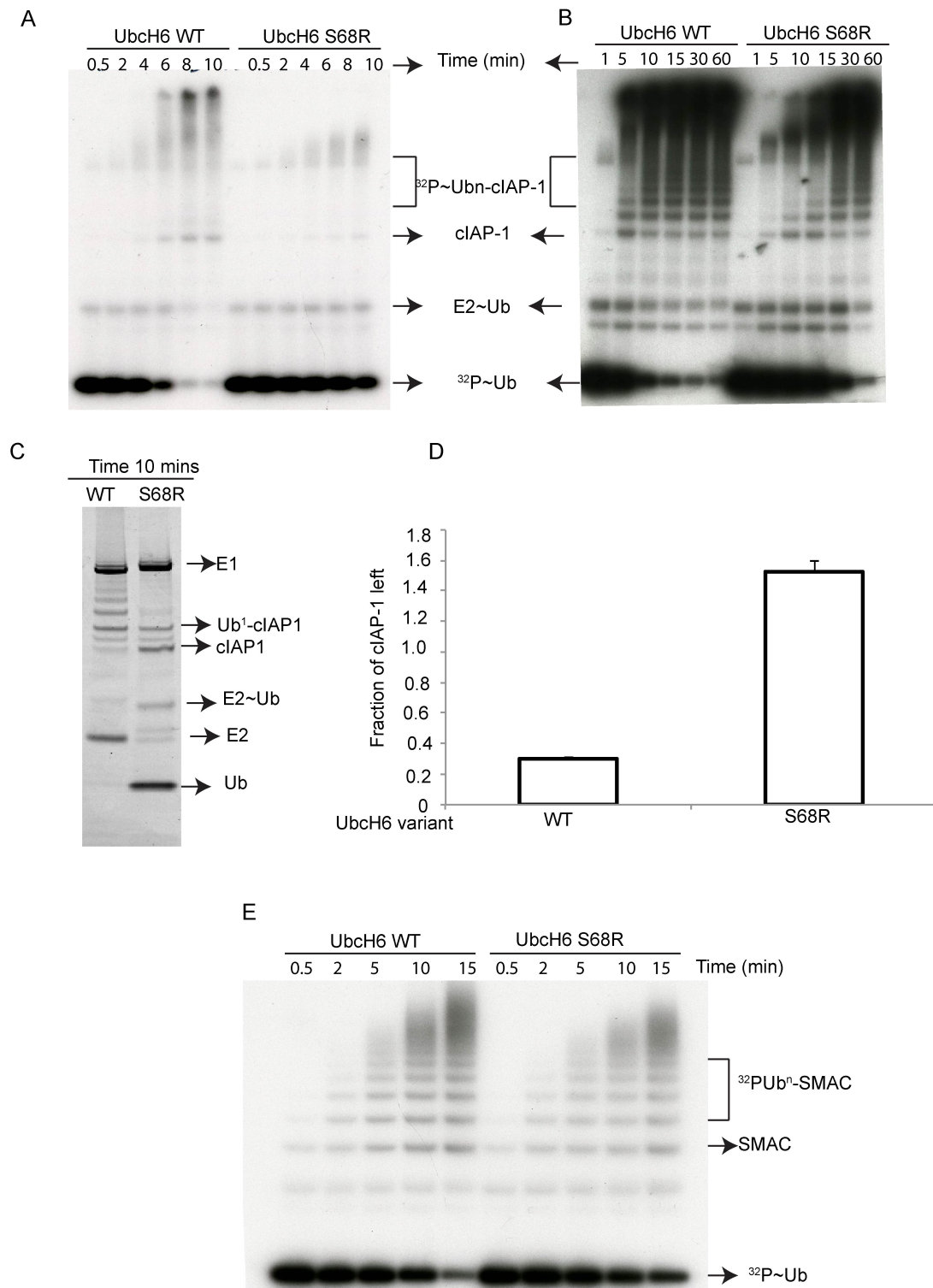


Figure 4-7: Ubiquitination assays for UbcH6^{core} WT and S68R. (A) Autoradiogram showing cIAP1(B3-C) autoubiquitination in presence of UbcH6^{core} WT and UbcH6^{core} S68R over the time with 10 μM ³²P-Ub. (B) Autoradiogram of cIAP1(B3-C) autoubiquitination in presence of UbcH6^{core} WT and UbcH6^{core} S68R over the time with 50 μM ³²P-Ub. (C) A representative non-reduced SDS-PAGE gel showing effects of UbcH6 mutations in cIAP1 autoubiquitination at the end of 10 mins. (D) A bar graph showing fraction of cIAP1 left in (C). (E) Autoradiogram of cIAP1(B3-C)-mediated ubiquitination of mature SMAC with UbcH6^{core} WT or UbcH6^{core} S68R over time with 50 μM ³²P-Ub.

4.2.6 Ubiquitinated cIAP1 acts as the source of Ub^B

Our lab has previously shown that polyUb modified-BIRC4 can serve as a source of Ub^B to stimulate UbcH5B-catalysed Ub transfer [40, 92]. To determine whether polyUb modified-cIAP1(B3-C) can function as a source of Ub^B to stimulate UbcH6-catalysed Ub transfer, I performed lysine discharge assays using UbcH6^{core} WT and S68R with autoubiquitinated cIAP1(B3-C). I generated polyUb-cIAP1(B3-C) by incubating cIAP1(B3-C) with E1, Mg²⁺-ATP, UbcH5B and Ub and stopped the reaction by adding EDTA and apyrase. For control reactions, E1 was omitted. In a separate reaction, I charged UbcH6^{core} WT or S68R with ³²P-Ub and stopped charging after 15 minutes by adding apyrase and EDTA. I then added polyUb-cIAP1(B3-C) or control (described above) to the precharged reactions of UbcH6^{core} WT~³²P-Ub or UbcH6^{core} S68R~³²P-Ub and monitored the disappearance UbcH6^{core}~³²P-Ub band. Similar rates of discharge were observed for UbcH6^{core} WT and S68R with the control cIAP1(B3-C) mixture, whereas the polyUb-cIAP1(B3-C) mixture stimulated the discharge of UbcH6^{core} WT~³²P-Ub but had no effect on the discharge of UbcH6^{core} S68R~³²P-Ub as compared to the control (Figure 4-8). Together these results demonstrate that covalently attached Ub molecules on cIAP1 function as a source of Ub^B to stimulate UbcH6-catalysed Ub transfer.

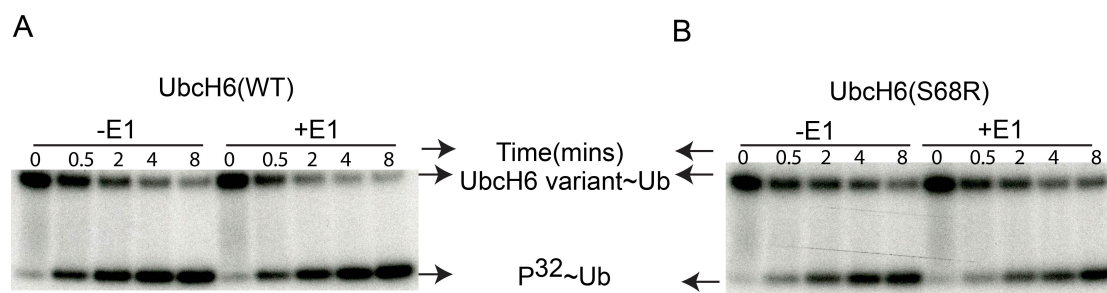


Figure 4-8: Non-reduced autoradiogram showing disappearance of UbcH6^{core} WT~³²P-Ub (A) Lysine discharge assays showing the disappearance of UbcH6^{core} WT~³²P-Ub catalysed by control (-E1, left) and polyUb-cIAP1 (B3-C) (+E1, right). (B) Lysine discharge assays showing the disappearance of UbcH6^{core} S68R~³²P-Ub catalysed by control (-E1, left) and polyUb-cIAP1(B3-C) (+E1, right).

4.2.7 Ubiquitination of cIAP2 with UbcH6^{core} WT and S68R

I was curious to find out why I see a difference between UbcH6^{core} WT and S68R with cIAP1 while Frances-Rose Schumacher et al., observed no difference between the two in their study with cIAP2. To further explore this difference, I decided to perform autoubiquitination assays with cIAP2 with UbcH6^{core} WT and S68R. I generated the same fragment of cIAP2 (residues 255-C) that was used by Frances-Rose Schumacher et al. in their study. My assay conditions were exactly the same as mentioned in section 4.2.5 and I again performed autoubiquitination assays with low (10 μ M) and high (50 μ M) ³²P-Ub concentrations (Figure 4-9A and B respectively). I further went ahead and quantified the gel. I performed three (n=3) independent autoubiquitination assays of cIAP2 with UbcH6 WT and S68R under same conditions as mentioned above with 10 μ M Ub. Results from quantification were analysed on Imagelab from Biorad. (Figure 4-9C and D). The error bars in Figure 4-9D indicate standard deviation. Consistent with my cIAP1 results presented in Section 4.2.5, I found that cIAP2 catalysed autoubiquitination faster with UbcH6^{core} WT than UbcH6^{core} S68R, regardless of whether the Ub concentration was high or low. Thus, it seems likely that the E1 concentration used in the study by Frances-Rose Schumacher et al. was too low to keep UbcH6 constantly charged with Ub, thereby causing the E1-E2 reaction to become the rate-limiting step.

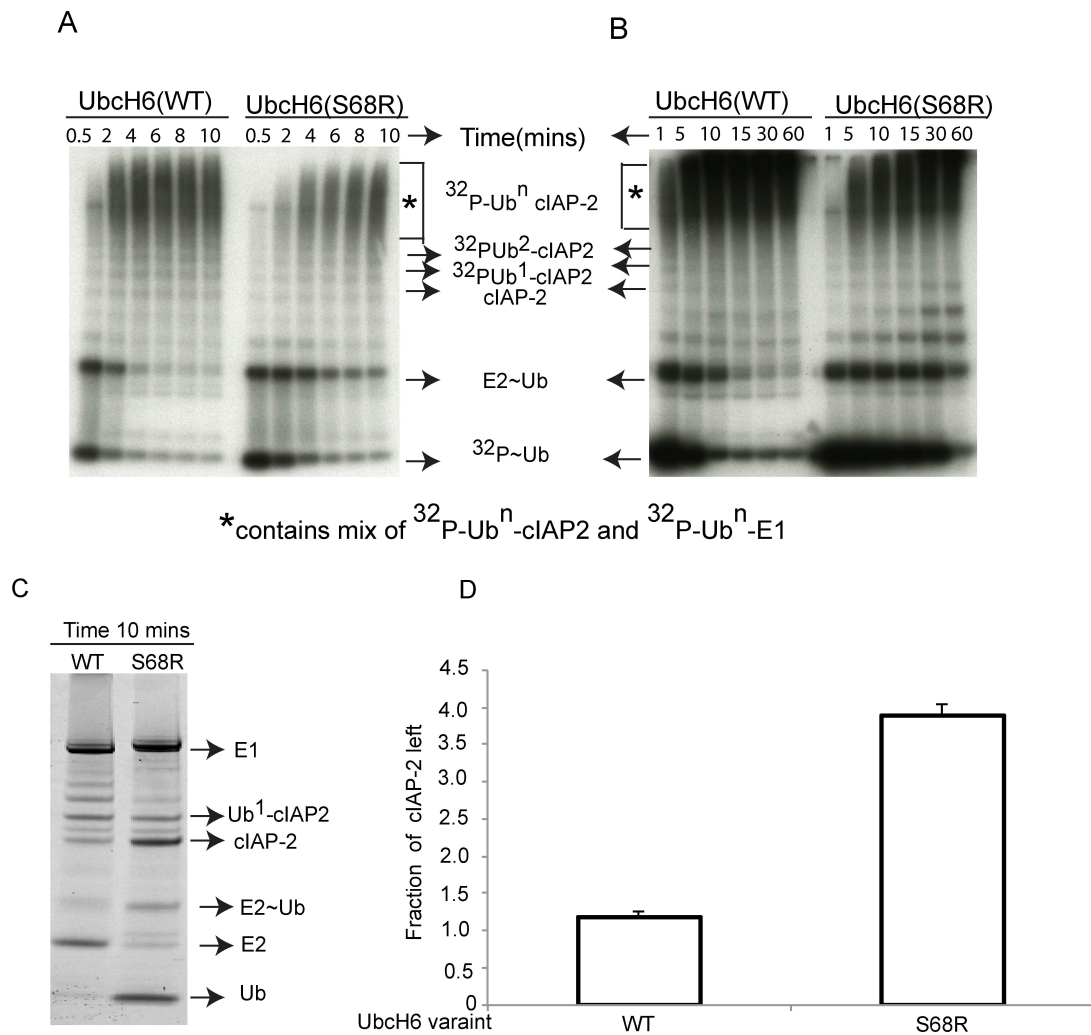


Figure 4-9: Autoubiquitination assays of cIAP-2 for UbcH6 WT and S68R . (A) Autoradiogram of pulsed-chased assay showing cIAP-2 autoubiquitination with UbcH6 WT and UbcH6 S68R over time with 10 μM $^{32}\text{P-Ub}$. (B) Autoradiogram of pulsed chased assay showing cIAP-2 autoubiquitination with UbcH6 WT and UbcH6 S68R over time with 50 μM $^{32}\text{P-Ub}$. (C) A representative non-reduced SDS-PAGE gel showing effects of UbcH6 mutations in cIAP2 autoubiquitination at the end of 10 mins. (D) A bar graph showing fraction of cIAP2 left in (C).

4.3 Discussion

At the beginning of the project, I was interested in understanding why UbcH6 lacks backside binding and stimulation as reported previously [41] despite sharing sequence and structural homology with the UbcH5 family of E2s (Section 1.5.3, Figure 1-8). To study this, I used the core domain of UbcH6 (the same construct that was previously used by Frances-Rose Schumacher et al.,) to investigate the role of UbcH6-backside binding of Ub. In 2015, our lab showed that non-covalent binding of Ub to the backside of UbcH5B enhances RING E3's affinity for UbcH5B~Ub and the overall catalytic efficiency of the RING E3-UbcH5B~Ub complex to facilitate Ub transfer. Initially I examined whether I could observe binding between the backside of UbcH6^{core} and non-covalent Ub. First I performed NMR experiments using ¹⁵N-labelled Ub and found that addition of UbcH6^{core} WT caused CSPs in Ub, suggesting binding between Ub and UbcH6. Furthermore these CSPs were similar to CSPs observed when UbcH5B was added to ¹⁵N-labelled Ub, suggesting the same surface on Ub is involved in binding both UbcH6 and UbcH5B. When these CSPs were mapped onto Ub, I found that this surface is involved in non-covalent Ub interaction with UbcH5's backside. Thus, my data suggest that UbcH6 harbours a backside Ub-binding property. However, the backside Ub binding affinity is very weak. The estimated K_d is likely greater than 1 mM since I only observed binding on SPR when 1 mM Ub was added to UbcH6 and at 2 mM UbcH6^{core} was insufficient to saturate ¹⁵N-labelled Ub in NMR experiments.

Given that UbcH6 harbours a Ub^B binding site, I then explored whether Ub^B could stimulate UbcH6-catalysed Ub transfer similar to that observed in the UbcH5 family of E2s (see Section 4.3; [36, 40]). First I performed lysine discharge assays and found that addition of 1 mM of Ub was necessary to stimulate cIAP1-UbcH6-catalysed Ub transfer. This process is initiated via UbcH6's backside, as S68R substitution was unable to support stimulation. These data are consistent with the weak Ub-UbcH6 interactions observed in SPR and NMR analyses. However, my data contradicted a previous finding [41], where there were no observable differences between UbcH6^{core} WT and S68R in cIAP2-catalysed autoubiquitination assay. I performed similar reactions as described in this previous study using cIAP1 and cIAP2. In contrast to these previous findings [43], I found that both cIAP1 and cIAP2 catalysed autoubiquitination faster in the presence of UbcH6^{core} WT than UbcH6^{core} S68R. My reaction conditions were nearly identical to that reported previously [41] except I used

a higher E1 concentration and I precharged UbcH6 with Ub prior adding E3. Frances-Rose et al. used only 10 nM E1 and did not precharge UbcH6 with Ub. I used a high E1 concentration and precharged UbcH6 with Ub to ensure that UbcH6 is constantly charged with Ub throughout the reaction cycle so that the E2-E3 reaction is the rate-limiting step and not the E1-E2 reaction. It seems likely that in their reaction, the E1-E2 reaction is rate-limiting. Hence they did not observe differences because the E1-UbcH6^{core} WT and E1-UbcH6^{core} S68R transthioylation reactions probably occur at the same rate.

One surprising observation is that in my autoubiquitination assays, 10 μ M Ub was sufficient to enable Ub^B-stimulation whereas in the lysine discharge assay, 1 mM Ub was required to stimulate Ub transfer. The major difference between the two assays is the generation of polyUb-cIAP1 during the autoubiquitination reaction. To assess whether a Ub molecule from polyUb-modified cIAP1 could serve as the source of Ub^B for UbcH6, I generated polyUb-cIAP1 and used that in lysine discharge assays. I found the polyUb-cIAP1 readily stimulated the discharge of UbcH6^{core} WT~Ub but not the S68R counterpart. It is noteworthy that with lysine discharge assay, I only observed stimulation in the presence of 1 mM Ub but now in the absence of 1 mM Ub, polyUb-cIAP1 readily stimulated the discharge.

Collectively my results show that UbcH6 harbours a weak backside Ub-binding affinity. Cellular Ub concentrations are \sim 20-85 μ M and therefore UbcH6 is unlikely to use free Ub as the source of Ub^B. Our lab previously showed that RING E3 binding could lower the K_d for UbcH5B~Ub's affinity for Ub^B (from \sim 300 to 17 μ M; [40]). I do not know whether RING E3 binding to UbcH6 could low Ub^B binding affinity. Given that at 300 μ M Ub, there was no observable stimulation in lysine discharge assays, I speculate that the K_d for Ub^B-UbcH6 would remain quite high even in the presence of RING E3. Thus it is unlikely that UbcH6 could use free Ub as the source of Ub^B. However, once E3 is decorated with Ub via autoubiquitination, the ubiquitin molecules attached to the E3 can serve as a source of Ub^B (see Section 4.2.6). This would greatly increase the effective concentration of Ub owing to the *cis* arrangement, thereby overcoming the weak UbcH6-backside Ub binding affinity. This mechanism is somewhat different to UbcH5 family E2s, where these E2s can also utilise free Ub as the source of Ub^B.

Together with all the above discussions, it is clear that in spite of weak binding between Ub and UbcH6, UbcH6 still retains its backside binding ability. A previous

study by our group suggests that Ub^B stabilises RING-E2~Ub complex by modulating the flexibility of E2's $\alpha 1\beta 1$ loop. [40] This mechanism of backside stimulation via the $\alpha 1\beta 1$ loop was also observed in my UbB-UbcH5B-Ub-cIAP1 structure (see chapter 3). UbcH6's UBC domain resembles the UBC domains of UbcH5 family E2s, but its $\alpha 1\beta 1$ loop contains an Asn substitution in place of the UbcH5 Gln that mediates Ub^B interactions with Ub^D. Initially, I believed this could be the reason for UbcH6's weak binding, so I substituted UbcH6's $\alpha 1\beta 1$ Asn with Gln and but observed no differences in Ub transfer in lysine discharge or autoubiquitination assays. These data suggest that there is more to the mechanism of Ub^B-stimulation than stabilising the $\alpha 1\beta 1$ loop of E2. It will require more structural, biophysical and biochemical understanding to elucidate Ub^B's mechanism for stimulating RING-catalysed Ub transfer.

Chapter 5

Study of RING mediated substrate poly- ubiquitination

5.1 Aims and Objectives

How RING E3s coordinate Ub transfer from E2~Ub to a particular substrate lysine residue and subsequently promote Ub chain elongation are poorly understood. To investigate the latter step of the reaction, we sought to develop a model system for crystallisation trials that contains an E3 bound to E2~Ub and a monoubiquitinated substrate. Since numerous Cbl structures have been determined previously and several Cbl substrates are well-characterised, this ubiquitin ligase system was selected [62, 73, 85].

In 2000, Zheng *et al.* solved the first structure of c-Cbl in complex with UbcH7 and ZAP70 peptide, where E2's catalytic cysteine faces away from substrate and is ~70 Å from the substrate-binding site. This raised the question of how substrate ubiquitination occurs (Figure 5-1A) [62]. Subsequently our lab showed that phosphorylation of Tyr371 in c-Cbl activates its ligase activity by inducing conformational changes that enable juxtaposition of E2's catalytic cysteine and the substrate binding site [85] (Figure 5-1B). Furthermore, our lab has determined a crystal structure of Tyr363 phosphorylated Cbl-b bound to E2~Ub and a ZAP70 peptide [73] (Figure 5-1C).

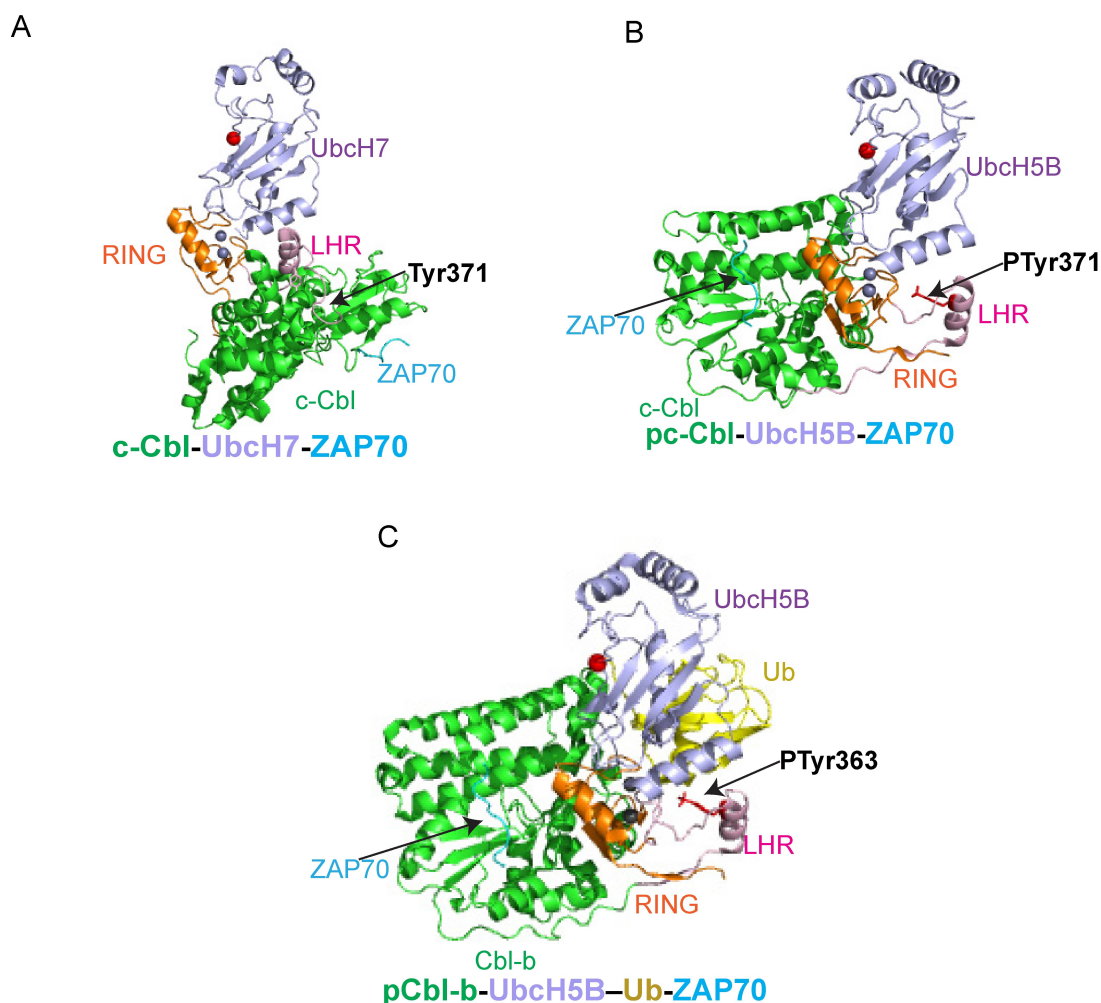
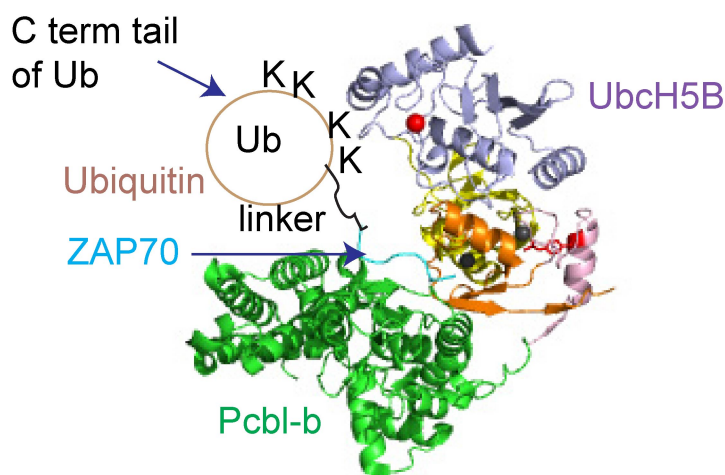


Figure 5-1: Structures of Cbl with E2 and ZAP70 peptide. Cbl is coloured in orange, LHR in pink, UbcH5B and UbcH7 is in light blue, ZAP70 peptide in cyan, catalytic Cys is shown in red sphere and Zn^{2+} ions in grey spheres. (A) Structure of c-Cbl-UbcH7-ZAP70 (PDB ID: 1FBV) (B) Structure of pc-Cbl-UbcH5B-ZAP70 (PDB ID: 4A4C) (C) Structure of pCbl-b-UbcH5B-Ub-ZAP70 (PDB ID: 3ZNI)[73]. The distance between E2's catalytic cysteine and ZAP70 peptide is $\sim 27\text{\AA}$. ZAP70 peptide does not have any lysines.

In this structure, E2-Ub faces ZAP70 peptide in an arrangement similar to that observed in the structure of pTyr371-c-Cbl-E2-ZAP70 peptide complex (Figure 5-1B). In the aforementioned complex structures, no lysine residues are present in ZAP70 peptide. Given the proximity of ZAP70 peptide to the E2-Ub thioester bond, we reasoned that generation of a Ub fused to ZAP70 (referred to as Ub-ZAP70 from now onwards) peptide or other Cbl substrate peptides might function as a “ubiquitinated substrate” mimetic. Since it is difficult to generate a site-specific monoubiquitinated substrate to study Ub chain elongation process, in this chapter I

discuss my development of a Ub-fusion strategy to study Cbl-mediated Ub chain elongation. A model demonstrating the objective of this chapter is shown in Figure 5-2.



Schematic of
pCbl-b-UbcH5B-Ub-Ub-ZAP70

Figure 5-2: Schematic of Ub-ZAP70 peptide in pCbl-b-UbcH5B-Ub ZAP70 structure (PDB ID: 3ZNI) [73]. In this figure, Ub's C-terminus is attached to a linker, which in turn is attached to the N-terminus of ZAP70 peptide. The model suggests that several Ub lysine residues are in close proximity to E2's catalytic Cys85.

In the above figure, Ub is fused via its C-terminal tail to a linker that is followed by ZAP70 peptide. The model suggests that Ub can fill the gap between E2's active site and the substrate-binding site. In the model, my substrate mimetic, Ub-linker-ZAP70, has several lysine sites that potentially sit in close proximity to E2's active site (Figure 5-1C).

5.2 Results

5.2.1 Generation of Ub fused to Cbl substrate peptide (Ub-peptide)

To generate a monoubiquitinated substrate mimetic, I fused Ub to the N-terminus of several Cbl substrate peptides. Given the proximity of ZAP70 peptide and the E2~Ub thioester bond in the crystal structure (Figure 5-1C), we hypothesised that each Ub moiety in our Ub-fused Cbl substrate peptides would be sufficiently proximal to the E2~Ub thioester bond to function as an acceptor. Using this strategy, I fused Ub to the N-terminus of ZAP70, Src, EGFR and c-MET peptides (Table 5-1). These peptides

have been shown to bind c-Cbl and Cbl-b's substrate-binding domain upon tyrosine phosphorylation [105, 121, 157]. Initially, my supervisor Danny Huang designed several constructs in which three Gly-Gly-Ser linkers were used to fuse Ub to the N-terminus of these peptides as illustrated in Figure 5-3A.

Table 5-1: Protein sequences of ZAP70, Src, EGFR and c-MET with phosphorylated Tyrosine (Y) residue shown in red

ZAP70	TLNSDGYTPEPA
Src	RLIEDNEYTARQG
EGFR	SNESVDYRATFPE
c-MET	LQRYSSDPTGA

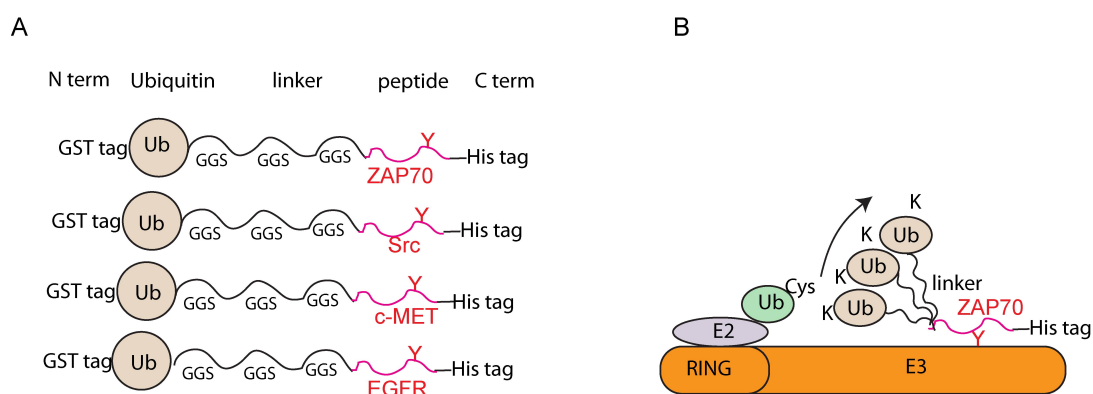


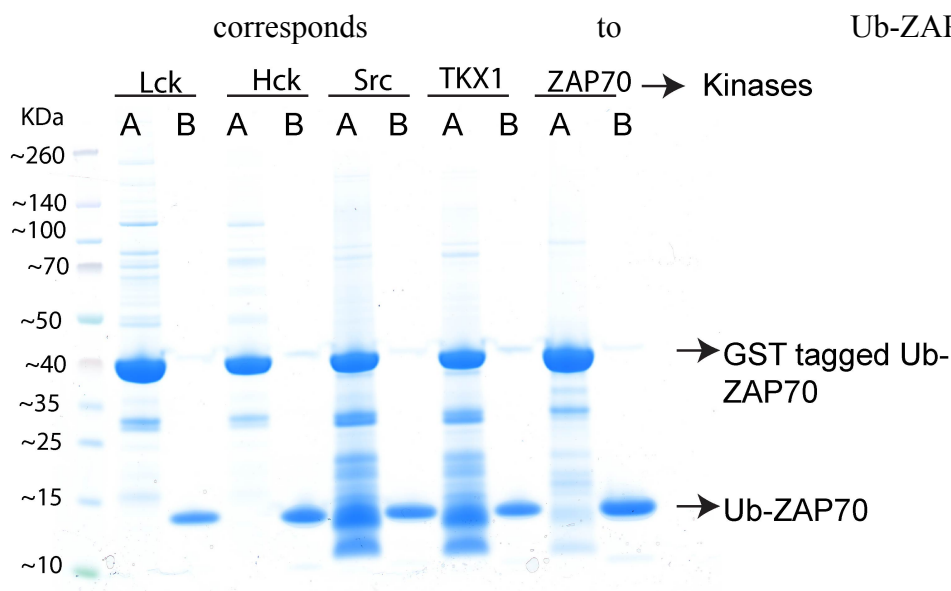
Figure 5-3: Generation of Ub fusion peptides to function as substrates to elucidate RING-mediated substrate polyUbiquitination. (A) All Ub fusion constructs contain an N-terminal GST followed by Ub, a flexible linker (3GGS repeats) and a substrate peptide (ZAP70, Src, c-MET, EGFR). The TYR residue marked in red must be phosphorylated to bind to E3. There is a His tag at the C-terminus of each construct. (B) Desired E3-E2-Ub-substrate system with RING E3 bound to E2-Ub and substrate (Ub fusion peptide).

All the constructs were cloned into the vector pGEX-4T1, which contains an N-terminal GST-tag followed by a thrombin cleavage site. We also inserted a 6xHis-tag at the C-terminus to facilitate purification. To phosphorylate the tyrosine on the substrate peptide, I co-expressed these constructs with His-MBP-tagged tyrosine kinases. It is noteworthy that these Ub-peptides only contain one tyrosine within the peptide sequence. This co-expression strategy has been previously used in our lab to generate tyrosine phosphorylated Cbl in *E. coli* [85]. Since I didn't know which

kinase would phosphorylate these substrate peptides, I tried several kinases such as Src, ZAP70, Hck, Lck, Fyn and TKX1 that were available in the lab.

5.2.2 Test expression and purification of Ub-peptides

I transformed Ub-fused ZAP70 peptide (Ub-ZAP70) together with ZAP70, Src, Hck, Fyn, Lck or TKX1 tyrosine kinase. Small-scale protein expression and purifications were performed (see Method Section 2.3) in these GST-tagged Ub-peptides were pulled down with GSH-sepharose and cleaved with thrombin. Following thrombin cleavage, bands corresponding to the size of Ub (~10 kDa) were present in GST-Ub-ZAP70 co-expressed with ZAP70, Fyn, Lck and Src whereas co-expressions with Hck and TKX1 yielded bands of ~10 and 12 kDa that correspond to the predicated size of Ub and Ub-ZAP70 (~12 kDa), respectively. Notably, only a small fraction of the total protein



A: After Ni²⁺ pull down of Ub-ZAP70 co-expressed with kinase

B: After thrombin cleavage and GST passback of lane A

Figure 5-4: Small-scale purifications of Ub-ZAP70 co-expressed with different kinases visualised by SDS-PAGE. Lane A indicates Ni²⁺ pull down and lane B subsequent thrombin cleavage for Ub-ZAP70 co-expressed with indicated tyrosine kinases.

These bands were then subjected to analyses with mass spectrometry. Mass spectrometry analyses showed that lanes 4 and 8 contained a mixture of Ub-ZAP70 and Ub. These findings were consistent with cleavage of Ub-ZAP70 just after the C-terminal diglycine motif of the Ub moiety, thereby generating Ub rather than Ub-

ZAP70. A literature search showed that *E. coli* contains protease(s) that can cleave Ub after the C-terminal diglycine motif and this cleavage is prevalent when Ub is fused to a peptide, but reduced when fused to a folded protein [158]. Several strategies were implemented previously to resolve this issue: (1) growing cells at lower temperature [158]; (2) shorter expression time (3 hours, not overnight); (3) addition of a proline residue immediately after Ub (the Ub-Proline bond is not cleaved by Ub-specific proteases [159]); and (4) replacing C-terminal Gly-Gly motif with Ala-Ala or Ala-Ala-Pro (Figure 5-5).

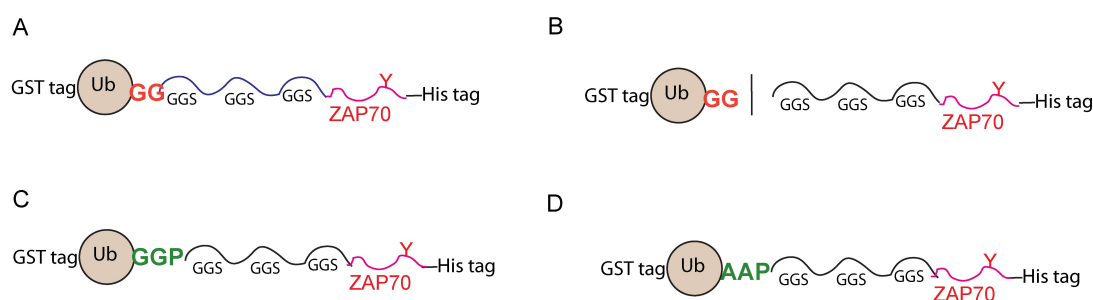


Figure 5-5: Trouble-shooting Ub-peptide cleavage in *E. coli*. (A) Design of Ub-peptide. (B) Cleavage of Ub-peptide during protein expression. (C) Replacement of Ub's C-terminal Gly-Gly motif with Gly-Gly-Pro. (D) Replacement Ub's C-terminal Gly-Gly motif with Ala-Ala to overcome cleavage problem.

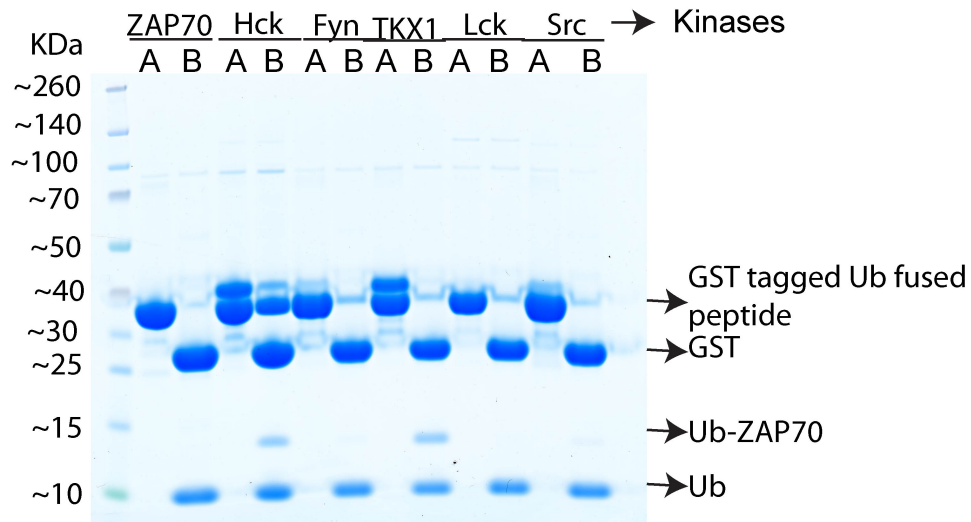
Based on these findings, I re-engineered my Ub-ZAP70 by replacing Ub's C-terminal Gly-Gly motif with Ala-Ala-Pro.

5.2.3 Test expression and purification of re-engineered Ub fused peptide

A small-scale protein expression and purification test was performed on co-expressions of the newly designed Ub-ZAP70 with Ala-Ala-Pro substitution and various kinases in *E. coli*. A new purification protocol was implemented to avoid pulling down Ub products in which the peptide fragment was cleaved. For these purifications, Ni²⁺-affinity chromatography was initially performed followed by thrombin cleavage and then GSH-sepharose chromatography to remove the GST tag (Figure 5-6). Strikingly, intact Ub-ZAP70 was recovered in every case. Thus, substitution of Ub's C-terminal Gly-Gly motif with Ala-Ala-Pro resolved the cleavage issue.

Next, to assess the phosphorylation status of Ub-ZAP70, I performed western blots using anti-phospho-tyrosine antibody on the products from the above purifications

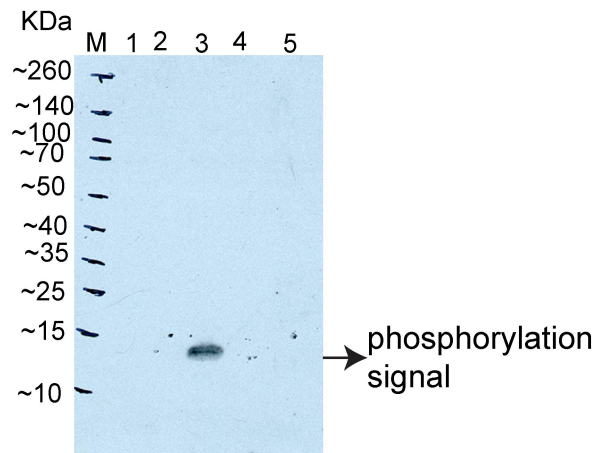
and found that Ub-ZAP70 is only phosphorylated when co-expressed with Src kinase (Figure 5-7). Hence, I was successful in developing a method for expressing phosphorylated Ub-ZAP70 (Ub-ZAP70p). Next, I scaled up production of Ub-ZAP70 and developed a method to separate phosphorylated (Ub-ZAP70p) and unphosphorylated Ub-ZAP70. In the remaining chapter, all Ub-peptide constructs contain a C-terminal Ala-Ala-Pro substitution in Ub.



A: After Ni^{2+} pull down of Ub-ZAP70 co-expressed with kinase

B: After thrombin cleavage and GST passback of lane A

Figure 5-6: SDS-PAGE of Ub-ZAP70 with a C-terminal Ala-Ala-Pro substitution after Ni^{2+} -affinity pull down and cleavage with thrombin. *E. coli* lysate was subjected to Ni^{2+} -affinity purification and eluted product was loaded in lanes A and treated with thrombin followed by GSH-sepharose pass-back to remove GST-tag in lane B



- 1: Ub-ZAP70 co-expressed with Lck
- 2: Ub-ZAP70 co-expressed with Hck
- 3: Ub-ZAP70 co-expressed with Src
- 4: Ub-peptide co-expressed with TKX1
- 5: non phosphorylated Ub-ZAP70 (control)

Figure 5-7: Western Blot of purified Ub-ZAP70 from co-expressions with tyrosine kinases. Ub-ZAP70 containing a C-terminal Ala-Ala-Pro substitution in Ub was co-expressed with indicated kinases and purified as described in Figure 5-6. Purified samples were probed with anti-phospho-tyrosine antibody to determine which kinases phosphorylated Ub-ZAP70.

5.2.4 Developing a method to separate tyrosine phosphorylated and unphosphorylated Ub-ZAP70

As mentioned in section 5.2.3, I developed a method for generating phosphorylated Ub-ZAP70. Based on our experience in generating tyrosine phosphorylated Cbl [85], it is difficult to achieve 100% phosphorylation. Thus, it is important to separate phosphorylated Ub-ZAP70 from the unphosphorylated species. To achieve this, I used anion exchange chromatography. Following GSH-sepharose chromatography, protein was subsequently applied to a SourceQ column and eluted using a gradient of NaCl (Figure 5-8). Eluted fractions were loaded onto an SDS-PAGE gel and subsequently analysed by Coomassie staining (Figure 5-8B) or Western blot using an anti-phospho-tyrosine antibody (Figure 5-8C). Fractions that eluted at higher salt concentrations were phosphorylated whereas those that eluted at lower salt concentrations were not.

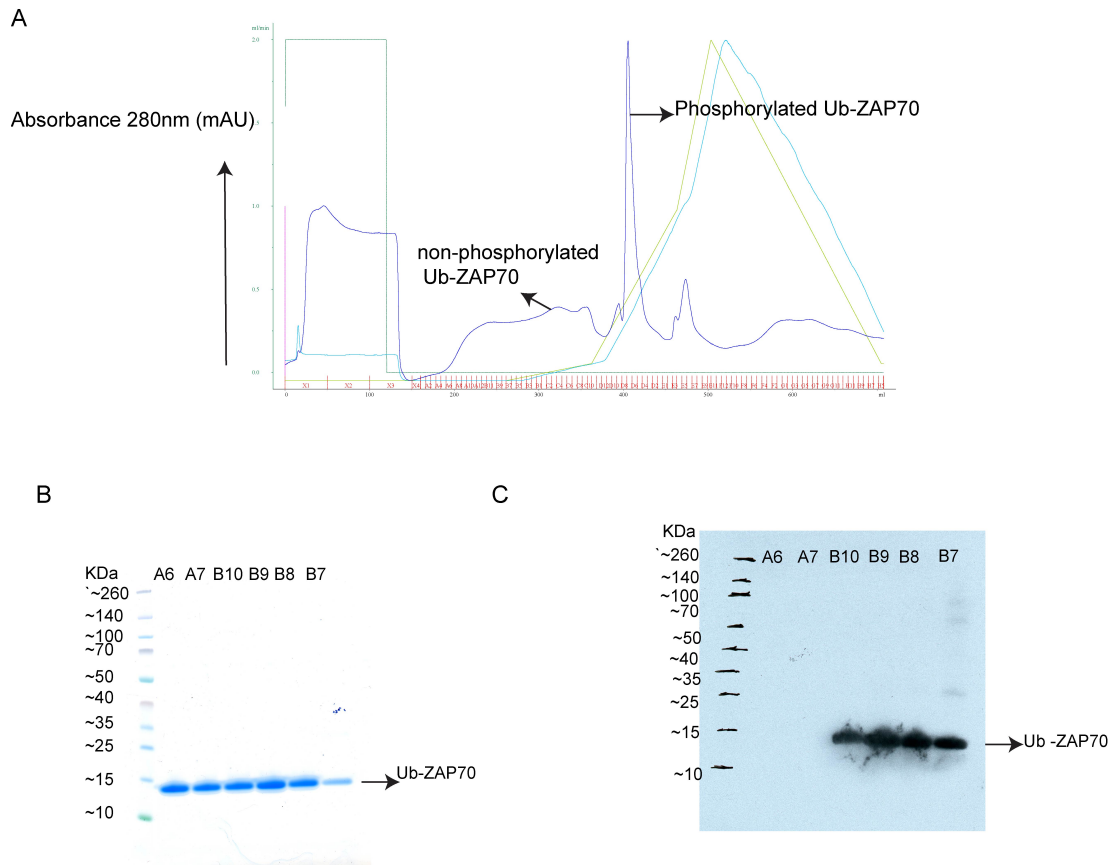


Figure 5-8: Separation of phosphorylated and unphosphorylated Ub-ZAP70. (A) Chromatogram obtained from anion exchange using a 20ml Source Q column. (B) SDS-PAGE separation and Coomassie stain of eluted fractions from (A) (Fractions A6, A7, B10, B9, B8 and B7). (C) Western blot of fractions from (B) probed with an anti-phospho-tyrosine antibody. Phosphorylated Ub-ZAP70 is indicated.

Next, I re-engineered and purified phosphorylated Ub-fused Src peptide (Ub-Srcp) and Ub-fused c-Met peptide (Ub-Metp) using methods similar to those described in sections 5.2.3, 5.2.4 and 5.2.5. These three phosphorylated Ub-peptides were used in the subsequent experiments.

5.2.5 Biochemical assay to validate Ub-ZAP70p as a substrate

To validate whether Ub-ZAP70p acts as a ubiquitinated substrate mimetic for Cbl, I performed ubiquitination assays to assess whether activated c-Cbl (pCbl; c-Cbl 47-435, Y368F, pY371; [85]) can transfer Ub to Ub-ZAP70p. pCbl only ubiquitinates Ub-ZAP70p but not its unphosphorylated counterpart. Thus, the interactions between Cbl and the phosphorylated ZAP70 moiety of Ub-ZAP70p presumably placed the Ub moiety proximal to the E2~Ub thioester bond, thereby enabling Ub-ZAP70p to function as a ubiquitinated substrate mimetic.

Next I wondered whether the length of the linker connecting Ub and ZAP70p influenced the efficiency of Ub transfer. Hence, I introduced various linker size sequences (no linker, 1, 3, and 5 Gly-Gly-Ser linkers) between Ub and ZAP70p and performed ubiquitination assay to assess the effect of the linker length on pCbl-mediated Ub transfer. Ub-ZAP70p functioned as a substrate mimetic with all of these linkers, but multiple Ub transfers were only observed with no linker or with one Gly-Gly-Ser linker (Figure 5-10).

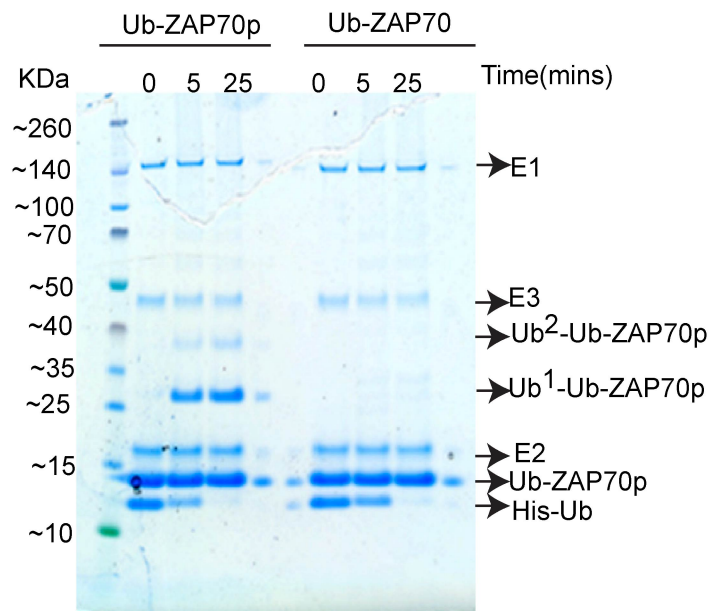


Figure 5-9: SDS-PAGE showing ubiquitination of Ub-ZAP70p catalysed by pCbl. Phosphorylated and unphosphorylated Ub-ZAP70p and ubiquitinated products are indicated.

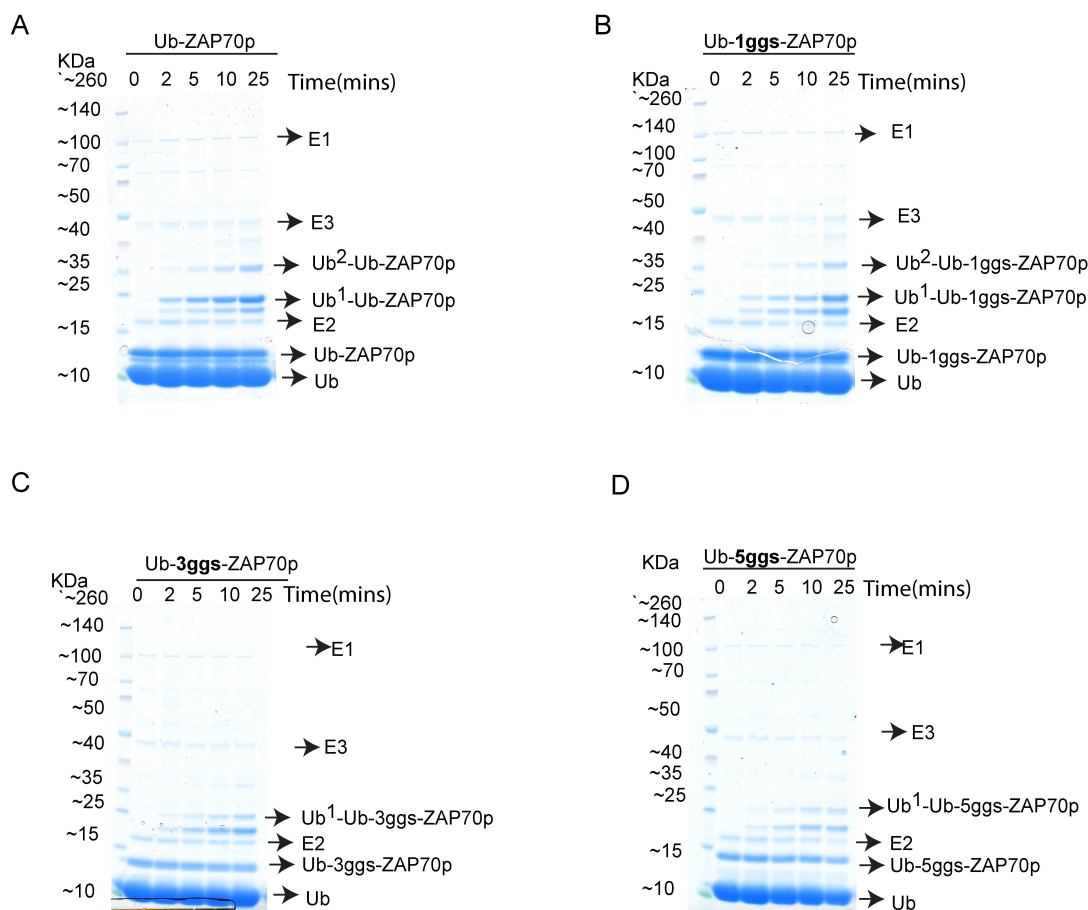


Figure 5-10: SDS-PAGE showing ubiquitination of Ub-ZAP70p with varying linker lengths catalysed by pCbl. (A) Ubiquitination Ub-ZAP70p with no linker. (B) Ubiquitination Ub-ZAP70p with one Gly-Gly-Ser linker. (C) Ubiquitination Ub-ZAP70p with three Gly-Gly-Ser linkers. (D) Ubiquitination Ub-ZAP70p with five Gly-Gly-Ser linkers.

5.2.6 Assembling pCbl-E2-Ub complex bound to phosphorylated Ub-peptides

To investigate how Cbl promotes polyubiquitination, I wanted to elucidate a structure of a complex of my substrate mimetic bound to activated Cbl and E2-Ub. Previously, our lab determined structures of pCbl-b-UbcH5B-Ub-ZAP70 peptide complex and pCbl-UbcH5B-Ub-ZAP70 peptide[73]. In both of these complexes, the catalytic site of E2 faces ZAP70 peptide. Hence, I purified phosphorylated c-Cbl and Cbl-b variants by co-expressing them with Src kinase to generate activated Cbl (see Methods Section 2.4). For E2-Ub conjugates, a variety of stable E2-Ub complexes with an amide or oxyester bond were generated (see Methods Section 2.6). Using different combinations of phosphorylated Cbl, E2-Ub and phosphorylated Ub-peptide, I setup crystallisation trials on various complexes as shown below.

5.2.6.1 pc-Cbl-UbcH5B_{S22R}-Ub-Ub-3ggs-Srcp

The first complex I assembled for crystallisation was pc-Cbl-UbcH5B_{S22R}-Ub-Ub-3ggs-Srcp. Previous studies have shown that the UbcH5 family has surface opposite the active site that binds Ub non-covalently and stimulates Ub transfer [36, 40]. To eliminate the possibility of the Ub moiety from Ub-3ggs-Srcp binding the backside of UbcH5B, I used UbcH5B_{S22R}-Ub to generate my complex because this UbcH5B mutation prevents backside binding by Ub. The stock concentration of pc-Cbl, UbcH5B_{S22R}-Ub, Ub-3ggs-Srcp was 8.5mg/ml, 24.5mg/ml and 19.5mg/ml respectively. We know from previous study the binding affinity of pc-Cbl to UbcH5B-Ub is very tight[73]. Hence I mixed the complex with molar ratio of 1:1:1.5 pc-Cbl: UbcH5B-Ub-Ub-3ggs-Srcp, such that final concentration of pc-Cbl was approx. between 5.5-6mg/ml. I screened the complex for crystal formation using more than 1000 conditions at 19°C. After 48 hours, I obtained crystals in several conditions, most of which contained low percentage of PEG or AmSO₄ as the precipitant (Figure 5-11A and B). I optimised both crystallisation conditions and ran crystals on an SDS-PAGE gel to confirm that all components of the protein complex were present in the crystals (Figure5-11D). Initially the crystals simply dissolved upon adding cryoprotectant such 20% ethylene glycol, MPD or glycerol. I then had to screen lot of cryoprotectants to find a condition where my crystals did not dissolve. I tried a series of cryoprotectants like glucose, sucrose, xylitol, MPD, several low molecular weight PEGS and found that 20% sucrose worked best as a cryoprotectant for my crystals. After, I overcame the dissolving issues, I tested the diffraction quality of my crystals. Unfortunately, crystals grown in AmSO₄ conditions did not diffract at all. I then optimised growth conditions for crystals using PEG as a precipitant. Despite using a variety of different cryoprotectants/techniques and regardless of my crystallisation conditions, the highest resolution diffraction I obtained was 6 Å. This included test shots of my crystals at room temperature in the absence of any cryoprotectant. Nonetheless, the diffracted crystals were indexed and assigned to the space group P 21 21 2 with the following unit cell dimensions: a=127.9, b= 286.78, c= 60.48, $\alpha=\beta=\gamma=90^\circ$

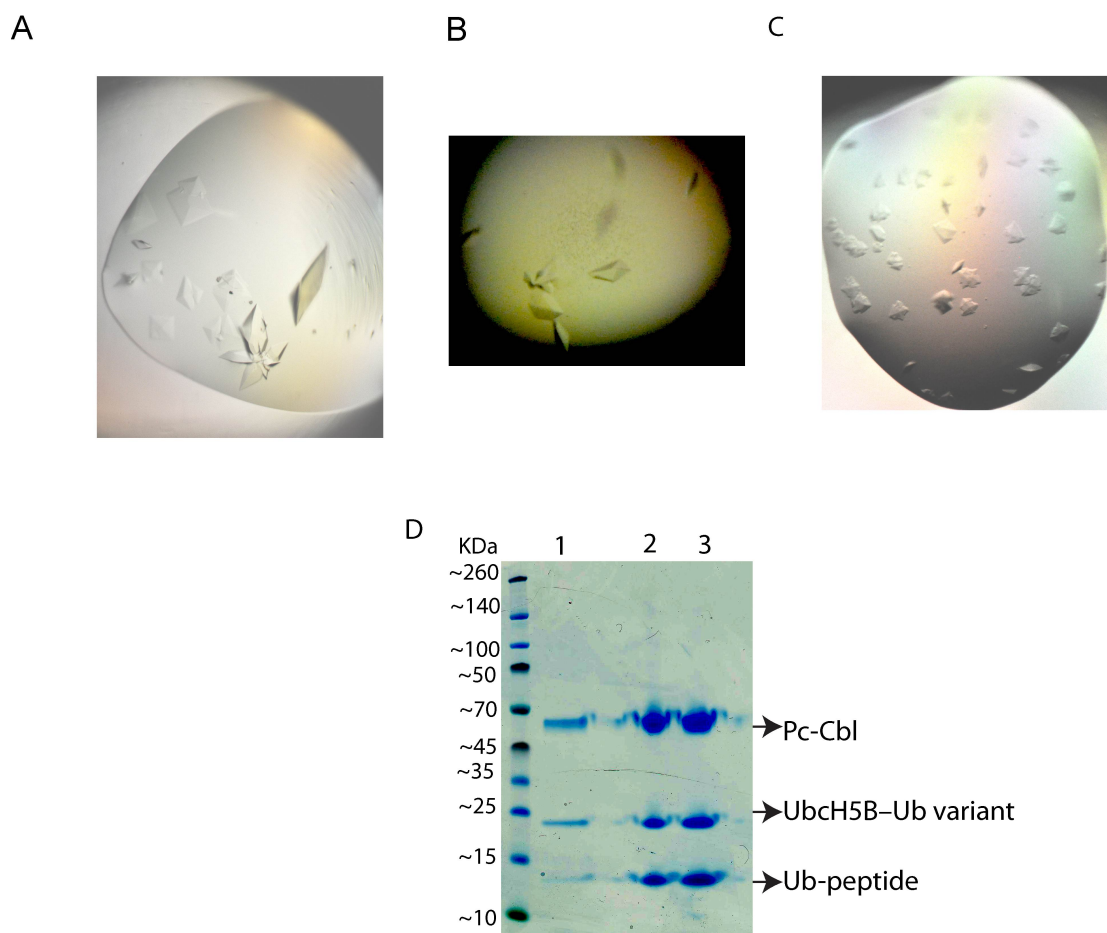


Figure 5-11: Results from crystallisation experiments obtained from Table 5.2. (A) Crystals of pCbl-UbcH5B_{S22R}-Ub-Ub-Srcp grown in 1.6 M AmSO₄ and 0.1 M Tris-HCl 8.5. (B) Crystals of pCbl-UbcH5B_{S22R}-Ub-Ub-Srcp grown in 5.5% PEG3350 0.1 M MES 6.5. (C) Crystals of pc-Cbl-UbcH5B-Ub-Ub-ZAP70p-Ub grown in 20 %(v/v) ethylene glycol, 10 %(v/v) PEG8K, 0.1M Tris HCl pH 8.5. (D) SDS-PAGE showing the protein components of the crystals in (A), (B) and (C) as indicated (just put A, B, C over the lanes instead).

5.2.6.2 pc-Cbl-UbcH5B_{C85K}-Ub-Ub-3ggs-Srcp with free Ub

Since crystals from pc-Cbl-UbcH5B_{S22R}-Ub-Ub-3ggs-Srcp complex diffracted poorly, I decided to set up alternative complexes that might involve different crystal packing. To do this, I decided to use UbcH5B_{C85K}-Ub (UbcH5B's active Cy85 mutated to lys85 to generate a stable isopeptide linkage)[66]. I also added free Ub to saturate UbcH5B's backside surface. The stock concentration of pc-Cbl was same as described above, whereas UbcH5B_{C85K}-Ub, Ub-3ggs-Srcp and Ub were at 22.5mg/ml, 19.5mg/ml and 100 mg/ml respectively. I mixed the complex pc-Cbl-UbcH5B_{C85K}-Ub-Ub-3ggs-Srcp-Ub in 1:1:1.5:1 molar ratio, such that final concentration of the complex was approx. between 7-8 mg/ml. I screened the complex with and without free Ub for crystal formation in over 1000 conditions. I only

observed crystal formation for complex containing free Ub in similar conditions to pc-Cbl-UbcH5B_{S22R}-Ub-Ub-3ggs-Srcp complex, that is in low PEG and low AmSO4 conditions, but these crystals did not diffract any better than what I had earlier, even after optimisation.

5.2.6.3 pc-Cbl-UbcH5B-Ub-Ub-3ggs-ZAP70p

Alternatively, I also set up complex with another substrate mimetic, Ub-3ggs-ZAP70. This time I screened complex with UbcH5B_{S22R}-Ub or UbcH5B_{C85K}-Ub in two separate drops on the same plate. Crystallisation screening and complex set up was the same as mentioned above in the previous crystallisation experiments. Crystals obtained are shown in figure 5-11C. I again observed numerous crystal hits in conditions containing low PEG, low pH and glycerol, but they all diffracted poorly.

5.2.6.4 Other E3-E2-Ub-substrate complex

After my initial crystallisation attempts to obtain high-resolution crystallisation data failed, I used a different strategy to generate a complex. I made modifications to my substrate, used different E2-Ub and tried alternative E3s. These strategies are discussed briefly below. Additionally, these alternative complexes are listed in Table 5-2.

Substrate: As shown in Figure 5-10, substrate mimetics with smaller linkers or lacking linker are more active in ubiquitination. Therefore, I used Ub-ZAP70p, Ub-Srcp, Ub-ggs-ZAP70p, and Ub-ggs-Srcp for additional crystallisation trials. I thought that a longer linker might be more flexible and contribute to conformational variability. To eliminate flexibility and to try and capture a more restrained complex, I set up screens with pc-Cbl-E2-Ub and ZAP70p or Srcp with no linker or 1ggs linker. I obtained crystals of these complexes but the diffraction quality did not improve.

E2-Ub: Initially I used UbcH5B_{S22R}-Ub and UbcH5B_{C85K}-Ub in my crystallisation complexes for reasons explained above. Because all my crystals with UbcH5B diffracted poorly, I decided to try another E2. UbcH5B has the ability to make a variety of polyUb chains and is very promiscuous [160]. I thought this might contribute to the poor diffraction. Therefore I chose UbcH6, which makes lys48-specific chains. I set up complex with UbcH6_{C131K,S68R}-Ub, which was cloned, expressed and purified by my supervisor Danny Huang. For this E2-Ub, the catalytic

cys is mutated to lys (C131K) to generate a stable isopeptide linkage and S68R abrogates backside binding to Ub. Unfortunately I did not get any crystal hits from complex containing UbcH6_{C131K,S68R}-Ub.

E3: I used pc-Cbl for all my initial crystallisation experiments. When none of the complexes with pc-Cbl diffracted to high resolution, I decided to use pCbl-b. I set up the following complexes with pCbl-b: pCblb-UbcH5B_{S22R}-Ub-Ub-1ggs-Srcp, pCblb-UbcH5B_{C85K}-Ub-Ub-1ggs-ZAP70p-Ub, pCblb-UbcH6_{C131K,S68R}-Ub-Ub-1ggs-Srcp and pCbl-b- UbcH6_{C131K,S68R}-Ub- Ub-1ggs-ZAP70p. I obtained crystals of all of these complexes except UbcH6-Ub; as observed with pc-Cbl, all the crystals diffracted poorly .

Table: 5-2 E3-E2-Ub-Ub-peptide complexes used for crystallisation trials

E3	E2~Ub	Substrate	Concentration (mg/ml)
pc-Cbl	UbcH5B _{C85K,S22R} -Ub	Ub-3ggs-ZAP70	~7.5
pc-Cbl	UbcH5B _{C85K,S22R} -Ub	Ub-3ggs-Src	~7.0
pc-Cbl	UbcH5B _{C85K} -Ub	Ub-3ggs-ZAP70	~7.0
pc-Cbl	UbcH5B _{C85K} -Ub	Ub-3ggs-Src	~7.5
pCbl-b	UbcH5B _{C85K,S22R} -Ub	Ub-3ggs-ZAP70	~8.0
pCbl-b	UbcH5B _{C85K,S22R} -Ub	Ub-3ggs-Src	~8.0
pCbl-b	UbcH5B _{C85K,S22R} -Ub	Ub-1ggs-ZAP70	~7.0
pCbl-b	UbcH5B _{C85K,S22R} -Ub	Ub-1-ggs-Src	~7.5
pCbl-b	UbcH6 _{C131K, S68R} -Ub	Ub-1ggs-Src	~7.5

5.3 Discussion

Zheng et al., (2000) determined the first structure of a RING E3 bound to an E2: the N-terminal fragment of c-Cbl bound to UbcH7 and a peptide fragment of the substrate ZAP70. In this structure, ZAP70 peptide and E2's catalytic Cys are separated by 67 Å (Figure 5-1A). Subsequently our lab showed that phosphorylation of a conserved tyrosine in Cbl's LH induces conformational changes that juxtapose E2's catalytic Cys and the substrate-binding site (Dou et al., in 2012), leaving a gap between E2's catalytic Cys and ZAP70 peptide of about 27 Å (Figure 5-1B). In these structural studies, the ZAP70 peptide fragment lacks lysine residues and therefore cannot be ubiquitinated. It seems likely that a longer fragment of substrate or a full-length substrate could bridge such gap. At the start of my PhD, Danny had designed Ub-peptides to mimic ubiquitinated substrate to enable studies of the mechanism of poly Ub chain formation. Modelling studies suggested that the 27-Å gap between E2's catalytic Cys and ZAP70 peptide in the structure could be bridged by an Ub moiety. Thus the goal of my project was to develop and optimise methods to generate Ub-peptide substrate mimetics for biochemical analyses and structural determination. Generation of Ub-peptide was challenging in the beginning. Initially, Ub-ZAP70 was cleaved following the C-terminal diglycine motif in Ub; hence, Ub was purified rather than Ub-ZAP70 (Figure 5-5 and section 5.2.2). I then re-engineered the construct to overcome the cleavage problem by replacing the diglycine motif at the C-terminus of Ub with a dialanine motif and introducing a proline residue (See section 5.2.2). This solved the cleavage issue and I was able to obtain Ub-ZAP70 (Section 5.2.2, Figure 5-7). The next challenge was to determine which kinase could phosphorylate Ub-ZAP70 and how to separate the phosphorylated and unphosphorylated Ub-ZAP70. I showed that Src kinase phosphorylates Ub-ZAP70 and other Ub-peptides. To separate the phosphorylated and unphosphorylated Ub-ZAP70, I developed a method using anion exchange chromatography to separate the two species (Section 5.2.4, Figure 5-4). Next, I performed ubiquitination assays to determine if Ub-ZAP70p is ubiquitinated by pCbl. (Section 5.2.5, Figure 5.9). Indeed, I showed that Ub-ZAP70p was ubiquitinated readily by pCbl whereas the unphosphorylated Ub-ZAP70 was not. These results showed the suitability of our model suitable for studying the mechanism of RING E3-catalysed polyUb chain formation.

I then setup various complexes of pCbl bound to E2-Ub and phosphorylated Ub-peptide (Section 5.2.6). Most of my crystallisation experiments yielded crystal hits (Figure 5-11) but the diffraction quality of these crystals was poor. I then used various methods like crystal dehydration and growing complex in different conditions to improve diffraction quality.. The highest quality diffraction I obtained was 6 Å. Since I could not improve the diffraction resolution of my complex, I then started setting up complex with Cbl-b, additional E2-Ub variants and other phosphorylated Ub-peptides that I generated (Table 5-2). Although I obtained crystals for many of these complexes, none diffracted better than my earliest crystals. I also wondered if the length of linker in between my fusion peptide might be too flexible and hence the Ub moiety in the phosphorylated Ub-peptide is loosely packed. I generated linker of varying lengths, all tested previously with ubiquitination assay to be optimal to act as substrate mimetic (Figure 5-10). I set up crystallisation trials with phosphorylated Ub-peptides with varying lengths, but still did not improve the diffraction.

Unfortunately, I was unable to obtain crystals of suitable diffraction quality to gain insights into how these components pack together and to assess whether we could capture E2~Ub bound to acceptor Ub at the E2's active site (a transient event in Ub transfer) using this strategy. During my PhD, Christopher Lima's group published a structure of SUMO E3, Siz1, bound to Ubc9-SUMO and a substrate, PCNA where they use a chemical crosslinking strategy to link PCNA's Lys164 to Ubc9's catalytic cysteine [161]. This strategy reduces conformational flexibility and eliminates potential non-specific protein-protein packing arrangement during protein crystallisation and would be worth investigating in the context of an E3-E2~Ub-Ub-substrate complex. Another possibility is to capture full-length substrate in complex with E3-E2~Ub instead of peptide which can be too flexible or too short to reach E2's active site. Of course all of these alternatives are equally challenging and will require great precision and biochemical understanding to capture E3-E2~Ub-substrate complex.

Chapter 6

Conclusions and future work

6. Conclusions and future work

6.1 Uncovering mechanisms of non-covalent binding of Ub in other E3s and E2s

My structure of cIAP1R with UbcH5B–Ub shows how the C-terminal tail of cIAP1 locks UbcH5B–Ub in a closed conformation primed for Ub transfer (chapter 3). Apart from RING E3s stabilising E2~Ub, there are various other components that provide further stability to the complex. One such component is non-covalent binding of Ub to the backside of the UbcH5 family of E2s. It is now evident that the mechanism of non-covalent binding of Ub increases the processivity of E2~Ub transfer in the UbcH5 family of E2s by stabilising the E3-E2~Ub complex. Crystal structures of the monomeric RING E3 RNF38 with UbcH5B–Ub and Ub^B [40] and dimeric RING cIAP1 bound to UbcH5B–Ub and Ub^B (chapter 3) both showed that the $\alpha 1\beta 1$ loop of UbcH5B is oriented in the presence of Ub^B in a conformation that helps to further stabilise the donor Ub in a primed conformation in the complex. The mechanism seems to be conserved across RING E3s, but whether this mechanism is conserved in other E2 families needs to be further investigated.

To address the role of Ub^B in other E2s, I studied the core domain of UbcH6 (chapter 4). The backside surface of UbcH6 is very similar to that of the UbcH5 family, but a previous study reported that UbcH6 lacks backside binding of Ub. Contrary to this previous studies, my results showed that non-covalent binding of Ub does stimulate UbcH6. However, my results showed that Ub^B binds UbcH6 more weakly than members of the UbcH5 family. My results also suggest that the mechanism of stimulation in UbcH6 differs than that observed in the UbcH5 family. This opens up new opportunities for investigating Ub^B mechanisms in other E2s. In addition, it will also be interesting to study full length UbcH6 and determine whether the regions outside of the core domain of the E2 affect non-covalent binding of Ub since the estimated affinity of Ub^B to the core domain of UbcH6 is higher than 1 mM. Together my results from chapters 3 and 4 suggest that there is more to the Ub^B mechanism that is not yet fully understood and requires further investigation. It is very interesting to see how two different families of E2s, which share similar UBC domains, have different mechanisms for Ub^B stimulation. This has opened new opportunities for studies in the field of E2 backside stimulation. This is the second structural and biochemical report of a Ub^B mechanism following that of Buetow *et al.* in 2015, and

it will be interesting to determine how it functions in cells and characterise its mechanism of action.

6.2 Generation of substrate mimetics to study polyUb chain formation

How RING E3s promote Ub transfer from E2~Ub to a lysine residue in substrate remains elusive. To understand the mechanism of polyUb chain formation, I generated several Ub-substrate mimetics to investigate how c-Cbl primes E2~Ub and ubiquitinated substrate to catalyse polyUb chain formation (chapter 5). I hypothesised that Ub-fused substrate peptide would be in close proximity of the thioester in E2~Ub and could function as an acceptor for studying polyUb chain formation. Biochemical studies showed that my substrate mimetics underwent ubiquitination. I assembled various Cbl-E2~Ub complexes bound to Ub-fused peptide and attempted to crystallise these complex to understand the mechanism of RING E3-catalysed polyUb chain formation. Unfortunately none of my crystals diffracted better than 6Å. Capturing an E3-E2~Ub-substrate complex is not trivial. During my PhD, I tried several optimisation techniques to get higher resolution diffraction, but none of them gave me resolution of sufficient quality to determine a structure. There are various factors that might contribute to the poor diffraction quality of my complexes including conformational flexibility, low binding affinities and lack of specificity. To eliminate these factors, future work could include using a full-length substrate to study the complex. Other techniques like chemical cross-linking to cross-link E2's active site to substrate might also be beneficial; this technique will restrict the conformational flexibility within the complex and might help in the crystal packing arrangement.

6.3 Characterisation of IAPs and Cbls

The IAP family of proteins play a significant role in many cellular processes including cell death and survival. Currently, there are no full length crystal structures of any member of the IAP family of proteins, hence we still do not completely understand their regulatory mechanisms. The longest structure available is that of cIAP1 extending from the BIR3 domain to the C-terminus; this structure reveals that cIAP1 is in an autoinhibited conformation in which it exists as a monomer. Upon binding SMAC or caspases, cIAP1 undergoes conformational changes in which it forms a RING-mediated dimer and undergoes autoubiquitination [139]. Overexpression of IAPs has been linked to tumour growth and poor prognosis for several types of cancer. Recently, SMAC mimetics that target IAP BIR domains have

emerged as a promising platform in the development of anticancer therapeutics [162]. Although IAPs are recognised as favourable drug target, how they are regulated still remains elusive and merits further investigation..

Cbls act as adaptor proteins and as E3 ubiquitin ligases. The latter function plays an important role in ubiquitination of RTKs. Based on its different functions in regulating immune response and development of cancer, they have emerged as a new class of therapeutic targets [163]. Certain mutations in Cbls lead to loss of E3 ligase activity. For example, mutation of Y371, which undergoes phosphorylation and activates Cbls' E3 ligase activity, is frequently found in patients with leukemia. In this case, development of drugs that can mimic the phosphorylated tyrosine can provide new therapeutic opportunities.

Bibliography

1. Pickart, C.M. and M.J. Eddins, *Ubiquitin: structures, functions, mechanisms*. Biochim Biophys Acta, 2004. **1695**(1-3): p. 55-72.
2. Finley, D., et al., *Inhibition of proteolysis and cell cycle progression in a multiubiquitination-deficient yeast mutant*. Mol Cell Biol, 1994. **14**(8): p. 5501-9.
3. Zhao, Y., et al., *Ubiquitin ligase components Cullin4 and DDB1 are essential for DNA methylation in Neurospora crassa*. J Biol Chem, 2010. **285**(7): p. 4355-65.
4. Ordureau, A., et al., *Defining roles of PARKIN and ubiquitin phosphorylation by PINK1 in mitochondrial quality control using a ubiquitin replacement strategy*. Proc Natl Acad Sci U S A, 2015. **112**(21): p. 6637-42.
5. Akutsu, M., I. Dikic, and A. Bremm, *Ubiquitin chain diversity at a glance*. J Cell Sci, 2016. **129**(5): p. 875-80.
6. Kim, W., et al., *Systematic and quantitative assessment of the ubiquitin-modified proteome*. Mol Cell, 2011. **44**(2): p. 325-40.
7. Wagner, S.A., et al., *A proteome-wide, quantitative survey of in vivo ubiquitylation sites reveals widespread regulatory roles*. Mol Cell Proteomics, 2011. **10**(10): p. M111 013284.
8. Swatek, K.N. and D. Komander, *Ubiquitin modifications*. Cell Res, 2016. **26**(4): p. 399-422.
9. Castaneda, C.A., et al., *Linkage via K27 Bestows Ubiquitin Chains with Unique Properties among Polyubiquitins*. Structure, 2016. **24**(3): p. 423-36.
10. Liu, J., et al., *Rhbdd3 controls autoimmunity by suppressing the production of IL-6 by dendritic cells via K27-linked ubiquitination of the regulator NEMO*. Nat Immunol, 2014. **15**(7): p. 612-22.
11. Cao, Z., et al., *Ubiquitin Ligase TRIM62 Regulates CARD9-Mediated Anti-fungal Immunity and Intestinal Inflammation*. Immunity, 2015. **43**(4): p. 715-26.
12. Birsa, N., et al., *Lysine 27 ubiquitination of the mitochondrial transport protein Miro is dependent on serine 65 of the Parkin ubiquitin ligase*. J Biol Chem, 2014. **289**(21): p. 14569-82.

13. Al-Hakim, A.K., et al., *Control of AMPK-related kinases by USP9X and atypical Lys(29)/Lys(33)-linked polyubiquitin chains*. *Biochem J*, 2008. **411**(2): p. 249-60.
14. Kerscher, O., R. Felberbaum, and M. Hochstrasser, *Modification of proteins by ubiquitin and ubiquitin-like proteins*. *Annu Rev Cell Dev Biol*, 2006. **22**: p. 159-80.
15. Johnson, E.S., *Protein modification by SUMO*. *Annu Rev Biochem*, 2004. **73**: p. 355-82.
16. Xirodimas, D.P., et al., *Mdm2-mediated NEDD8 conjugation of p53 inhibits its transcriptional activity*. *Cell*, 2004. **118**(1): p. 83-97.
17. Reverter, D., et al., *Structure of a complex between Nedd8 and the Ulp/Senp protease family member Den1*. *J Mol Biol*, 2005. **345**(1): p. 141-51.
18. Watson, I.R. and M.S. Irwin, *Ubiquitin and ubiquitin-like modifications of the p53 family*. *Neoplasia*, 2006. **8**(8): p. 655-66.
19. Lee, I. and H. Schindelin, *Structural insights into E1-catalyzed ubiquitin activation and transfer to conjugating enzymes*. *Cell*, 2008. **134**(2): p. 268-78.
20. Walden, H., et al., *The structure of the APPBP1-UBA3-NEDD8-ATP complex reveals the basis for selective ubiquitin-like protein activation by an E1*. *Mol Cell*, 2003. **12**(6): p. 1427-37.
21. Lois, L.M. and C.D. Lima, *Structures of the SUMO E1 provide mechanistic insights into SUMO activation and E2 recruitment to E1*. *EMBO J*, 2005. **24**(3): p. 439-51.
22. Lake, M.W., et al., *Mechanism of ubiquitin activation revealed by the structure of a bacterial MoeB-MoaD complex*. *Nature*, 2001. **414**(6861): p. 325-9.
23. Haas, A.L. and I.A. Rose, *The mechanism of ubiquitin activating enzyme. A kinetic and equilibrium analysis*. *J Biol Chem*, 1982. **257**(17): p. 10329-37.
24. Haas, A.L., et al., *Ubiquitin-activating enzyme. Mechanism and role in protein-ubiquitin conjugation*. *J Biol Chem*, 1982. **257**(5): p. 2543-8.
25. Hershko, A., et al., *Components of ubiquitin-protein ligase system. Resolution, affinity purification, and role in protein breakdown*. *J Biol Chem*, 1983. **258**(13): p. 8206-14.

26. Schulman, B.A. and J.W. Harper, *Ubiquitin-like protein activation by E1 enzymes: the apex for downstream signalling pathways*. Nat Rev Mol Cell Biol, 2009. **10**(5): p. 319-31.
27. Olsen, S.K., et al., *Active site remodelling accompanies thioester bond formation in the SUMO E1*. Nature, 2010. **463**(7283): p. 906-12.
28. Ozkan, E., H. Yu, and J. Deisenhofer, *Mechanistic insight into the allosteric activation of a ubiquitin-conjugating enzyme by RING-type ubiquitin ligases*. Proc Natl Acad Sci U S A, 2005. **102**(52): p. 18890-5.
29. Wu, P.Y., et al., *A conserved catalytic residue in the ubiquitin-conjugating enzyme family*. EMBO J, 2003. **22**(19): p. 5241-50.
30. Ye, Y. and M. Rape, *Building ubiquitin chains: E2 enzymes at work*. Nat Rev Mol Cell Biol, 2009. **10**(11): p. 755-64.
31. Wenzel, D.M., K.E. Stoll, and R.E. Klevit, *E2s: structurally economical and functionally replete*. Biochem J, 2011. **433**(1): p. 31-42.
32. Eletr, Z.M., et al., *E2 conjugating enzymes must disengage from their E1 enzymes before E3-dependent ubiquitin and ubiquitin-like transfer*. Nat Struct Mol Biol, 2005. **12**(10): p. 933-4.
33. van Wijk, S.J. and H.T. Timmers, *The family of ubiquitin-conjugating enzymes (E2s): deciding between life and death of proteins*. FASEB J, 2010. **24**(4): p. 981-93.
34. Jensen, J.P., et al., *Identification of a family of closely related human ubiquitin conjugating enzymes*. J Biol Chem, 1995. **270**(51): p. 30408-14.
35. Scheffner, M., J.M. Huibregtse, and P.M. Howley, *Identification of a human ubiquitin-conjugating enzyme that mediates the E6-AP-dependent ubiquitination of p53*. Proc Natl Acad Sci U S A, 1994. **91**(19): p. 8797-801.
36. Brzovic, P.S., et al., *A UbcH5/ubiquitin noncovalent complex is required for processive BRCA1-directed ubiquitination*. Mol Cell, 2006. **21**(6): p. 873-80.
37. Stewart, M.D., et al., *E2 enzymes: more than just middle men*. Cell Res, 2016. **26**(4): p. 423-40.
38. Sakata, E., et al., *Crystal structure of UbcH5b~ubiquitin intermediate: insight into the formation of the self-assembled E2~Ub conjugates*. Structure, 2010. **18**(1): p. 138-47.

39. Page, R.C., et al., *Structural insights into the conformation and oligomerization of E2~ubiquitin conjugates*. *Biochemistry*, 2012. **51**(20): p. 4175-87.
40. Buetow, L., et al., *Activation of a primed RING E3-E2-ubiquitin complex by non-covalent ubiquitin*. *Mol Cell*, 2015. **58**(2): p. 297-310.
41. Frances-Rose, *The N terminal extension*. 2013.
42. Uversky, V.N., *The UBE2E proteins as conjugating dispersers: extending function with extended extensions*. *J Mol Biol*, 2013. **425**(22): p. 4067-70.
43. Schumacher, F.R., G. Wilson, and C.L. Day, *The N-terminal extension of UBE2E ubiquitin-conjugating enzymes limits chain assembly*. *J Mol Biol*, 2013. **425**(22): p. 4099-111.
44. Ardley, H.C. and P.A. Robinson, *E3 ubiquitin ligases*. *Essays Biochem*, 2005. **41**: p. 15-30.
45. Metzger, M.B., et al., *RING-type E3 ligases: master manipulators of E2 ubiquitin-conjugating enzymes and ubiquitination*. *Biochim Biophys Acta*, 2014. **1843**(1): p. 47-60.
46. Scheffner, M. and S. Kumar, *Mammalian HECT ubiquitin-protein ligases: biological and pathophysiological aspects*. *Biochim Biophys Acta*, 2014. **1843**(1): p. 61-74.
47. Huibregtse, J.M., et al., *A family of proteins structurally and functionally related to the E6-AP ubiquitin-protein ligase*. *Proc Natl Acad Sci U S A*, 1995. **92**(11): p. 5249.
48. Buetow, L. and D.T. Huang, *Structural insights into the catalysis and regulation of E3 ubiquitin ligases*. *Nat Rev Mol Cell Biol*, 2016. **17**(10): p. 626-42.
49. Rotin, D. and S. Kumar, *Physiological functions of the HECT family of ubiquitin ligases*. *Nat Rev Mol Cell Biol*, 2009. **10**(6): p. 398-409.
50. Metzger, M.B., V.A. Hristova, and A.M. Weissman, *HECT and RING finger families of E3 ubiquitin ligases at a glance*. *J Cell Sci*, 2012. **125**(Pt 3): p. 531-7.
51. Bernassola, F., et al., *The HECT family of E3 ubiquitin ligases: multiple players in cancer development*. *Cancer Cell*, 2008. **14**(1): p. 10-21.
52. Scheffner, M. and O. Staub, *HECT E3s and human disease*. *BMC Biochem*, 2007. **8 Suppl 1**: p. S6.

53. Deshaies, R.J. and C.A. Joazeiro, *RING domain E3 ubiquitin ligases*. *Annu Rev Biochem*, 2009. **78**: p. 399-434.
54. Morreale, F.E. and H. Walden, *Types of Ubiquitin Ligases*. *Cell*, 2016. **165**(1): p. 248-248 e1.
55. Capili, A.D., et al., *Structure of the C-terminal RING finger from a RING-IBR-RING/TRIAD motif reveals a novel zinc-binding domain distinct from a RING*. *J Mol Biol*, 2004. **340**(5): p. 1117-29.
56. Eisenhaber, B., et al., *The ring between ring fingers (RBR) protein family*. *Genome Biol*, 2007. **8**(3): p. 209.
57. Marin, I., et al., *Parkin and relatives: the RBR family of ubiquitin ligases*. *Physiol Genomics*, 2004. **17**(3): p. 253-63.
58. Chaugule, V.K., et al., *Autoregulation of Parkin activity through its ubiquitin-like domain*. *EMBO J*, 2011. **30**(14): p. 2853-67.
59. Smit, J.J., et al., *The E3 ligase HOIP specifies linear ubiquitin chain assembly through its RING-IBR-RING domain and the unique LDD extension*. *EMBO J*, 2012. **31**(19): p. 3833-44.
60. Stieglitz, B., et al., *LUBAC synthesizes linear ubiquitin chains via a thioester intermediate*. *EMBO Rep*, 2012. **13**(9): p. 840-6.
61. Kelsall, I.R., et al., *TRIAD1 and HHARI bind to and are activated by distinct neddylated Cullin-RING ligase complexes*. *EMBO J*, 2013. **32**(21): p. 2848-60.
62. Zheng, N., et al., *Structure of a c-Cbl-UbcH7 complex: RING domain function in ubiquitin-protein ligases*. *Cell*, 2000. **102**(4): p. 533-9.
63. Wenzel, D.M., et al., *UBCH7 reactivity profile reveals parkin and HHARI to be RING/HECT hybrids*. *Nature*, 2011. **474**(7349): p. 105-8.
64. Bailly, V., et al., *Specific complex formation between yeast RAD6 and RAD18 proteins: a potential mechanism for targeting RAD6 ubiquitin-conjugating activity to DNA damage sites*. *Genes Dev*, 1994. **8**(7): p. 811-20.
65. Chen, B., et al., *The activity of a human endoplasmic reticulum-associated degradation E3, gp78, requires its Cue domain, RING finger, and an E2-binding site*. *Proc Natl Acad Sci U S A*, 2006. **103**(2): p. 341-6.
66. Dou, H., et al., *BIRC7-E2 ubiquitin conjugate structure reveals the mechanism of ubiquitin transfer by a RING dimer*. *Nat Struct Mol Biol*, 2012. **19**(9): p. 876-83.

67. Plechanovova, A., et al., *Structure of a RING E3 ligase and ubiquitin-loaded E2 primed for catalysis*. Nature, 2012. **489**(7414): p. 115-20.
68. Pruneda, J.N., et al., *Structure of an E3:E2~Ub complex reveals an allosteric mechanism shared among RING/U-box ligases*. Mol Cell, 2012. **47**(6): p. 933-42.
69. Huang, L., et al., *Structure of an E6AP-UbcH7 complex: insights into ubiquitination by the E2-E3 enzyme cascade*. Science, 1999. **286**(5443): p. 1321-6.
70. Zhang, M., et al., *Chaperoned ubiquitylation--crystal structures of the CHIP U box E3 ubiquitin ligase and a CHIP-Ubc13-Uev1a complex*. Mol Cell, 2005. **20**(4): p. 525-38.
71. Yin, Q., et al., *E2 interaction and dimerization in the crystal structure of TRAF6*. Nat Struct Mol Biol, 2009. **16**(6): p. 658-66.
72. Benirschke, R.C., et al., *Molecular basis for the association of human E4B U box ubiquitin ligase with E2-conjugating enzymes UbcH5c and Ubc4*. Structure, 2010. **18**(8): p. 955-65.
73. Dou, H., et al., *Essentiality of a non-RING element in priming donor ubiquitin for catalysis by a monomeric E3*. Nat Struct Mol Biol, 2013. **20**(8): p. 982-986.
74. Nomura, K., et al., *Structural analysis of MDM2 RING separates degradation from regulation of p53 transcription activity*. Nat Struct Mol Biol, 2017. **24**(7): p. 578-587.
75. Soss, S.E., R.E. Klevit, and W.J. Chazin, *Activation of UbcH5c~Ub is the result of a shift in interdomain motions of the conjugate bound to U-box E3 ligase E4B*. Biochemistry, 2013. **52**(17): p. 2991-9.
76. Scott, D.C., et al., *Structure of a RING E3 trapped in action reveals ligation mechanism for the ubiquitin-like protein NEDD8*. Cell, 2014. **157**(7): p. 1671-84.
77. Mace, P.D., et al., *Structures of the cIAP2 RING domain reveal conformational changes associated with ubiquitin-conjugating enzyme (E2) recruitment*. J Biol Chem, 2008. **283**(46): p. 31633-40.
78. Berndsen, C.E., et al., *A conserved asparagine has a structural role in ubiquitin-conjugating enzymes*. Nat Chem Biol, 2013. **9**(3): p. 154-6.

79. Joazeiro, C.A., et al., *The tyrosine kinase negative regulator c-Cbl as a RING-type, E2-dependent ubiquitin-protein ligase*. Science, 1999. **286**(5438): p. 309-12.
80. Levkowitz, G., et al., *c-Cbl/Sli-1 regulates endocytic sorting and ubiquitination of the epidermal growth factor receptor*. Genes Dev, 1998. **12**(23): p. 3663-74.
81. Levkowitz, G., et al., *Ubiquitin ligase activity and tyrosine phosphorylation underlie suppression of growth factor signaling by c-Cbl/Sli-1*. Mol Cell, 1999. **4**(6): p. 1029-40.
82. Yokouchi, M., et al., *Ligand-induced ubiquitination of the epidermal growth factor receptor involves the interaction of the c-Cbl RING finger and UbcH7*. J Biol Chem, 1999. **274**(44): p. 31707-12.
83. Kassenbrock, C.K. and S.M. Anderson, *Regulation of ubiquitin protein ligase activity in c-Cbl by phosphorylation-induced conformational change and constitutive activation by tyrosine to glutamate point mutations*. J Biol Chem, 2004. **279**(27): p. 28017-27.
84. Kobashigawa, Y., et al., *Autoinhibition and phosphorylation-induced activation mechanisms of human cancer and autoimmune disease-related E3 protein Cbl-b*. Proc Natl Acad Sci U S A, 2011. **108**(51): p. 20579-84.
85. Dou, H., et al., *Structural basis for autoinhibition and phosphorylation-dependent activation of c-Cbl*. Nat Struct Mol Biol, 2012. **19**(2): p. 184-92.
86. Das, R., et al., *Allosteric activation of E2-RING finger-mediated ubiquitylation by a structurally defined specific E2-binding region of gp78*. Mol Cell, 2009. **34**(6): p. 674-85.
87. Hibbert, R.G., et al., *E3 ligase Rad18 promotes monoubiquitination rather than ubiquitin chain formation by E2 enzyme Rad6*. Proc Natl Acad Sci U S A, 2011. **108**(14): p. 5590-5.
88. Cook, W.J., et al., *Crystal structure of a class I ubiquitin conjugating enzyme (Ubc7) from Saccharomyces cerevisiae at 2.9 angstroms resolution*. Biochemistry, 1997. **36**(7): p. 1621-7.
89. Metzger, M.B., et al., *A structurally unique E2-binding domain activates ubiquitination by the ERAD E2, Ubc7p, through multiple mechanisms*. Mol Cell, 2013. **50**(4): p. 516-27.

90. Li, S., et al., *Insights into Ubiquitination from the Unique Clamp-like Binding of the RING E3 AO7 to the E2 UbcH5B*. J Biol Chem, 2015. **290**(51): p. 30225-39.
91. Saha, A., et al., *Essential role for ubiquitin-ubiquitin-conjugating enzyme interaction in ubiquitin discharge from Cdc34 to substrate*. Mol Cell, 2011. **42**(1): p. 75-83.
92. Ranaweera, R.S. and X. Yang, *Auto-ubiquitination of Mdm2 enhances its substrate ubiquitin ligase activity*. J Biol Chem, 2013. **288**(26): p. 18939-46.
93. Waterman, H., et al., *A mutant EGF-receptor defective in ubiquitylation and endocytosis unveils a role for Grb2 in negative signaling*. EMBO J, 2002. **21**(3): p. 303-13.
94. Pierce, N.W., et al., *Detection of sequential polyubiquitylation on a millisecond timescale*. Nature, 2009. **462**(7273): p. 615-9.
95. Yoshida, Y., et al., *A comprehensive method for detecting ubiquitinated substrates using TR-TUBE*. Proc Natl Acad Sci U S A, 2015. **112**(15): p. 4630-5.
96. Busino, L., et al., *SCFFbxl3 controls the oscillation of the circadian clock by directing the degradation of cryptochrome proteins*. Science, 2007. **316**(5826): p. 900-4.
97. Davis, M.A., et al., *The SCF-Fbw7 ubiquitin ligase degrades MED13 and MED13L and regulates CDK8 module association with Mediator*. Genes Dev, 2013. **27**(2): p. 151-6.
98. Iconomou, M. and D.N. Saunders, *Systematic approaches to identify E3 ligase substrates*. Biochem J, 2016. **473**(22): p. 4083-4101.
99. Guo, Z., et al., *Proteomics strategy to identify substrates of LNX, a PDZ domain-containing E3 ubiquitin ligase*. J Proteome Res, 2012. **11**(10): p. 4847-62.
100. Guo, Z., et al., *Screening E3 substrates using a live phage display library*. PLoS One, 2013. **8**(10): p. e76622.
101. Xu, G., J.S. Paige, and S.R. Jaffrey, *Global analysis of lysine ubiquitination by ubiquitin remnant immunoaffinity profiling*. Nat Biotechnol, 2010. **28**(8): p. 868-73.

102. Dammer, E.B., et al., *Polyubiquitin linkage profiles in three models of proteolytic stress suggest the etiology of Alzheimer disease*. J Biol Chem, 2011. **286**(12): p. 10457-65.
103. Langdon, W.Y., et al., *v-cbl, an oncogene from a dual-recombinant murine retrovirus that induces early B-lineage lymphomas*. Proc Natl Acad Sci U S A, 1989. **86**(4): p. 1168-72.
104. Swaminathan, G. and A.Y. Tsygankov, *The Cbl family proteins: ring leaders in regulation of cell signaling*. J Cell Physiol, 2006. **209**(1): p. 21-43.
105. Thien, C.B. and W.Y. Langdon, *Cbl: many adaptations to regulate protein tyrosine kinases*. Nat Rev Mol Cell Biol, 2001. **2**(4): p. 294-307.
106. Bartkiewicz, M., A. Houghton, and R. Baron, *Leucine zipper-mediated homodimerization of the adaptor protein c-Cbl. A role in c-Cbl's tyrosine phosphorylation and its association with epidermal growth factor receptor*. J Biol Chem, 1999. **274**(43): p. 30887-95.
107. Mohapatra, B., et al., *Protein tyrosine kinase regulation by ubiquitination: critical roles of Cbl-family ubiquitin ligases*. Biochim Biophys Acta, 2013. **1833**(1): p. 122-39.
108. Haglund, K., P.P. Di Fiore, and I. Dikic, *Distinct monoubiquitin signals in receptor endocytosis*. Trends Biochem Sci, 2003. **28**(11): p. 598-603.
109. Mosesson, Y., et al., *Endocytosis of receptor tyrosine kinases is driven by monoubiquitylation, not polyubiquitylation*. J Biol Chem, 2003. **278**(24): p. 21323-6.
110. Miyake, S., et al., *Cbl-mediated negative regulation of platelet-derived growth factor receptor-dependent cell proliferation. A critical role for Cbl tyrosine kinase-binding domain*. J Biol Chem, 1999. **274**(23): p. 16619-28.
111. Lee, P.S., et al., *The Cbl protooncogene product stimulates CSF-1 receptor multiubiquitination and endocytosis, and attenuates macrophage proliferation*. EMBO J, 1999. **18**(13): p. 3616-28.
112. Lupher, M.L., Jr., et al., *Cbl-mediated negative regulation of the Syk tyrosine kinase. A critical role for Cbl phosphotyrosine-binding domain binding to Syk phosphotyrosine 323*. J Biol Chem, 1998. **273**(52): p. 35273-81.
113. Andoniou, C.E., et al., *The Cbl proto-oncogene product negatively regulates the Src-family tyrosine kinase Fyn by enhancing its degradation*. Mol Cell Biol, 2000. **20**(3): p. 851-67.

114. Rao, N., et al., *Negative regulation of Lck by Cbl ubiquitin ligase*. Proc Natl Acad Sci U S A, 2002. **99**(6): p. 3794-9.
115. Melander, F., T. Andersson, and K. Dib, *Fgr but not Syk tyrosine kinase is a target for beta 2 integrin-induced c-Cbl-mediated ubiquitination in adherent human neutrophils*. Biochem J, 2003. **370**(Pt 2): p. 687-94.
116. Kyo, S., et al., *Negative regulation of Lyn protein-tyrosine kinase by c-Cbl ubiquitin-protein ligase in Fc epsilon RI-mediated mast cell activation*. Genes Cells, 2003. **8**(10): p. 825-36.
117. Soubeyran, P., et al., *Cbl-CIN85-endophilin complex mediates ligand-induced downregulation of EGF receptors*. Nature, 2002. **416**(6877): p. 183-7.
118. Lupher, M.L., Jr., et al., *The Cbl phosphotyrosine-binding domain selects a D(N/D)XpY motif and binds to the Tyr292 negative regulatory phosphorylation site of ZAP-70*. J Biol Chem, 1997. **272**(52): p. 33140-4.
119. Meng, W., et al., *Structure of the amino-terminal domain of Cbl complexed to its binding site on ZAP-70 kinase*. Nature, 1999. **398**(6722): p. 84-90.
120. Duan, L., et al., *The Cbl family and other ubiquitin ligases: destructive forces in control of antigen receptor signaling*. Immunity, 2004. **21**(1): p. 7-17.
121. Yokouchi, M., et al., *Src-catalyzed phosphorylation of c-Cbl leads to the interdependent ubiquitination of both proteins*. J Biol Chem, 2001. **276**(37): p. 35185-93.
122. Sanjay, A., et al., *Cbl associates with Pyk2 and Src to regulate Src kinase activity, alpha(v)beta(3) integrin-mediated signaling, cell adhesion, and osteoclast motility*. J Cell Biol, 2001. **152**(1): p. 181-95.
123. Fulda, S. and D. Vucic, *Targeting IAP proteins for therapeutic intervention in cancer*. Nat Rev Drug Discov, 2012. **11**(2): p. 109-24.
124. Dolcet, X., et al., *NF-kB in development and progression of human cancer*. Virchows Arch, 2005. **446**(5): p. 475-82.
125. Idriss, H.T. and J.H. Naismith, *TNF alpha and the TNF receptor superfamily: structure-function relationship(s)*. Microsc Res Tech, 2000. **50**(3): p. 184-95.
126. de Almagro, M.C. and D. Vucic, *The inhibitor of apoptosis (IAP) proteins are critical regulators of signaling pathways and targets for anti-cancer therapy*. Exp Oncol, 2012. **34**(3): p. 200-11.
127. Dynek, J.N., et al., *c-IAP1 and UbcH5 promote K11-linked polyubiquitination of RIP1 in TNF signalling*. EMBO J, 2010. **29**(24): p. 4198-209.

128. Varfolomeev, E., et al., *IAP antagonists induce autoubiquitination of c-IAPs, NF-kappaB activation, and TNFalpha-dependent apoptosis*. *Cell*, 2007. **131**(4): p. 669-81.
129. Vucic, D., V.M. Dixit, and I.E. Wertz, *Ubiquitylation in apoptosis: a post-translational modification at the edge of life and death*. *Nat Rev Mol Cell Biol*, 2011. **12**(7): p. 439-52.
130. Salvesen, G.S. and C.S. Duckett, *IAP proteins: blocking the road to death's door*. *Nat Rev Mol Cell Biol*, 2002. **3**(6): p. 401-10.
131. Crook, N.E., R.J. Clem, and L.K. Miller, *An apoptosis-inhibiting baculovirus gene with a zinc finger-like motif*. *J Virol*, 1993. **67**(4): p. 2168-74.
132. Birnbaum, M.J., R.J. Clem, and L.K. Miller, *An apoptosis-inhibiting gene from a nuclear polyhedrosis virus encoding a polypeptide with Cys/His sequence motifs*. *J Virol*, 1994. **68**(4): p. 2521-8.
133. Ni, T., W. Li, and F. Zou, *The ubiquitin ligase ability of IAPs regulates apoptosis*. *IUBMB Life*, 2005. **57**(12): p. 779-85.
134. Samuel, T., et al., *Distinct BIR domains of cIAP1 mediate binding to and ubiquitination of tumor necrosis factor receptor-associated factor 2 and second mitochondrial activator of caspases*. *J Biol Chem*, 2006. **281**(2): p. 1080-90.
135. Phillips, A.H., et al., *Internal motions prime cIAP1 for rapid activation*. *Nat Struct Mol Biol*, 2014. **21**(12): p. 1068-74.
136. Hu, S. and X. Yang, *Cellular inhibitor of apoptosis 1 and 2 are ubiquitin ligases for the apoptosis inducer Smac/DIABLO*. *J Biol Chem*, 2003. **278**(12): p. 10055-60.
137. Silke, J., et al., *Determination of cell survival by RING-mediated regulation of inhibitor of apoptosis (IAP) protein abundance*. *Proc Natl Acad Sci U S A*, 2005. **102**(45): p. 16182-7.
138. Cheung, H.H., et al., *The RING domain of cIAP1 mediates the degradation of RING-bearing inhibitor of apoptosis proteins by distinct pathways*. *Mol Biol Cell*, 2008. **19**(7): p. 2729-40.
139. Dueber, E.C., et al., *Antagonists induce a conformational change in cIAP1 that promotes autoubiquitination*. *Science*, 2011. **334**(6054): p. 376-80.

140. Herman, M.D., et al., *Structures of BIR domains from human NAIP and cIAP2*. Acta Crystallogr Sect F Struct Biol Cryst Commun, 2009. **65**(Pt 11): p. 1091-6.
141. Bradford, M.M., *A rapid and sensitive method for the quantitation of microgram quantities of protein utilizing the principle of protein-dye binding*. Anal Biochem, 1976. **72**: p. 248-54.
142. Winter, M.J., et al., *Using data from drug discovery and development to aid the aquatic environmental risk assessment of human pharmaceuticals: concepts, considerations, and challenges*. Integr Environ Assess Manag, 2010. **6**(1): p. 38-51.
143. Kaelin, W.G., Jr., et al., *Expression cloning of a cDNA encoding a retinoblastoma-binding protein with E2F-like properties*. Cell, 1992. **70**(2): p. 351-64.
144. Quinn, J.G., et al., *Development and application of surface plasmon resonance-based biosensors for the detection of cell-ligand interactions*. Anal Biochem, 2000. **281**(2): p. 135-43.
145. Gao, G., J.G. Williams, and S.L. Campbell, *Protein-protein interaction analysis by nuclear magnetic resonance spectroscopy*. Methods Mol Biol, 2004. **261**: p. 79-92.
146. Koliopoulos, M.G., et al., *Functional role of TRIM E3 ligase oligomerization and regulation of catalytic activity*. EMBO J, 2016. **35**(11): p. 1204-18.
147. Wickliffe, K.E., et al., *The mechanism of linkage-specific ubiquitin chain elongation by a single-subunit E2*. Cell, 2011. **144**(5): p. 769-81.
148. Yunus, A.A. and C.D. Lima, *Lysine activation and functional analysis of E2-mediated conjugation in the SUMO pathway*. Nat Struct Mol Biol, 2006. **13**(6): p. 491-9.
149. Bocik, W.E., et al., *Mechanism of polyubiquitin chain recognition by the human ubiquitin conjugating enzyme Ube2g2*. J Biol Chem, 2011. **286**(5): p. 3981-91.
150. Miura, T., et al., *Characterization of the binding interface between ubiquitin and class I human ubiquitin-conjugating enzyme 2b by multidimensional heteronuclear NMR spectroscopy in solution*. J Mol Biol, 1999. **290**(1): p. 213-28.

151. Nakatani, Y., et al., *Regulation of ubiquitin transfer by XIAP, a dimeric RING E3 ligase*. *Biochem J*, 2013. **450**(3): p. 629-38.
152. Lopez, J., et al., *CARD-mediated autoinhibition of cIAP1's E3 ligase activity suppresses cell proliferation and migration*. *Mol Cell*, 2011. **42**(5): p. 569-83.
153. Bosanac, I., et al., *Modulation of K11-linkage formation by variable loop residues within UbcH5A*. *J Mol Biol*, 2011. **408**(3): p. 420-31.
154. Haas, A.L. and P.M. Bright, *The immunochemical detection and quantitation of intracellular ubiquitin-protein conjugates*. *J Biol Chem*, 1985. **260**(23): p. 12464-73.
155. Job, F., et al., *Ubiquitin is a versatile scaffold protein for the generation of molecules with de novo binding and advantageous drug-like properties*. *FEBS Open Bio*, 2015. **5**: p. 579-93.
156. Fredrickson, E.K., et al., *Means of self-preservation: how an intrinsically disordered ubiquitin-protein ligase averts self-destruction*. *Mol Biol Cell*, 2013. **24**(7): p. 1041-52.
157. Lupher, M.L., Jr., et al., *A novel phosphotyrosine-binding domain in the N-terminal transforming region of Cbl interacts directly and selectively with ZAP-70 in T cells*. *J Biol Chem*, 1996. **271**(39): p. 24063-8.
158. Moon, W.J., et al., *Recombinant expression, isotope labeling, refolding, and purification of an antimicrobial peptide, piscidin*. *Protein Expr Purif*, 2007. **51**(2): p. 141-6.
159. Gilchrist, C.A., D.A. Gray, and R.T. Baker, *A ubiquitin-specific protease that efficiently cleaves the ubiquitin-proline bond*. *J Biol Chem*, 1997. **272**(51): p. 32280-5.
160. Brzovic, P.S. and R.E. Klevit, *Ubiquitin transfer from the E2 perspective: why is UbcH5 so promiscuous?* *Cell Cycle*, 2006. **5**(24): p. 2867-73.
161. Streich, F.C., Jr. and C.D. Lima, *Capturing a substrate in an activated RING E3/E2-SUMO complex*. *Nature*, 2016. **536**(7616): p. 304-8.
162. Dubrez, L., J. Berthelet, and V. Glorian, *IAP proteins as targets for drug development in oncology*. *Onco Targets Ther*, 2013. **9**: p. 1285-304.
163. Liyasova, M.S., K. Ma, and S. Lipkowitz, *Molecular pathways: cbl proteins in tumorigenesis and antitumor immunity-opportunities for cancer treatment*. *Clin Cancer Res*, 2015. **21**(8): p. 1789-94.